AN EXPERIMENTAL INVESTIGATION INTO THE PERFORMANCE OF A NANOFLUID BASED CONCENTRATING PARABOLIC SOLAR COLLECTOR (NCPSC)

A Thesis Report Submitted
in partial fulfillment of the requirements for
the award of degree of

MASTER OF ENGINEERING
IN
THERMAL ENGINEERING

Submitted by
KAPIL SHARMA
Roll No.: 801283012

Under the Guidance of

Mr. Kundan Lal
(Assistant Professor)

Department of Mechanical Engineering
Thapar University, Patiala

DEPARTMENT OF MECHANICAL ENGINEERING
THAPAR UNIVERSITY, PATIALA-147004, INDIA
July 2014
Established under section 3 of UGC Act, 1956 vide notification # F-12/84-U.3 of Government of India

DECLARATION

I, "Kapil Sharma", hereby certify that the work which is being presented in this thesis report entitled **"An Experimental Investigation into the Performance of a Nanofluid Based Concentrating Parabolic Solar Collector (NCPSC)"** by me in partial fulfilment of the requirements for the award of degree of **Master of Engineering** in **Thermal Engineering** from **Thapar University, Patiala,** is an authentic record of my own work carried out under the supervision of Mr. Kundan Lal, Assistant Professor, **Department of Mechanical Engineering**, Thapar University, Patiala.

The matter embodied in this thesis has not been submitted in any other University / Institute for the award of any other degree.

Date: 11/07/14

Kapil Sharma

(KAPIL SHARMA)

Reg. No. 801283012

This is to certify that the above statement made by the student concerned is correct to the best of my knowledge and belief.

Date: 11/07/14

(Mr. KUNDAN LAL)

Assistant Professor,

Mechanical Engineering Department,

Thapar University, Patiala (Punjab)

Countersigned by

(Dr. AJAY BATISH)

Professor and Head,

Mechanical Engineering Department,

Thapar University,

Patiala (Punjab)

(Dr. S.K. MOHAPATRA)

Dean of Academic Affairs,

Thapar University,

Patiala (Punjab)

ACKNOWLEDGEMENT

With deep sense of gratitude I express my sincere thanks to my guide **Mr. Kundan Lal**, *Assistant Professor*, Mechanical Engineering Department (MED), Thapar University, Patiala for his valuable guidance, constructive suggestions and constant encouragement during the course of my work on this thesis report.

I also pay thanks to **Dr. Ajay Batish**, *Prof. & Head*, Mechanical Engineering Department (MED), **Dr. Rajeev Mehta,** *Associate Prof. & Head,* Chemical Engineering Department (CHED), Dr. Madhup Mittal, *Assistant Professor*, Mechanical Engineering Department (MED), for providing the facilities for the completion of research work.

I am grateful to Mr. Charanjeet Singh, *Lab Technician*, Mechanical Engineering Department (MED) & Mr. Rakesh Lal, *Lab Technician*, Mechanical Workshop for providing help in my research work.

I would like to thank TEQIP-II for providing the grant for funds to carry out research work.

I am grateful to my parents for giving me inspiration and moral support, which enable me to pursue my studies.

Above all, I express my thanks to the **"ALMIGHTY"** for blessings and kindness.

Kapil Sharma

KAPIL SHARMA

ABSTRACT

Solar collectors are widely used to harvest the solar energy and performance of these solar collectors depends upon various factors like collector & receiver material, solar intensity, nature of working fluid etc. It has been observed that nature & properties of the working fluid which flows through the collectors, greatly effects its performance. In the present study an attempt has been made to improve the performance of a parabolic solar collector by using nanofluids instead of conventional fluid like water as working fluid. The present investigation mainly focus on the nanofluid based concentrating parabolic solar collector (NCPSC). Nanofluids are the suspensions of metallic or non-metallic nanoparticles like aluminium, aluminium oxide, copper oxide etc. in base fluids like water, ethylene glycol, oil etc. The performance of a parabolic solar collector is investigated experimentally by studying the effect of alumina (Al_2O_3) & copper oxide (CuO) nanoparticles in water, as working fluids. Three mass flow rates (20, 40 & 60) l/hr and two particles volume concentrations 0.01% & 0.05% have been examined. The average size of nanoparticle is 20-30 nm. Nanofluids are prepared without using any surfactant. For water based copper oxide (CuO) & for water based alumina (Al_2O_3) nanofluid, for a concentration of 0.01% (vol.) the maximum instantaneous efficiency is found to be 13.57% and 10.1% whereas, thermal efficiency is 4.87% and 3.67% for a mass flow rate of 60 l/hr. Similarly for same mass flow rate & at volume concentration of 0.05% the maximum instantaneous efficiency is 18.4% and 10.37% & thermal efficiency found to be 6.6% and 3.74%. Comparison of water based alumina nanofluid is done with copper oxide nanofluid and it is observed that by using CuO nanofluid as a working fluid the value for maximum instantaneous & thermal efficiency is 8.16% & 5.14% for 60 l/hr & 20 l/hr mass flow rates with 0.01% concentration. Similarly, for 60 l/hr mass flow rate the observed value of maximum instantaneous & thermal efficiency is 8.75% & 3.06% with 0.05% volume concentration. Therefore, from the results it can be concluded that the performance of solar collector is remarkably enhanced by using nanofluids as working fluid in the solar collector.

Keywords: parabolic solar collector, efficiency, nanofluid, mass flow rate, concentration

CONTENTS

Page No.

LIST OF FIGURES

Page No.

LIST OF TABLES

Page No.

NOMENCLATURE

Symbols

$A_{aper.}$	aperture area, m^2
Al_2O_3	aluminium oxide or alumina
Al	aluminium
C_r	concentration ratio
c_p	specific heat, J/kg K
c_{pnf}	specific heats of nanofluid, J/kg K
c_{bf}	specific heats of base fluids, J/kg K
c_{np}	specific heats of nanoparticles, J/kg K
CO_2	Carbon-dioxide
CuO	copper oxide
D_i	inner diameter of receiver tube, m
D_0	outer diameter of receiver tube, m
D_{ci}	inner diameter Glass cover tube, m
D_{co}	outer diameter of glass cover tube, m
F'	collector efficiency factor
F_R	heat removal factor
f_v	volume fraction of the nanoparticles in percent
G_T	solar intensity, W/m^2
$G_{avg.}$	average solar intensity, W/m^2
h_f	convective heat transfer coefficient, W/m^2K
I_t	total solar intensity, $W.m^2$
k	thermal conductivity, W/m-K
k_{nf}	thermal conductivity of nanofluid, W/m-K
k_{bf}	thermal conductivity base fluids, W/m-K
k_{np}	thermal conductivity nanoparticles in W/m-K
L	length of collector, m
l/hr	litres per hour
$\dot{m}$	mass flow rate, kg/sec

m	mass, kg
MWe	megawatt electrical
N_u	nusselt number
ppm	parts per million
P_r	prandtl number
q_u	useful heat gain, W
R_b	bond resistance
R_e	reynolds number
S	absorbed flux, W/m^2
SiO_2	silicon oxide
TiO_2	titanium oxide
T_m	mean temperature, °C
T_a	ambient temperature, °C
T_{out}	outlet temperatures, °C
T_{in}	inlet temperatures, °C
T_{max}	maximum temperatures, °C
T_{min}	minimum temperatures, °C
U_l	overall loss coefficient, W/m^2K
$V_{bf,}$	quantity of base fluid
V_{np}	quantity of nanoparticle
V_{nf}	quantity of nanofluid
V	average velocity, m/sec
W	width of collector, m
W_{nf}	weight of nanofluid , gm
W_{np}	weight of nanoparticles , gm

Greek symbols

α	absorptivity of receiver tube
τ	glass cover transmissivity for solar radiation
β	specular reflectivity of concentrated surface
ϒ	intercept factor
ν	viscosity, m^2/s
μ	dynamic viscosities, m^2/s

μ_{nf}	dynamic viscosity of nanofluids, m^2/s
μ_{bf}	dynamic viscosity base fluids, m^2/s
ρ	density, kg/m^3
ρ_{nf}	density of nanofluid, kg/m^3
ρ_{np}	density of nanoparticle, kg/m^3
ρ_{bf}	density of base fluids, kg/m^3
η_{ov}	overall efficiency
η_{th}	thermal efficiency
η_i	instantaneous Efficiency
η_{opt}	optical efficiency

Subscripts

a	ambient
aper	aperture
avg.	average
bf	base fluid
ci	inner glass cover tube
co	outer glass cover tube
in	inlet
i	instantaneous
max.	maximum
min	minimum
m	mean
nf	nanofluid
np	nanoparticle
out	outlet
ov	overall
opt	optical
r	ratio
v	volume
t	total
th	thermal
u	useful

Abbreviations

BTU	British thermal unit
CSP	concentrated solar power
CNT	carbon nanotube
DASC	direct absorption solar collector
FPSC	flat plate solar collector
FDM	finite difference method
GW	gigawatt
HTF	heat transfer fluid
HDC	hamilton–crosser model
kW	kilowatt
MWCNT	multiwall carbon nanotubes
NCSWHS	nanofluid-based concentrating solar water heating system
NIR	near-infrared
PSC	parabolic solar collector
PVT	photovoltaic thermal
PTC	parabolic trough collector
PW	petawatt
SEM	scanning electron microscopy
SDS	sodium dodecyl sulphate
SWCNH	single wall carbon nanohorns
TEM	transmission electron microscopy
TPTC	transparent parabolic trough collector
W	watt
XRD	X-ray diffraction

CHAPTER-1

INTRODUCTION

1.1 General

As we all know that the entire world faces a big challenge of global warming. There is a great need to tackle the issue of global warming mainly induced by the gas CO_2. Sun is the major resource of renewable energy. In order to reduce carbon dioxide emission and global warming the utilization solar energy is very essential. There are various type of renewable energy resources like wind energy, solar energy, tidal energy. Of all the renewable sources of energy available like wind, solar, tidal, ocean thermal, solar thermal energy is the most plentiful source and is available in both direct as well as indirect forms. Hence, solar energy is promising to be the best option for renewable source. The proper or efficient utilisation of this source i.e. solar energy is increasingly being considered to be the suitable solution to solve the global warming like issues. By the usage of solar energy we can also achieve the concept of sustainable development.

The sun releases a huge quantity of radiation to its surroundings: 174 PW (1 PW = 1015 W) at upper atmosphere of the earth When the energy coming from the sun reaches to the earth's surface it has been attenuated two times (Tian and Zhao, 2013):-

1. by the earth's atmosphere (6% by reflection and 16% by absorption) and
2. by the clouds (20% by reflection and 3% by absorption)

The Sun releases energy at a rate of 3.8×10^{23} kW, of which, approximately 1.8×10^{14} kW is intercepted by the earth. About 60% of this amount or 1.08×10^{14} reaches the earth's surface. The remaining is reflected back into space and absorbed by the atmosphere. Around 0.1% of this energy, when converted at an efficiency of 10% would generate four times the world's total generating capacity of about 3000 GW. Within the next two decades, the demand for fossil fuels like coal, petroleum, and natural gas is expected to surpass annual production. Moreover, the harmful emissions such as carbon dioxide, nitrogen oxides, etc. release by the burning of fossil fuels affect the environmental condition (Thirugnanasambandam et al., 2010).

Solar energy has been discovered through solar thermal utilization, & the generation of power by photovoltaic technology. The most popular application among these is solar thermal utilization. In solar thermal collectors like devices, plates or tubes are used to absorb solar energy. These plates or tubes are coated with a layer of selectively absorbing material, and then energy is carried away by working fluids in the form of heat energy (Han et al. 2011).

Solar energy is very large, unlimited and clean form of energy. Thus to fulfil the present and future needs of the world solar energy has the great potential. The most essential advantage of using renewable energy sources is the decrease of environmental pollution. The crisis of the energy cost and its demand rises exponentially with the lack of fossil fuels (Chaji et al. 2013). In today's world economy Renewable energies are gaining a lead role because they are sustainable and safe. Renewable energies are expected to grow at higher rate because of the following reasons (Sani et al. 2011):-

1. World energy demand is expected to rise in future with a corresponding decline in oil production.
2. Due to changing climatic conditions.

To meet increasing energy demands, there is a big necessity for clean and inexpensive renewable energy sources because there is a shortage of the supply of fossil fuels in the world (Barlev et al., 2011). The perceived shortage of fossil fuels like coal, petroleum, natural gas as well as environmental considerations will limit the use of fossil fuels in the future. Therefore, the continuous investigation for an alternative power source is still going on.

Solar thermal energy is a very suitable source of heating and it is a technology that does not depend on scarce, finite energy resources. Solar collector transforms solar radiation into heat and transfer the heat to a medium. The main application of solar energy is that it is used for heating or cooling systems (Yousefi et al., 2012b). Today our society faces the most important challenges regarding the generation of sustainable energy. Consumption of electricity is increasing year by year and generation of electricity has become a main issue in the industry.

To the world's total energy demand electricity supplies contributes a big share, and is growing a faster sector than liquid fuels, natural gas, and coal. Coal, petroleum and natural gas like fossil fuels are used to generate the steam in boilers of power plants and these plants has a major contribution in the electricity power plant in the entire world. On the other hand, air pollution caused due to burning of fossil fuels has become the major issue for the governments, investors, environmentalists and researchers (Saidur et al., 2012). Solar thermal collector devices are used to convert solar radiation energy to internal energy of the transport medium. These are also known as heat exchangers. On the other hand, non-concentrating solar collectors are used if a big quantity of solar radiation coming from the sun is concentrated on a relatively small collecting area (Saidur et al., 2012). In last 10–15 years innovation in concentrated solar energy has plays an important role or has a major contribution to increase the number of experimental and commercial thermal systems (Taylor et al., 2011a).

There are two typical categories of solar devices used to harvest and store the solar energy for power generation that is photovoltaic and concentrated solar power (CSP). Photovoltaic includes the use of solar cells to generate electricity directly by the photoelectric effect. The concentrated solar power employs dissimilar methods of capturing solar thermal energy for the usage in power-producing heat processes (Barlev et al., 2011).

In recent years, technological developments have greatly increased the growth in the energy sector especially in the solar energy field. Many improvements and investigations carried out in the field of solar energy. Technological developments carried out mainly in the field of concentrated solar power (CSP).

Concentrating Solar Power (CSP) technologies are used to obtain high quality electrical energy from solar energy. CSP technologies based on linear Fresnel reflector, parabolic trough, power tower and parabolic dish collectors. Among these all CSP technologies, parabolic trough collector is the most advanced technology with high capability for large scale generation of solar power (Reddy and Kumar, 2012).

1.2 Solar Collector

A solar energy collector is a heat-exchanging device that converts solar radiation into thermal energy that can be used for generation of power. The elementary role of a solar collector is to absorb incident solar radiation coming from the sun and transform it into heat, which is then carried away by a heat transfer fluid (HTF) flowing through the collector. The heat transfer fluid relates the solar collectors to the power generation system. As it circulates it carries thermal energy from each collector to a central steam generator or thermal storage system (Barlev et al., 2011). The conventional solar collector used in various applications like water heating, space heating and cooling.

There are numerous kinds of solar collectors. They can be categorise on the basis of maximum temperature obtainable in the receiver. Thus solar collectors fall in three categories of low, medium and high temperatures (Yahya S.M., 2012). In other words, solar collectors are typically classified into two categories according to concentration ratios as follows:

1. Non-concentrating collectors e.g. Flat-plate collectors, Hybrid PVT Collectors, Enhanced hybrid PVT collectors – Bifacial PVT (Tian and Zhao, 2013)
2. Concentrating collectors e.g. Heliostat field collectors, parabolic dish collectors, parabolic trough collectors (Tian and Zhao, 2013)

A non-concentrating collector are those which has the same absorbing area as its intercepting area, whereas a sun-tracking concentrating solar collector generally has concave reflecting

surfaces to intercept and focus the solar irradiation to a much smaller receiving area, resulting in an increased heat flux so that the thermodynamic cycle can attain higher Carnot efficiency when working under higher temperatures (Tian and Zhao, 2013).

1.2.1 Non-concentrating collectors or low temperature collectors

A flat plate collector comes under the category of a non-concentrating type low temperature collector (Yahya S.M., 2012). Flat-plate solar collectors are usually permanently fixed in position, and therefore need to be oriented appropriately. Flat plate solar collector usually comprises of glazing covers, absorber plates, insulation layers, recuperating tubes (filled with heat transfer fluids) and other auxiliaries (Tian and Zhao, 2013). In this type of collector the solar radiation is received by the bank of tubes mounted on a black metallic absorber plate. Water or some other suitable base fluid is circulated through the collector tubes for absorbing solar energy as a heat. The energy in the hot water (at about T_{max}=100°C) can be utilized for heating and power generation in small units (Yahya S.M., 2012).

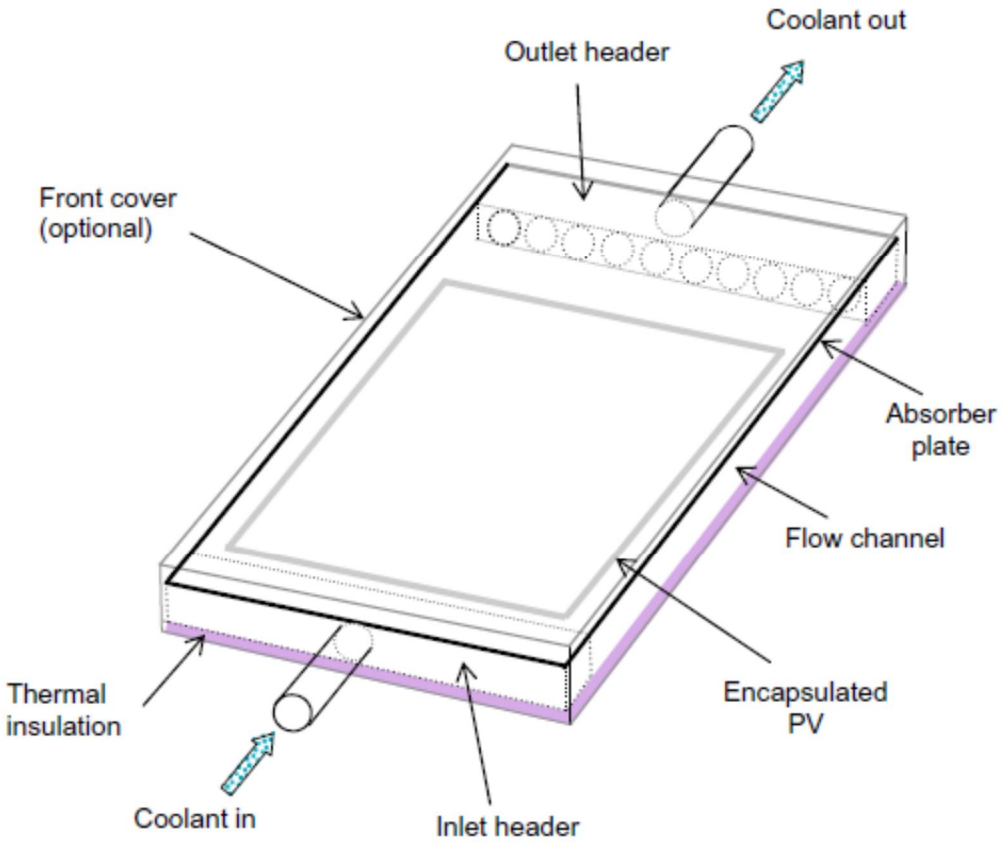

Figure 1.1: Main features of a Flat-plate PVT collector (Chow T.T., 2009)

It is easy to assemble such collectors from comparatively cheaper materials. They need very little maintenance. Energy losses in these collectors are generally due to heat losses by conduction, convection and radiation (Yahya S.M., 2012).

1.2.2 Concentrating collectors or high temperature collectors

These type of concentrating collectors can produce receiver temperatures above 350°C. They need accurate sun tracking by employing large number of heliostats. The concentration ratio of these collectrors is very high (greater than 50). Central receiver systems employing a great number of heliostats have high values of concentration ratio (50-300) and temperature (Yahya S.M., 2012). They are most appropriate for power generation. The main type of concentrating solar collector is parabolic trough collector (Barlev et al., 2011)

(1) Parabolic trough collector

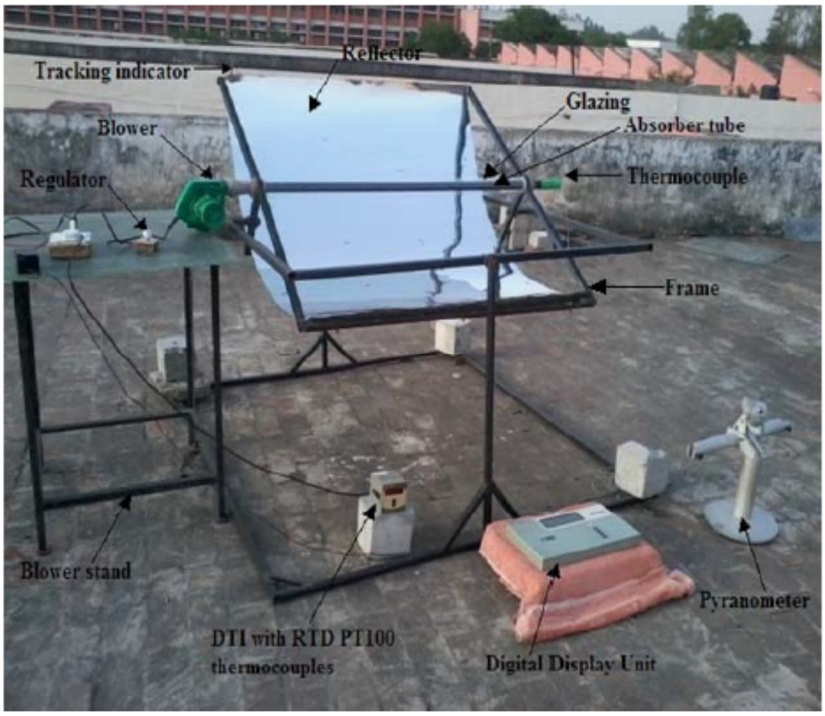

Figure 1.2: Parabolic trough collectors (Yadav et al., 2013)

Parabolic trough collectors can concentrate sunlight with a concentration rate of around 50, depending on the trough size. The focal line temperature can be as high as 350 °C to 400 °C. Parabolic mirrors are the main key component of such collectors, which has the ability to reflect the sunlight that is parallel to its symmetrical axis to its common focal line. At the focal line, a black metal receiver (covered by a glass tube to diminish heat loss) is placed to absorb collected heat. Parabolic trough collectors can be orientated either in an east–west direction, tracking the sun from north to south, or a north–south direction, tracking the sun from east to west (Tian and Zhao, 2013).

Parabolic trough technology is the most advanced concentrated solar power scheme. Presently it is used by numerous operational large-scale CSP farms around the world (Barlev et al., 2011). The advanced field of parabolic trough collectors provides an efficient, relatively low cost

power production scheme. In the last decade, numerous advances in reflector and receiver design have been made in order to improve efficiency and reduce losses. To achieve optimum power output throughout the day heat collection and transfer methods have been modelled and tested repeatedly in order. The PTC scheme also involves efficient thermal energy storage. (Barlev et al., 2011).

1.3 Nanofluids in Solar Energy

The field of using nanofluids for the devices like solar collectors as a working medium is a relatively an innovative idea. In order to improve the physical properties for enhancing direct solar collectors various studies has to be carried out. As solar power is readily available, researchers are interested to develop the various aspects to make usage of this energy (Saidur et al., 2012).

Nanofluids are defined as the colloidal suspensions of fine nanomaterials in the size range of 1–100 nm in carrier fluids like water, ethylene glycol, therminol-VP 1, and oil are known as nanofluids (Philip & Shima., 2012). In other words, Nanofluids are potential heat transfer fluids with improved thermophysical properties and heat transfer performance can be applied in many devices for better performances (i.e. energy, heat transfer and other performances) (Saidur et al., (2011). Nanoparticles provide the following possible advantages in solar power plants (Taylor et al., 2011a):

1. The very small size of the particles preferably lets them to pass through pumps without adverse effects.
2. Nanofluids can absorb energy directly--- skipping intermediate heat transfer steps.
3. The nanofluids has high absorption in the solar range and low emittance in the infrared).
4. A more uniform receiver temperature can be attained inside the collector.
5. Enhanced heat transfer via greater convection and thermal conductivity which may enhance the performance of a receiver, and
6. Absorption efficiency may be improved by modifying the nanoparticle size and shape to the application.

One of the most effective methods to increase the solar collector efficiency, is to replace the working fluid, water, by high thermal conductivity fluids. At present nanofluids are expected to excellent heat transfer properties as compare to the conventional heat transfer fluids (Yousefi et al., 2012b).

The suspension of nano-sized particles with average size ranging from 1nm to100 nm or below 100 nm in a conventional base fluid is called a nanofluid (Mahian et al., 2013). Nanofluids are

suspensions of metallic or nonmetallic nanoparticles like copper, aluminum silicon, alumina (Al_2O_3) in a base fluid such as water, ethylene glycol (Yousefi et al., 2012a).

Common fluids such as water, ethylene glycol, and heat transfer oil plays a vital role in various industrial processes such as generation of power, heating or cooling processes, chemical processes, and microelectronics. However, the thermal conductivity of these fluids is comparatively low and thus cannot able to reach high heat exchange rates in thermal engineering devices. A way to solve this obstacle is using excessive fine solid particles suspended in common fluids so that their thermal conductivity will be improved. Experiments have shown that nanofluids have substantial higher thermal conductivities compared to the base fluids. These suspended nanoparticles can change the transport and thermal properties of the base fluid (Sridhara & Narayan Satapathy, 2011). Nanofluids show better stability, rheological properties, and considerably higher thermal conductivities.

For various industrial and automotive applications nanofluids are the novel generation heat transfer fluids because they exhibit excellent thermal performance (Tiwari et al., 2013).Recently, many researchers have investigated the effects of nanofluids on the improvement of heat transfer in thermal engineering devices, both experimentally and theoretically (Mahian et al., 2013). The exceptional features of nanofluids are increase in liquid thermal conductivity, liquid viscosity, and heat transfer coefficient.

Using nanofluids as a DASC leads to following advantages (Otanicar et al., (2010)

1. Variability of the shape, size, material, and volume fraction of the nanoparticles allows for tuning to maximize spectral absorption of solar energy during the fluid volume.
2. Enhancement in the thermal conductivity can lead to efficiency improvements, although small, by more effective fluid heat transfer; and, finally.
3. Huge improvements in surface area due to the very small particle size, which makes nanofluid-based solar systems attractive for thermo chemical and photo-catalytic processes.

For several years the thermophysical properties of fluids like thermal conductivity, thermal diffusivity, viscosity and convective heat transfer coefficients containing various solid particles have been investigated. In order to measure the thermal conductivity of dispersed materials some predicting formulae have been proposed theoretically and experimentally (Zhang et al., 2007). Thermal conductivity is an important parameter in enhancing the heat transfer performance of a base fluid. Since the thermal conductivity of solid metals is higher than that of fluids, the suspended particles are expected to increase the thermal conductivity and heat transfer performance. Various methods have been used to measure the thermal conductivity of nanofluids like the temperature oscillation method, the steady-state parallel plate method and

transient hot-wire method (Sridhara & Narayan Satapathy, 2011). Various theoretical, numerical, and experimental results have reported by many researchers regarding thermophysical properties of nanofluids (Zhang et al., 2007).

For the last one decade, nanofluids have been a topic of intense research due to their enhanced thermal properties and possible heat transfer applications. The low thermal conductivity of conventional heat transfer fluid has been a serious impediment for improving the performance and compactness of engineering equipments (Philip & Shima., 2012).

1.3.1 Applications of nanofluids (Wong & De Leon et al. 2010)

1. Heat Transfer Applications (industrial cooling applications, nuclear reactors, smart fluids)
2. Automotive Applications (nanofluid coolant, nanofluid in fuel, brake and other vehicular nanofluids)
3. Electronic Applications (cooling of microchips, microscale fluidic applications, micro devices)
4. Biomedical Applications (nano drug delivery, cancer therapeutics, nano cryosurgery, Sensing and imaging, cryopreservation)

Other applications (Saidur et al., (2011)

1. Application in chillers in air conditioning systems
2. Application in domestic refrigerator
3. Application as a coolant in machining
4. Cooling of diesel electric generator
5. Solar water heating applications
6. Cooling and heating in buildings
7. Application in transformer
8. Space, defence and ships
9. Application in fuel cell
10. Application of nanofluids in thermal absorption systems
11. Application in grinding

1.3.2 Challenges of nanofluids (Saidur et al., (2011)

1. High cost of nanofluids
2. Difficulties in production process

3. Lower specific heat than base fluids
4. Higher viscosity
5. Long term stability of nanoparticles dispersion
6. Increased pressure drop and pumping power

CHAPTER-2

LITERATURE REVIEW

This literature review presents a detailed discussion about solar collectors and applications of nanofluids in solar energy. As nanofluids have a great potential to enhance the heat transfer characteristics, a detailed review is presented. Firstly the literatures based on solar energy collectors are reviewed and the variations of efficiency to some parameters e.g. solar radiation, mass flow rate, temperature difference, solar insolation, ambient/inlet temperature, volume concentration, diameter of fluids etc. is observed.

In the reviewed literature effect of volume fraction & diameter of nanofluid on the thermal performance of collectors is studied. The various types of nanofluids have been used like Al_2O_3-H_2O, TiO_2-H_2O, Carbon Nanotube (CNT), graphite, silver, single wall and multiwall carbon nanohorns.

Literature of Nanofluids application in solar collectors is studied in a great manner.

2.1 Investigations

Natarajan & Sathish (2009) carried out an investigation to study the role of nanofluids in solar water heater. The objective of this study was to examine and compare the heat transfer properties of the nanofluids with the conventional fluids. During this investigation water based Multiwall carbon nanotubes (MWCNTs) were used as nanofluids with volume fraction in percent taken as 0.2, 0.4, 0.6, 0.8, 1.0, and 1.2. For the preparation of CNTs sodium dodecyl sulphate (SDS) was used as a surfactant. Sodium dodecyl sulphate was used to obtain stable nanofluids. It was found that for the stable CNT dispersion SDS surfactant proves to be a suitable dispersant. Transient hot-wire method was used to measure the thermal conductivities of nanofluids. It was concluded that the thermal conductivity of water-based MWCNT nanofluid increases as a function of volume fraction of MWCNTs. At a volume fraction of 1.0% the thermal conductivity of nanofluid increased up to 41%. The comparison between the experimental data for MWCNT in deionized water was done and the values were calculated from Hamilton–Crosser model. It was concluded that the measured values of thermal conductivity is greater than those calculated from Hamilton–Crosser model (HDC). It was also concluded that if nanofluids are used as a heat transport medium, it increases the efficiency of the traditional solar water heater.

Tyagi et al. (2009) carried out theoretical and numerical investigations to study the effects of different parameters such as nanoparticle size, volume fraction, collector geometry on the efficiency of a low-temperature nanofluid based direct absorption solar collector (DASC).In this paper water based aluminum nanoparticles Al_2O_3 taken as a working fluid (i.e. mixture of water and aluminum nanoparticles). Numerical modelling of DASC was also done by using two dimensional heat transfer analysis. The variation of collector efficiency as a function of the particle volume fraction (0.1% to 5%), particle size, collector geometry was studied experimentally. The results revealed that by the addition of nanoparticles in the working fluid, the efficiency increases remarkably for low values of volume fraction of nanoparticles However, it was found that the addition of more nanoparticles is not beneficial because the efficiency remains approximately constant for a volume fraction higher than 2%. Investigations were also carried out regarding the effects of nanoparticles size and collector geometry on the collector efficiency. The results also revealed that the efficiency increases slightly with an increase in the size of nanoparticles. The collector efficiency increases as the collector's height increases and reaches up to the value of 80 %, and with the length factor the efficiency firstly increases with length and then gradually falloffs. It was observed that the rise of collector efficiency to the rise in attenuation of sunlight passing through the collector due to the nanoparticles addition leads to the increase of collector efficiency. On comparison, the DASC using nanofluid as a working fluid have 10 % efficiency higher than that of the conventional flat plate collector using water as a working fluid.

Otanicar et al. (2010) carried out an experimental and theoretical investigations to study the effects of different nanofluids such as carbon nanotubes, graphite, and silver on the performance of a direct absorption solar collector (DASC). The investigations were carried out to check the variation of collector efficiency as a function of volume fraction for different nanomaterials mentioned above. The DASC data are compared with the conventional collector configuration where the solar energy is absorbed on a black plate surface. It was concluded that by the addition of small amounts of nanoparticles leads to the remarkable improvement of the collector efficiency. The efficiency increases up to approximately 0.5% of volume fraction. After a volume fraction of 0.5%, the efficiency begins to level off and even fall slightly with increasing volume fraction.

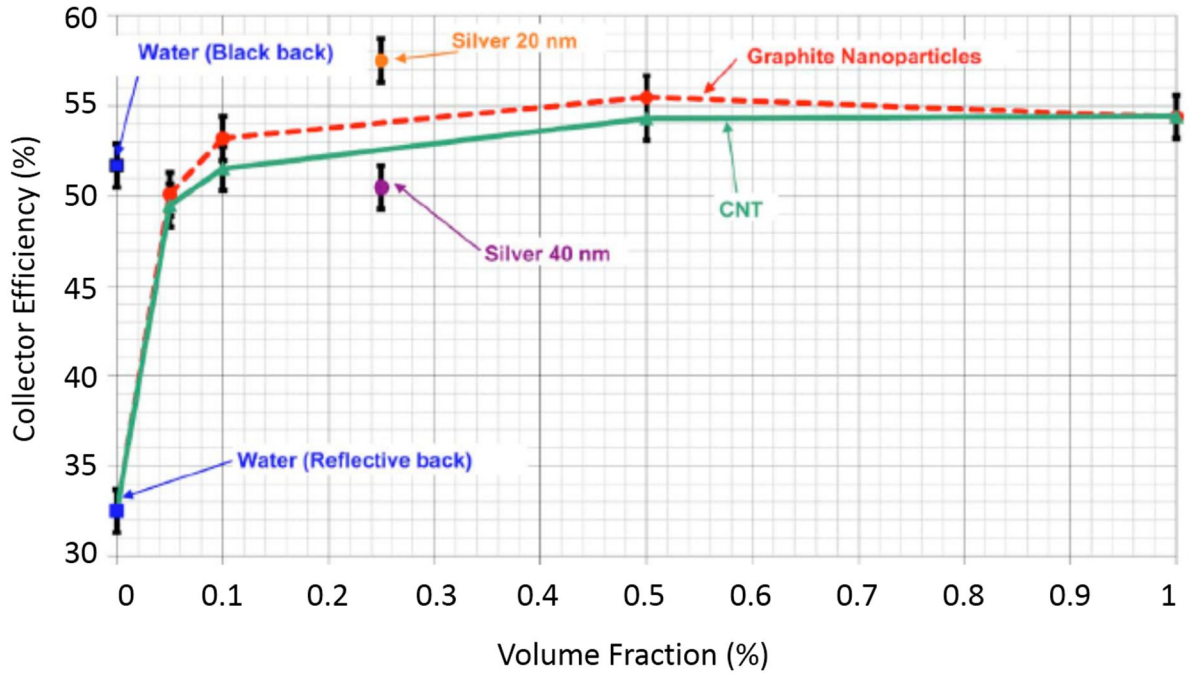

Figure 2.1: Variation of collector's efficiency with volume fraction

By using graphite nanoparticles of size 30 nm, the performance of DASC over a conventional flat surface absorber was increased up to 3% which was considered to be the maximum enhancement in its performance. In case of silver particles, the main difference in the steady-state efficiency between nanofluids occurred when the size of these particles is between 20 and 40 nm. It was found that when the size of silver nanoparticles reduces from 40 nm to 20 nm efficiency enhancement of 6 % was observed. The collector efficiency as a function of volume fraction was plotted for silver graphite and CNT nanoparticles in figure 2.1. It was seen that as the size of nanoparticles increases, the collector efficiency decreases.

Khullar et al. (2010) carried out theoretical & numerical investigation regarding the application of nanaofluids as the working fluid in concentrating parabolic solar collectors. In this paper mathematical modelling of heat transfer and flow aspects of the linear parabolic solar collectors had been done. Al-water based nanofluid was used as the working fluid and to solve the equations numerically FDM (finite difference method) technique has been used. Evaluation and comparison of the two dimensional temperature field, optical and thermal efficiencies, and mean-outlet temperatures had been done for both conventional parabolic collectors utilizing water as a working fluid and nanofluid based collectors using nanofluid as a working fluid. In order to achieve the desired output temperature the effect of various operating parameters such as concentration ratio, receiver length, fluid velocity, volume fraction of nanoparticles taken

into consideration. The results indicated that in terms of thermal and optical efficiencies and higher outlet temperatures under same working conditions the collector using nanofluid as a working fluid has a better performance as compare to the conventional collector. The results also showed that the addition of aluminium nanoparticles into the base fluid (water) significantly improves its absorption characteristics.

Sani et al. (2010) carried out an investigation about the optical and thermal properties of nanofluids as a function of the nanoparticle concentration consisting in aqueous suspensions of single wall carbon nanohorns (SWCNH). The characteristics of these nanofluids were evaluated in view of their use as sunlight absorber fluids in a solar device, hence characterization of SWCNH was done in aqueous suspensions as new nanofluids for the utilization in the field of solar energy. It was found that the thermal conductivity of the nanofluids was higher than the water used as the operating fluid. According to spectral transmission measurement SWCNHs play an important role in improving the photonic properties of the fluid, leading to a major increase of the light extinction level even at very low concentrations. At the investigated concentrations up to 10% rise in the thermal conductivity was observed. For the optimization of heat transfer efficiency, optical and thermal properties of the nanofluid provides valuable information to the sunlight collector designer. It was concluded that for efficiency enhancement the usage of SWCNH water nanofluid as absorber in solar devices appears a very promising step.

Taylor et al. (2011a) carried out theoretical & experimental investigations regarding the applicability of nanofluids in high flux solar collectors and to compare the performance of nanofluid-based concentrating solar thermal system with a conventional system. The results indicated that the usage of a nanofluid as the working fluid in the receiver enhance the efficiency by 10%. It was seen that Collector efficiency enhancement of 5%–10% is possible with a nanofluid used as the working fluid in the receiver. It was concluded that using graphite/therminol VP-1 nanofluid for 10–100 MWe power plants, with volume fractions approximately up to 0.001% or less could be advantageous. The authors estimated that in a solar resource like Tucson, Arizona combining solar thermal power tower with a nanofluid receiver with the capacity of 100 MWe operating, could generate $3.5 million more per year. It was observed that, nanofluids are not expected to be appropriate for using as the working fluid for parabolic dish or trough solar thermal systems, but further optimization or cost reductions might increase their range of applicability.

Taylor et al. (2011b) carried out theoretical and experimental investigations to study the optical property characterization of various nanoparticles such as graphite, silver, copper, gold, and aluminum suspended in water and therminol-VP1 as the base fluids to determine their potential to be utilized in direct absorption solar collectors (DASC). To determine the optical property of nanofluids like graphite, aluminum measurement and modelling techniques were used. For several concentrations of aqueous graphite nanofluids extinction coefficients were studied by using modelling and experimental methods. The results showed that approximately 95% of incoming sunlight coming from the sun can be absorbed by a nanofluid having thickness greater than equal to 10 cm with very small nanoparticle volume fractions (less than 0.00001 or 10 ppm). Thus, nanofluids could be utilized to absorb sunlight with a small amount of viscosity and/or density. It was concluded that absorption is generally due to the nanoparticles at shorter wavelengths and due to the base fluids at longer wavelengths.

Sani et al. (2011) carried out an experimental investigation to study the potential of carbon nanohorn (CNH)-based suspensions for solar thermal collectors. In this paper the optical characterization of new fluid made up of single-wall carbon nanohorns (SWCNH) and ethylene glycol as a base fluid for solar energy applications were studied. In optical characterization to measure the potential of SWCNH-glycol suspension as direct sunlight absorbers, the optical properties of the nanofluid were examined as a function of the nanoparticle concentration. The measured spectral transmission showed that SWCNHs play an important role to enhance the photonic properties of the fluid, leads to a remarkable growth of the light extinction level even at very small concentrations. To evaluate the differences between SWCNHs and conventional commercial carbon forms, i.e. Carbon-black particles the obtained results had been compared with glycol-based amorphous carbon suspensions It was found that Carbon nanohorn (CNH) plays an vital role to increase the sunlight absorption with respect to the pure base fluid & SWCNHs spectral features are far more favourable than those of amorphous carbon-black particles for the specific application. It was concluded that, the use of SWCNH-glycol based nanofluid as direct absorber or working fluid in solar devices can be beneficial for increasing the collector efficiency and compactness of thermal solar devices, reducing both environmental impact and costs.

Mercatelli et al. (2011) carried out an investigation to study the scattering and absorption properties of carbon nanohorn-based nanofluids consisting in aqueous suspensions of single wall carbon nanohorns for solar energy applications. In order to use them as direct sunlight absorber fluids in solar devices the characteristics of these nanofluids were assessed. The investigation was carried out for nanohorns of different morphologies (dahlia-like, bud-like and seeds-like) and for suspensions prepared with different amounts of surfactant, hence measurements of extinction and absorption coefficients on Single Wall Carbon Nanohorn (SWCNH) suspensions as a function of the nanoparticle morphology was done. The differences in optical properties induced by carbon nanoparticles compared to those of pure water lead to a considerably higher sunlight absorption with respect to the pure base fluid. Scattering results indicating that the portion of light scattered by SWCNH suspensions was smaller than 5%. This means that approximately up to 95% of light was directly absorbed. Therefore, nanohorns suspensions behave as perfect absorbers for NIR wavelengths (833 nm) or for longer wavelengths. Finally it was concluded that for new-generation solar collectors SWCNHs seems to be very promising as innovative direct sunlight absorbers in the field of Solar Energy.

Han et al. (2011) carried out an experimental investigation about the thermal properties of carbon black aqueous nanofluids for solar absorption. In this paper carbon black nanofluids were prepared by dispersing the pre-treated carbon black powder into distilled water. During investigation optical properties of carbon black powder and nanofluids, photo thermal properties, rheological behaviours, thermal conductivity of carbon black nanofluids were measured. The volume concentration of nanofluids taken as 4.4%, 5.5%, 6.6%, 7.7% and wavelength ranges from 200-2500 nm. It was found that with high-volume fraction the nanofluids have better photo thermal properties which shows better solar energy adsorption properties. In the wavelength range from 200 to 2,500 nm both carbon black powder and nanofluids have good absorption characteristics. The results showed that the shear viscosity increases as the volume fraction increases and decreases as the temperature increases at the same shear rate and the thermal conductivity of carbon black nanofluids increases as the volume fraction and temperature increases. Finally it was concluded that, carbon black nanofluids have good absorption ability of solar energy and can effectively increase the solar absorption efficiency, hence carbon black nanofluids have high potentials for the utilization in solar application.

Yousefi et al. (2012a) carried out an experimental investigations to study the effects of Al_2O_3/water nanofluid on the efficiency of a flat-plate solar collector. The effect of using water as the working fluid, Al_2O_3 nanofluid as the working fluid without surfactant and with surfactant on the efficiency of solar collector was investigated. Triton X-100 was used as a surfactant. Two different weight fractions i.e.0.2% and 0.4% of the nanofluid taken into account with diameter of the particles taken as 15 nm. The effect of mass flow rate also taken into consideration. The mass flow rates were taken as 1, 2, 3 lit/min. their results showed that:
1. With 0.2% weight fraction (wt.) Al_2O_3 nanofluid the efficiency of the solar collector is greater as compare with the water by 28.3%.
2. The efficiency of the collector using 0.2% weight fraction Al_2O_3 nanofluid is higher as compared to 0.4 % weight fraction for a wide range of the reduced temperature parameter.
3. By using Triton X-100 as a surfactant the maximum enhanced efficiency of the collector is 15.63%.

Yousefi et al. (2012b) carried out an examination using the same experimental setup as in their previous work (Yousefi et al., 2012a), to study the effects of water–Multi wall carbon nanotubes (MWCNT)-H_2O nanofluid on the efficiency of the flat plate collector. The effect of using water as the working fluid, MWCNT nanofluid as the working fluid without surfactant and with surfactant on the efficiency of solar collector was investigated. Triton X-100 used as a surfactant. The authors examined the effect of two different weight fractions i.e.0.2% and 0.4% of the nanofluid with diameter of the particles taken in the range from 10 to 30 nm. The effect of mass flow rate also taken into account. The mass flow rates were taken as 1, 2, and 3 lit/sec. their results shows that:
1. The efficiency of the collector by using of MWCNT–H_2O nanofluid as a working fluid without surfactant is remarkably increased for 0.4 % weight fraction of nanofluid,
2. With 0.2 % weight fraction of MWCNT nanofluid with surfactant collector efficiency increases and without surfactant the efficiency decreases.
3. For small values of reduced temperature differences parameter, the efficiency of collector is increased by increasing the mass flow rate. Beyond these small values, the efficiency gets a reversed trend.

Yousefi et al. (2012c) carried out an experimental investigation to study the effect of pH variation of MWCNT–H_2O nanofluid on the efficiency of a flat-plate solar collector. The experimental work carried out by using weight fraction of 0.2 % with different pH values i.e.

3.5, 6.5, 9.5. Triton X-100 used as additive. The diameter of MWCNT taken as 10-30 nm. With mass flow rate of 0.0333 kg/s the efficiency of the flat-plate solar collector with MWCNT nanofluid as a working fluid at three pH values (3.5, 6.5, and 9.5.) was compared with water. It was observed that if the temperature differences higher than the mean temperature difference, the efficiency for pH = 3.5 is greater than that for pH = 9.5. On the other hand, if the temperature differences lower than the mean temperature difference, the efficiency of the flat-plate solar collector for pH = 9.5 is greater than that for pH = 3.5. It was also observed that, the absorbed energy parameter for pH=9.5 is higher than that of pH=3.5 and 6.5. Similarly, the removed energy parameter for pH=6.5 was higher than pH=9.5 and pH=3.5. Among these values pH values removed energy parameter of pH =3.5 was lower. From the experimental results it was concluded that, more differences between the pH of nanofluid and pH of isoelectric point leads to more improvement in the collector efficiency as the pH of the isoelectric point is 7.4 for MWCNT.

Saidur et al. (2012) carried out an experimental investigation to study the effect of using nanofluid as working fluid for direct solar collector. The objective of this study was:

(1) To investigate the appropriateness of nanofluid as a volumetric absorber.

(2) To discover the radioactive properties of the base fluid and the nanoparticle.

(3) To determine the effect of nanoparticle sizes and volume fractions for nanofluid as well as comparing its transmissivity of light.

The extinction coefficient of aluminum (Al) nanoparticle suspended in water as a base fluid was investigated and evaluated by changing nanoparticle size and volume fraction. It was seen that the nanoparticle size has negligible impact on the optical properties of nanofluid. On the other hand, the extinction coefficient of water based aluminium nanofluid is linearly proportional to volume fraction.

The authors observed that direct solar collector is expected to provide excellent optical properties and improved thermal transfer by utilizing nanofluids as a volumetric absorber. At shorter wavelength aluminum nanoparticle shows very strong extinction coefficient and peak at a wavelength of 0.3 μm. In spite of a lower extinction coefficient at longer wavelength, aluminium nanoparticle can be utilized to improve the light absorption ability of water at the visible and shorter wavelength region. It was observed that the improvement is promising within 1.0% volume fraction and is showing suitable enhancement to solar absorption, aluminium nanofluid is seems to be good solution for direct solar collector as a volumetric absorber.

Khullar et al. (2012a) studied the environmental impact of nanofluid based concentrating solar water heating system. This paper examines the potential of the nanofluid-based concentrating solar water heating system (NCSWHS) as a substitute to systems based on fossil fuels. Therefore, to save fossil fuels which are presently being widely used for water heating purposes the concept of NCSWHS and its potential was examined. It was found that the proposed water heating system has relatively better performance characteristics in comparison with the conventional flat plate collectors. The NCSWHS system also seems to be the best solution for fuel savings and it also promises the reduction of CO_2 emission so far as it substitutes for fossil fuel water heaters. It was seen that:-

1. The common water heating system of concentrating type would be more efficient and cost effective than flat plate collector.
2. The main advantage of NCSWHS is that it is being energy efficient.
3. Higher output temperatures can be attained by using NCSWHS hence it significantly reduces greenhouse gas emissions and save enormous amount of fossil fuels.

Khullar et al. (2012b) carried out theoretical investigations to study a nanofluid-based concentrating parabolic solar collector (NCPSC) and the results obtained were compared with the experimental results of conventional concentrating parabolic solar collectors operating under same conditions. Aluminium nanoparticle with 0.05 vol. % suspended in Therminol-VP-1 as the base fluid was used for the analysis. The results showed that the thermal efficiency of NCPSC compared to a conventional parabolic solar collector is about 5–10% higher under the similar weather conditions. The theoretical results indicated that the nanofluid-based concentrating parabolic solar collector has the potential to harness solar energy in a more efficient manner as compared to a conventional parabolic trough. It was observed that in order to get the desired output in terms of thermal efficiency and maximum outlet fluid temperatures, nanoparticle shape, size, and material need to be optimized and to transform this new concept of harvesting solar radiant energy into a commercial reality mathematical analysis needs to be validated with experimentation.

Chougule et al. (2012) carried out an experimental investigation to check the performance of nanofluid charged solar water heater using solar tracking system. In this investigation two identical flat plate collectors using heat pipes were fabricated. The nanoparticles used in the present study are CNT having diameter 10-12 nm and for the preparation of nanofluid the

concentration of nanoparticles taken as 0.15% by volume. Experimentations were carried in two steps i.e. by changing the collector's angle from Indian Standard i.e. normal angle 3l° to maximum performance angle of solar collector 50° with fixed position and other step is keeping the collectors on tracking mechanism. The effect of tilt angle, Solar Tracking System, & effect on average efficiency and on heat loss factor [T_m - T_a /I_t] was observed.

After the observation of CNTs nanofluid used as working fluid it was concluded that a very low quantity of nanoparticles results in a better performance and has remarkable potential as working fluid in high performance thermosyphon heat pipe collectors. It was also concluded that at 50° tilt angle working fluids gave better performance as compared to standard normal angle in both conditions (fixed and tracking) & average efficiencies are increased 12% and 11 % for water and nano working fluid at 31.50° tilt angle while 7% and 4% respectively at 50° tilt angle using tracking system, hence Solar tracking system adds an advantage to improve the efficiency in both water as well as nano working fluid solar heat pipe collector and also each of tilt angle for solar heat pipe collector.

De Risi et al. (2013) mathematically done the modelling and optimization of transparent parabolic trough collector based on gas-phase nanofluids as a working fluids. To directly absorb the solar energy a new concept of solar Transparent Parabolic trough Collector (TPTC) working with gas-based nanofluid as heat transfer fluid was suggested and examined. The model of the geometrical, thermal and fluid dynamic aspects of the TPTC was developed mathematically in order to attain global performance and to describe the main geometrical and operational parameters of the TPTC. In addition, to optimize the performance of the solar collector a genetic algorithm optimization was used.

Numerical results revealed that the gas-based nanofluids when combine with Transparent Parabolic trough Collector can be an effective substitute to conventional systems such as synthetic oils or molten salts. Simulation of the gas based nanofluids absorption showed that a complete absorption of the solar spectrum within the diameter of the receiver tube is attained by a correct mixture (0.25% CuO and 0.05% Ni). The results also indicated that the maximum TPTC solar to thermal efficiency is 62.5%.for a nanofluid outlet temperature of 650°C and a nanoparticles volume concentration of 0.3%.

Chaji et al. (2013) carried out an experimental investigation to check the Thermal Efficiency of Flat Plate Solar Collector (FPSC) using TiO_2/Water nanofluid. In this investigation to study the effects of different nanoparticle concentrations of TiO_2 in water as base fluid a small flat

plate solar collector (FPSC) was fabricated and tested, hence the effect of nanofluid on solar collector efficiency was evaluated for different mass flow rates (36, 72 and 108 lit/m^2.hr). Three levels of TiO_2 nano particles concentrations i.e. 0.1%, 0.2%, 0.3% (without using surfactants) were examined and the results were compared with those of water. It was concluded that the increase of mass flow rates of base fluid inside the solar collector enlarged the index of total collector efficiency area under the curves up to 15.7%. Also, adding the nano particles to water improved the index of collector efficiency -area under the curve - between 2.6 and 7% relative to base fluid at the same flow rate.

Tiwari et al. (2013) presents a comprehensive overview on thermal performance and environmental impact analysis of solar flat plate collector for water heating using Al_2O_3 water based nanofluid. The effect of utilizing the Al_2O_3 nanofluid as absorbing medium in a flat-plate solar collector was studied. The effect of mass flow rate and particle volume fraction on the efficiency of collector was also investigated. The mass flow rate taken as 30, 60, 90, and 120 in lit/hr and the volume concentration taken as 0.5, 1.0, 1.5, and 2.0 in percent were taken into account. It was concluded that using the 1.5% optimal particle volume fraction of Al_2O_3 nanofluid increase the thermal efficiency in comparison with water as working fluid by 31.64%.

Maddah et al. (2013) carried out an experimental investigation to study the effect of silver and aluminium oxide nanoparticles on thermo physical properties of nanofluids. Thermal conductivity, electrical conductivity, and viscosity are the thermo physical properties of nanofluids. For investigation the nominal diameters of Al_2O_3 and Ag nanoparticles taken as 40 and 20 nm. Nanofluids of various volume concentrations 0.25% to 5% taken into consideration at a temperature of 15°C. The nanofluid was prepared by dispersing aluminium oxide and silver nanoparticles in distilled water and then sonication process was done. It was concluded that

1. The viscosity and thermal conductivity of nanofluids increases as volume fraction of nanoparticles increases.
2. The electrical conductivity of nanofluids increases linearly with an increase in the volume fraction of the aluminium oxide and silver nanoparticles.

It was observed that higher the concentration of nanofluids, higher is the viscosity. On the other hand, electrical conductivity of aluminium oxide and silver nanofluid is significantly greater than that of the base fluid.

CHAPTER-3

GAP STUDY & OBJECTIVES

3.1 Gap Study

No doubt using nanofluids is relatively a new concept in the field of solar energy.Most of the work done by various researchers is on the non-concentrating type flat plate solar collectors in which nanofluid is used as a working fluid. Theoretical and experimental work were done by the various researchers on the flat plate type collectors. Papers also represent studies on direct solar collector, micro-scale direct absorption type collector.

If we talk about concentrating type collector only a limited literature is available. Limited information has been reported on the concentrating parabolic type collector as compare to the non-concentrating type flat plate collectors.

1. Khullar et al. (2010), carried out theoretical & numerical investigations regarding the application of nanofluids as the working fluid in concentrating parabolic solar collectors.
2. Taylor et al. (2011a), carried out theoretical & experimental investigations to compare a nanofluid based concentrating solar thermal system with a conventional system. Parabolic dish type concentrating collector was used to carry out Experimentations.
3. Khullar et al. (2012b), carried out theoretical investigations to study the nanofluid based concentrating type parabolic solar collector. No experimental work was done using nanofluids on the concentrating type parabolic solar collectors.
4. De Risi et al. (2013), carried out modelling and optimization of transparent parabolic trough collector based on gas-phase nanofluids. No experimentations were carried using gas-phase nanofluids on the concentrating type parabolic solar collectors

Therefore, it is clear that only few research papers deal with concentrating type collectors. Only theoretical and mathematical modelling was done on the concentrating parabolic type collector. A very limited experimental work has been reported on the parabolic type concentrating collector. The mathematical analysis is only related with theoretical work not with experimental work. Based on the above cited gap study it was decided to carry out the experimental work to study the performance of nanofluid based parabolic concentrating solar collector (NCPSC) using nanofluid as working fluid.

3.2 Study Objectives

The efficiency of solar collectors mainly depends on the thermophysical properties of fluid being used such as thermal conductivity, specific heat, viscosity and convective heat transfer coefficients which is used to absorb the heat. These thermal properties plays a significant role to absorb the energy which make the system more effective. By reviewing literature, it is found that the conventional fluids like water, ethylene glycol & oil have relatively low thermal conductivity and thus cannot reach high heat exchange rates in solar collector like devices and hence, can absorb heat up to a certain limits which leads to the lower efficiency of solar collectors. Whereas on the other hand, fluids with solid nanoparticles suspended called nanofluids developed recently are new class of fluids possesses very good thermal properties. So these nanofluids can be used to enhance the performance of solar collectors. The present thesis report lays a main emphasis on the performance evaluation of solar collectors by using nanofluid as a working fluid.

The main objectives of present experimental work are as follows:-

1. To investigate the variation of collector's efficiency by using water.
2. To investigate the variation of collector's efficiency by using Al_2O_3 water based nanofluid (sizes 20-30 nm).
3. To investigate the variation of collector's efficiency by using CuO water based nanofluid (sizes 20-30 nm).
4. To investigate the variation of collector's efficiency with varying volume fraction of nanoparticles.
5. To studied the temperature variation.
6. To investigate the efficiency of a collector with different mass flow rates of nanofluid and water.
7. To compare the performance of a solar collector in terms of efficiencies for nanofluid and water.

CHAPTER-4

EXPERIMENTAL SETUP & METHODOLOGY

In this chapter the following topics are covered:-

1. Experimental Setup
2. Preparation of Nanofluids
3. Characterization of Nanofluids
4. Sonication of Nanoparticles

4.1 Experimental setup

The experimental setup for testing the performance of collector consists of the parabolic shaped collector, parabolic reflector, receiver tube, glass cover tube, 10 litre Storage tank, supporting structure, tracking mechanism, piping system and ball valve as a throttling valve. The storage tank is fixed below the receiver's pipe level to allow the heating fluid to flow in a forced manner with pumping system. The storage tank is filled with water/nanofluid and flow takes place in a closed system. Storage tank is also known as heat transfer fluid tank. The test is repeated with three different water/nanofluid mass flow rates. The water/nanofluid inlet and outlet of the receiver tube, and the solar radiation intensity is measured in every 30 minutes (10:00 AM - 3:00 PM) during the experiment. The test was carried outdoor in the month of May and June 2014.

4.1.1 System operation

The parabolic trough collector is manually tracked on each day with the help of mechanism consisting of clutch wire and bicycle hub before the reading starts so that the solar radiations coming from the sun fall perpendicular to the plane of aperture area. When the solar radiations fall on the aperture area of the parabolic trough collector, these radiations are concentrated on the receiver tube. This causes the heat transfer from the surface of the receiver tube to the water/nanofluid flowing inside the receiver tube and fluid gets heated up.

The complete set-up of parabolic trough solar collector (PTSC) is shown in the figure 4.1. The specifications of Parabolic Trough solar Collector (PTSC) are given in Table 4.1.

Figure 4.1: Parabolic Trough Solar Collector (PTSC) set-up

Table 4.1: Specifications of Parabolic Trough solar Collector (PTSC)

Sr. No.	**Parameters**	**value**
1.	Length of collector, L	1.20 m
2.	Width of collector, W	0.91 m
3.	Thickness of the end plate	0.002 m
4.	Aperture area, $A_{aper.}$	1.0188 m^2
5.	Rim angle	90 °
6.	Receiver tube inside diameter, (D_i)	0.027 m
7.	Receiver tube outside diameter, (D_o)	0.028 m
8.	Glass cover tube inside diameter, (D_{ci})	0.064 m
9.	Glass cover tube outside diameter, (D_{co})	0.066 m
10.	Concentration ratio, C_r	9.66
11.	Focal distance	0.30 m
12.	Mass flow rate, $\dot{m}$	20 ,40 & 60 l.hr
13.	Storage tank capacity	10 ltr.
14.	Tank material	Plastic container

Contd…

15.	Tank insulation material	Glass wool
16.	Insulation of the pipes	SUPERLON
17.	Submersible pump	18 W with maximum height of 5ft
18.	Tracking mechanism	Manual

4.1.2 Components of Parabolic trough solar collector (PTC)

The main components of parabolic trough collector are:-

1. Reflector: The main function of parabolic reflector it to reflect and concentrates all the radiations coming from the sun on the receiver tube which is at the focal point of the parabola. Figure 4.2 shows the reflection of solar radiations to receiver tube via reflector.

Figure 4.2: Reflection of solar radiations to Receiver tube via Reflector

A Stainless steel sheet having dimensions (1.20 m × 0.91 m) is used to form the parabolic shape. The stainless steel sheet is used to provide the mechanical strength to the parabolic trough. Parabolic shaped mirrors are used as reflectors with a reflectivity of 96%. Mirrors stripes are pasted on the parabolic sheet with 26 in number having dimensions (5mm × 3ft) with the help of fevitite and double tape. The reflector made up of mirror stripes pasted on a stainless sheet is shown in the figure 4.3.

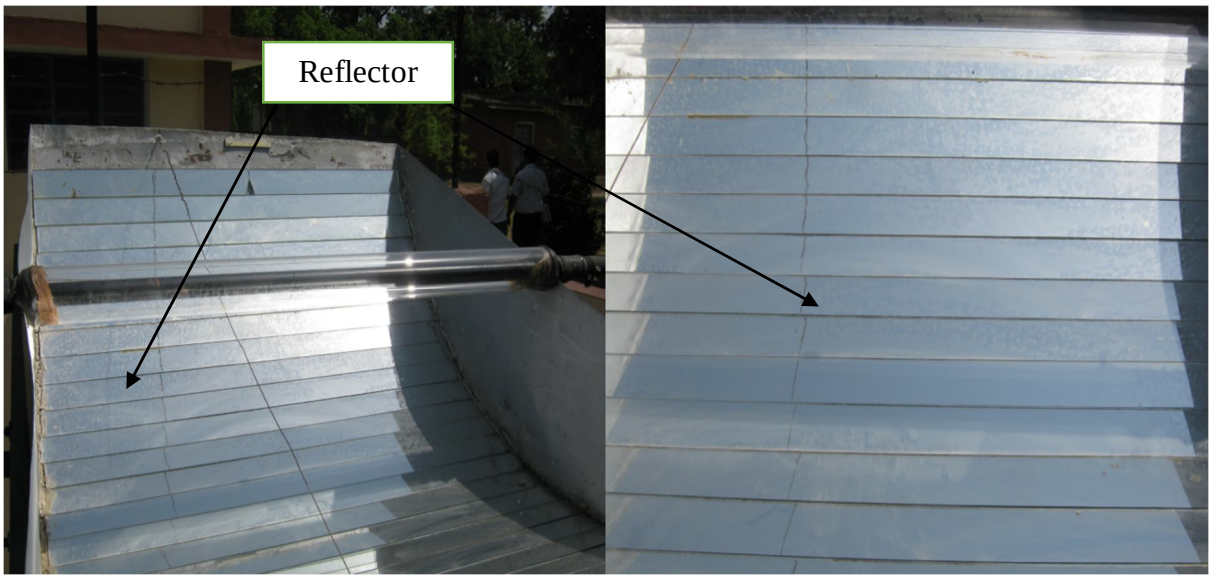

Figure 4.3: Reflector made up of mirror stripes

2. Receiver Tube: Receiver tube is one of the vital part of the parabolic trough collector. The receiver tube is composed an outer glass cover tube, a vacuum type enclosure or annular space & an inner black painted tube made of copper material. Copper tube (receiver) covered with glass cover tube is shown in the figure 4.4.

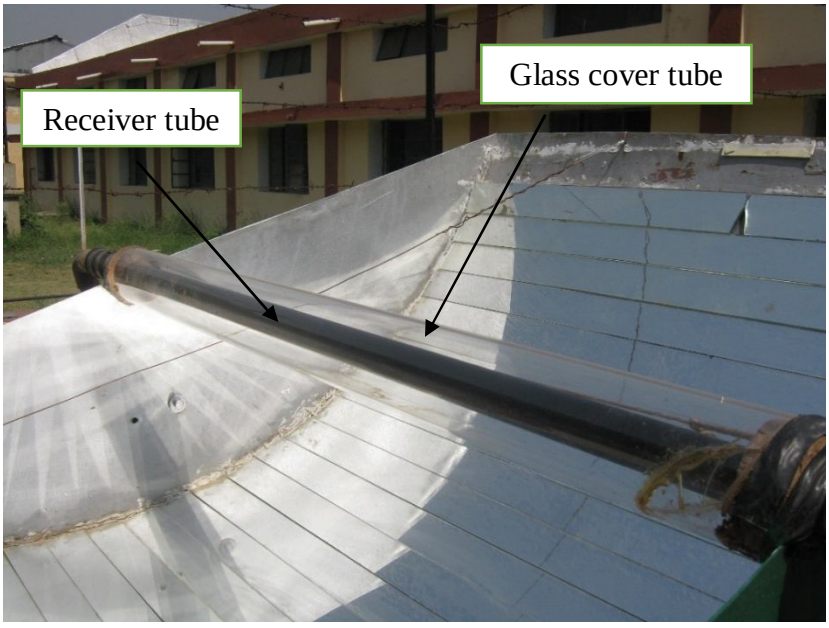

Figure 4.4: Receiver tube & Glass cover tube

In receiver tube the flowing heat transfer fluid (HTF) such as water or nanofluid gains heat from the solar radiation coming from the reflector part. A black painted copper tube which has higher thermal conductivity is used as a receiver tube and is covered by a glass cover tube. The main objective of providing glass cover tube is to reduce the conductive, convective, and radiative losses from the copper tube. A receiver tube has 4ft length with inside and outside

diameter of 27 mm & 28 mm. glass cover tube has 3ft length with inside and outside diameter of 64 mm & 66 mm.

3. Support Structure: The support structure for the parabolic solar collector is made of cast iron**.** The selection of cast iron material for the support structure is because of its greater rigidity, hardness and more flexibility. The support structure made up of cast iron is green painted shown in the figure 4.5. The robust design of support structure has an ability to withstand all type of loads like wind loads, stress loads etc. Its robust design could not affect the parabolic shape of the collector & also helps to minimize the alignment errors up to some extent.

Figure 4.5: Support structure

4. Tracking Mechanism: Mainly two types of tracking systems are used namely, manual tracking system and automatic tracking system. In this experiment manual tracking is used because it is inexpensive as compared to automatic tracking as, automatic tracking requires a motor and a gear mechanism. The angle is measured with the help of the magnetic base instrument provided with a needle. In this experiment manual tracking system is consists of a clutch wire and a bicycle hub shown in the figure 4.6.

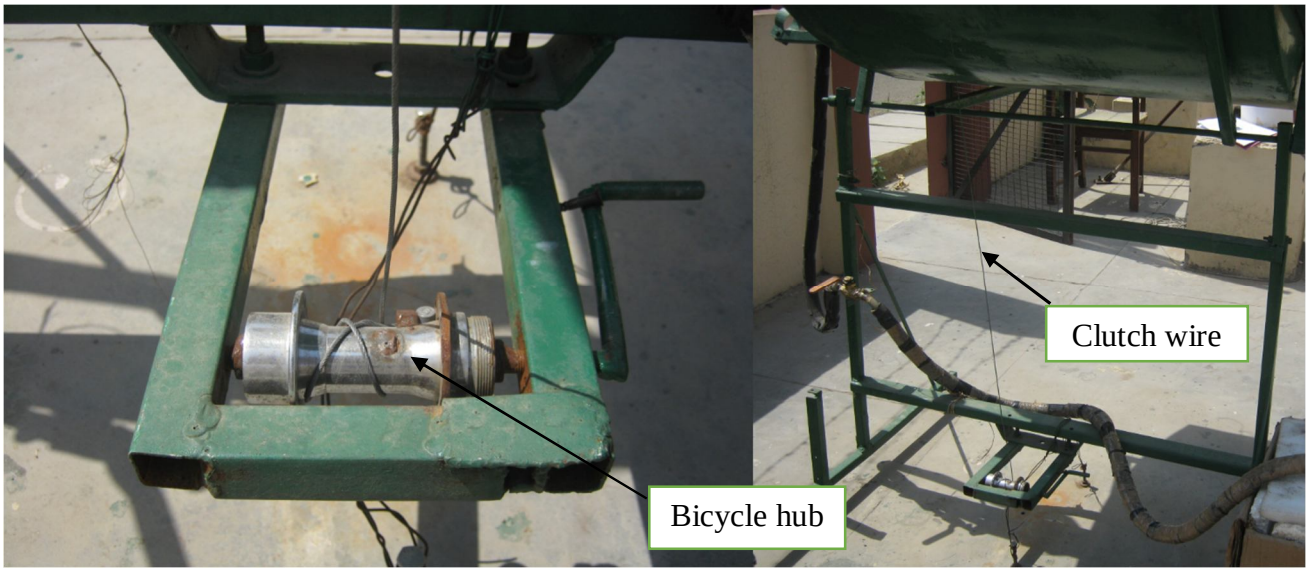

Figure 4.6: Manual tracking mechanism

The bicycle hub is inserted in the welded cast iron structure provided with a handle. The shape of the cast iron structure is like a rectangle and then clutch wire is fitted into the hub provided with a welded nut. In manual tracking system the parabolic trough is oriented in an north to south direction, because the sun travels from north to south direction. Manual tracking is done in such a way that the solar radiations fall perpendicular to the plane of aperture area so that these radiations are concentrated on the receiver tube.

5. Storage tank: A storage tank is a type of container made up of a plastic container having 10 litres capacity filled with water or nanofluid used as a working fluid. The water/nanofluid is circulated from the container with the help of a small pump of power 18 W to the inlet of the receiver tube. Water/nanofluid after gaining heat from the receiver tube is dropped in the same container and is re-circulated again with the help of a pump. The inlet and outlet of the receiver tube is from the storage tank. The Berger plastic bucket used a container in the storage tank is insulated with glass wool and then supported by a packaging thermo Cole sheet. Figure 4.7 shows the picture of storage tank used in the experiment.

Figure 4.7: Storage tank

6. Insulation: The entire piping system is insulated with SUPERLON insulation. The main objective of using insulation is to minimize all the heat losses during the transportation of water/nanofluid as a working fluid from inlet to the outlet in the receiver tube via storage tank. Glass wool is used as an insulation for the storage tank. It also reduces heat losses from the storage tank. These both insulations are easily available from the market in the Air Conditioners and Refrigerators spare parts shop. The insulation on the pipe and on the Storage tank is shown in figure 4.8.

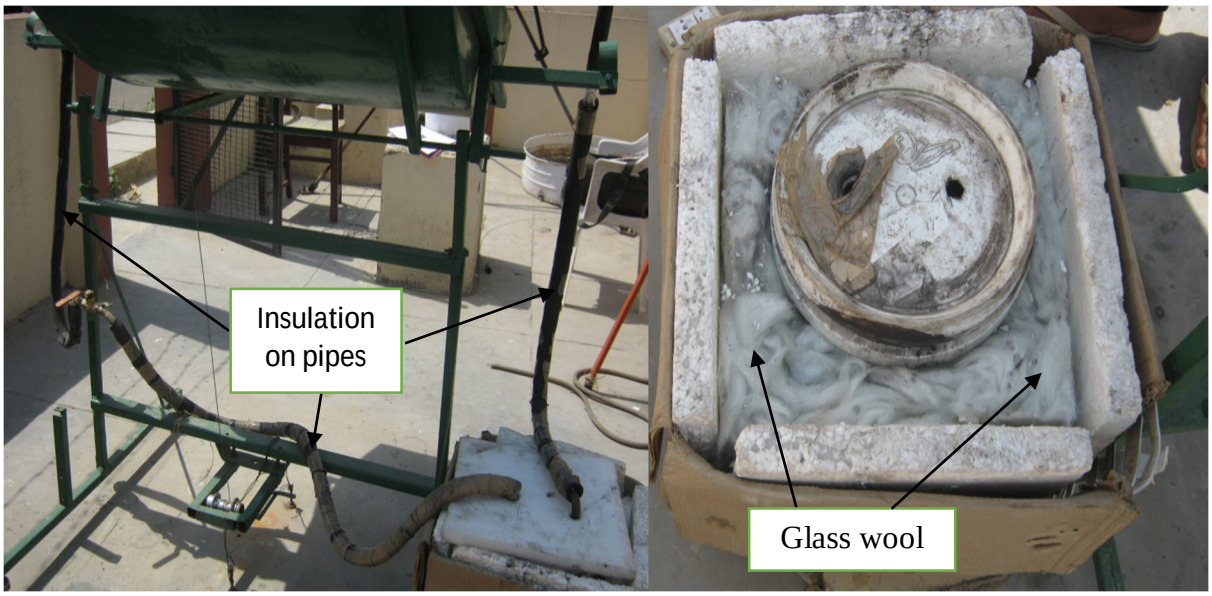

Figure 4.8: Insulation on the pipe and on the Storage tank

7. Control valve: Control valves are used to control conditions such as flow rate, liquid level by fully or partially opening or closing. In this experiment it is used to control the mass flow

rate of water & nanofluid. The mass flow rate taken as 20, 40, 60 lit/hr, the control valve is also known as throttling valve. The control valve is shown in the figure 4.9.

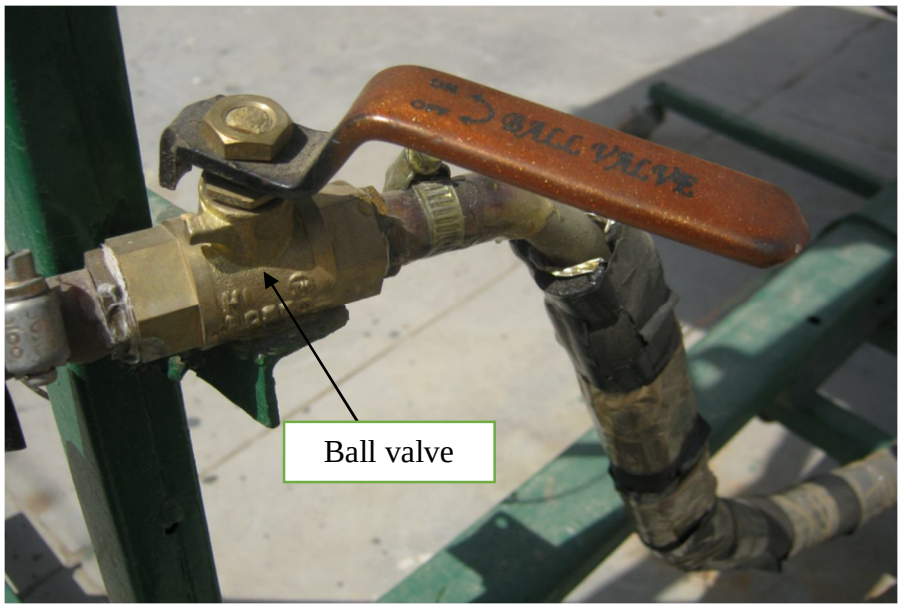

Figure 4.9: Control valve

8. Pump: Pump is used to circulate water or nanofluid from the storage tank to the inlet of the receiver tube at some appreciable height. In this experiment submersible pump is used with a maximum height of 5 ft., 1100 l/hr output and 18 W power. The pump used to carry out this experiment shown in the figure 4.10.

Figure 4.10: Pump

4.2 Preparation of Nanofluids

In order to carry out experimental studies with nanofluids, their preparation is the first main step. During preparation of nanofluids certain requirements are essential such as stability, negligible agglomeration of particles, no chemical alteration of nanofluid, etc. Nanofluids are prepared by dispersing nano sized solid particles like alumina (Al_2O_3), silicon oxide (SiO_2), copper oxide (CuO) into base liquids such as water, ethylene glycol therminol-VP-1 etc. There are mainly two techniques used to produce nanofluids: the single-step and the two-step method.

a) **Two-step method:** In this technique, first the nanoparticles are obtained by different methods and then are dispersed in an appropriate base fluid like water, ethylene glycol, therminol-VP 1 (Sridhara & Narayan Satapathy, 2011). In other words, the two step technique uses physical or chemical processes to produce nanoparticle and proceeds to disperse them into a base fluid. Widely two step method is used for the preparation of nanofluids.

b) **One-step method:** In single step method the nanoparticles are dispersed directly into a base fluid. This method suits best for metallic nanofluids like copper, aluminium.
In this technique the processes such as drying, storage, transportation, and dispersion of nanoparticles are avoided, so that the agglomeration of nanoparticles is minimized to some extent and the stability of fluids is increased (Yu et al. 2012).

4.3 Characterization of Nanofluids

Characterization of nanoparticles is essential for well understanding of nanoparticles synthesis and their applications. Commonly used techniques for the characterization of nanoparticles are X-ray Diffraction (XRD), Transmission Electron Microscopy (TEM), and Scanning Electron Microscopy (SEM). The present work is more related with the application of nanofluid so XRD is done for the confirmation of nanoparticles.

- **XRD:** X-ray Diffraction (XRD) is a fast diagnostic method utilized for the phase identification of a crystal-like material. It is a rapid technique works on the principle of X-rays i.e. when X-rays are focused on the sample of Nano powder, the electrons present in the material scatter the X-rays. This forms a pattern of maxima and minima which can be used to recognise the material of the structure being investigated. This technique uses the Bragg's Law. Bragg's Law gives the condition for two X-rays to be in phase with each other. In the present work XRD patterns range lies between 0 degrees to 110 degrees. The XRD image of alumina (Al_2O_3) sample (purchased) is shown in

the figure 4.11 (a) & the XRD image of alumina (Al_2O_3) sample (tested) is shown in the figure 4.11 (b).

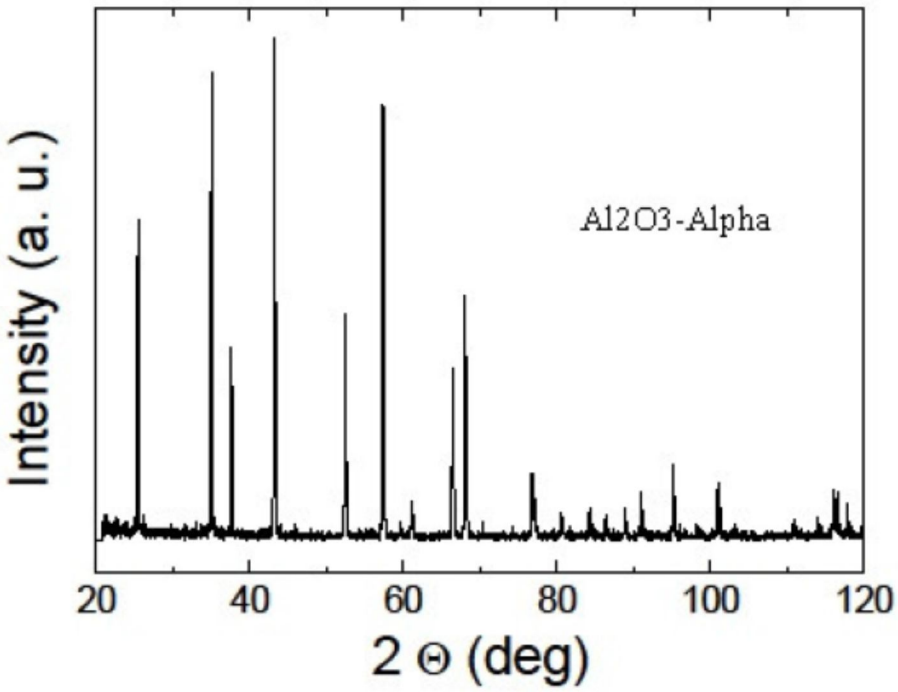

Figure 4.11 (a): XRD image of Alumina (Al_2O_3) sample (purchased)

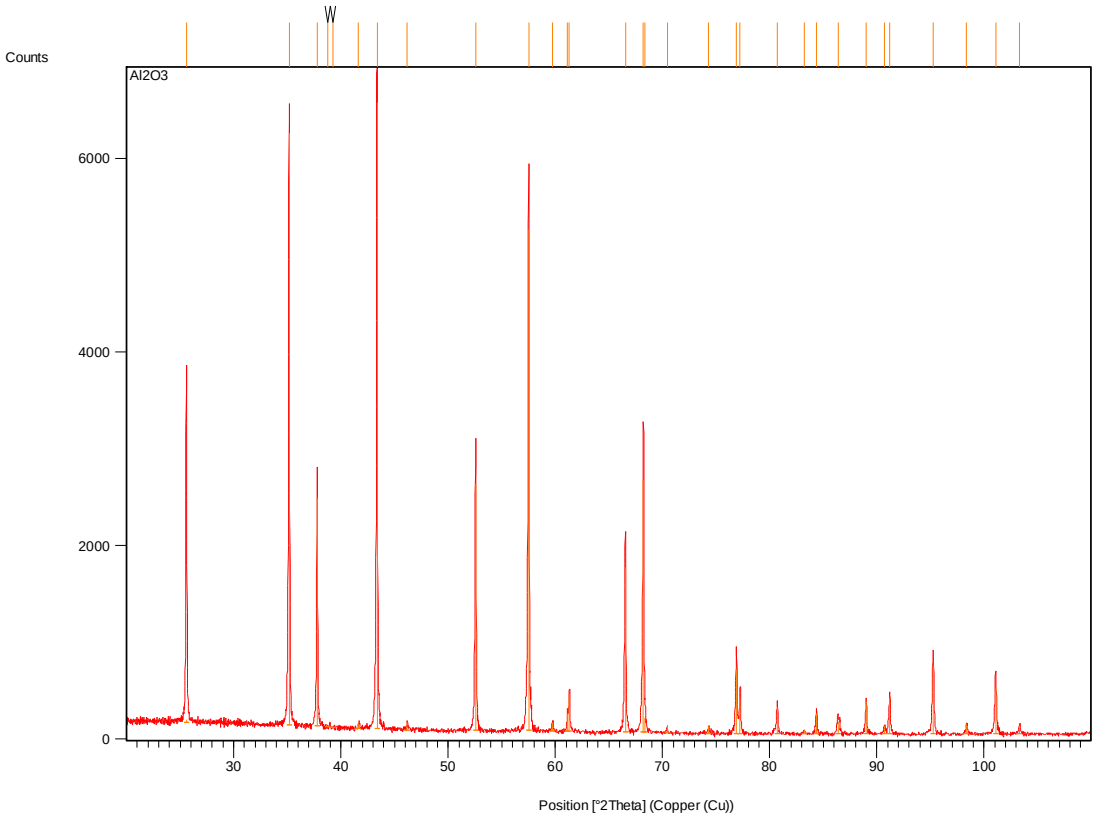

Figure 4.11 (b): XRD image of alumina (Al_2O_3) sample (tested)

The XRD image of copper oxide (CuO) sample (purchased) is shown in the figure 4.12 (a) & the XRD image of copper oxide (CuO) sample (tested) is shown in the figure 4.12 (b).

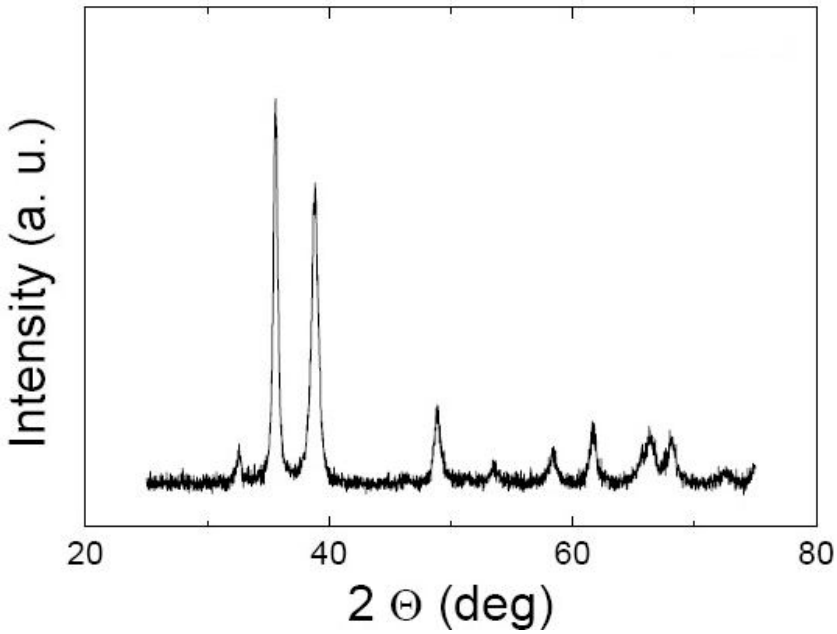

Figure 4.12 (a): XRD image of Copper oxide (CuO) sample (purchased)

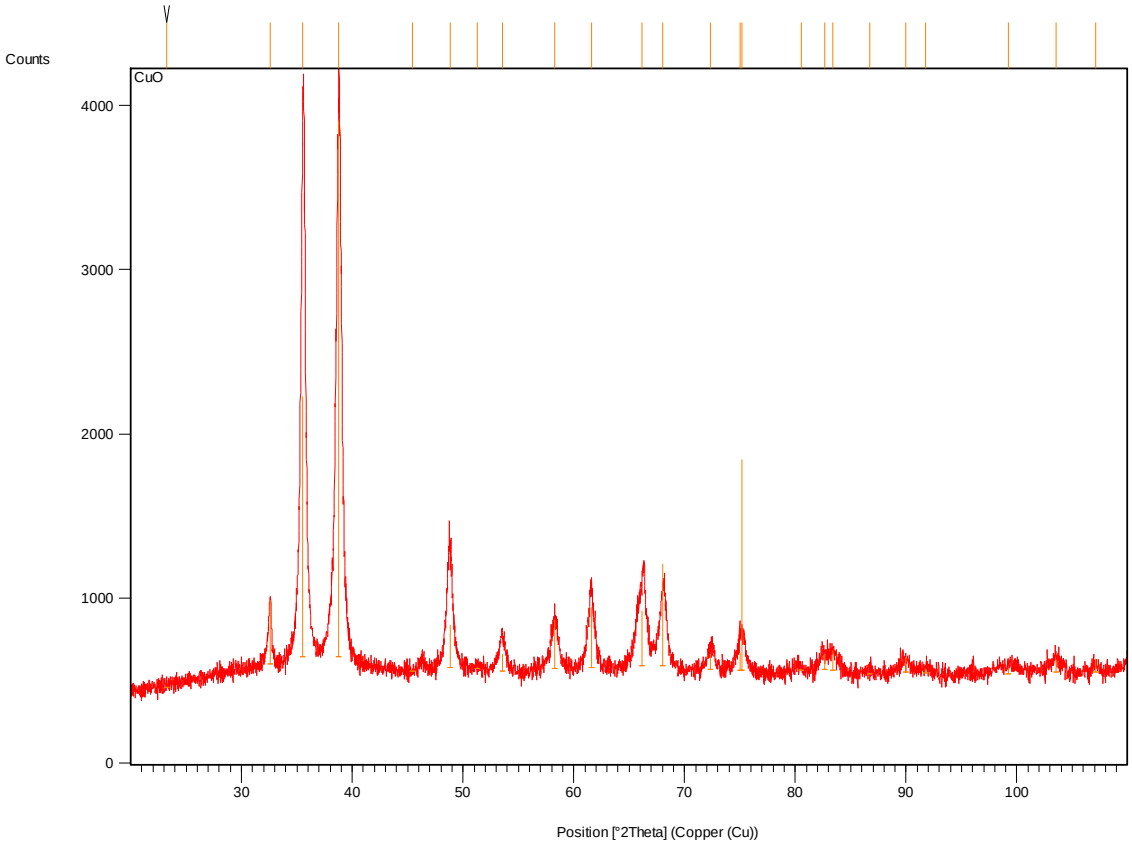

Figure 4.12 (b): XRD image of Copper oxide (CuO) sample (tested)

4.3.1 Properties of nanomaterials (purchased)

- Sample of alumina (Al_2O_3) nanoparticle was purchased from NANOSHEL Intelligent Materials Pvt. Ltd. Panchkula (Pb.).

Table 4.2: Properties of alumina (Al_2O_3) powder

Chemical name: Alumina Nanopowder
Particle Size: 20-30nm
Particle shape: Spherical
Appearance: White
pH Value: 6.6
True density: 3.97 g/cm^3
Specific Surface Area (SSA): 15-20 m^2/g
Crystal Form: Alpha
High purity: 99%
Thermal conductivity of particle: 36 W/m-K
Specific heat of particle: 765 J/kg K

- Sample of copper oxide (CuO) nanoparticle was purchased from NANOSHEL Intelligent Materials Pvt. Ltd. Panchkula (Pb.).

Table 4.3: Properties of copper oxide (CuO) nanopowder

Chemical name: CuO Nanopowder
Particle Size: 30-40 nm
Particle shape: Spherical
True density: 6.4 g/cm^3
Appearance: Black Powder
Specific Surface Area (SSA): >13m^2/g
Purity: >99%
Specific heat of particle: 531.8 J/kg K

4.4 Sonication of Nanoparticles

4.4.1 Sonication of alumina (Al_2O_3) nanoparticles

Sonication is a technique for dispersing the aggregated nanoparticle. The alumina (Al_2O_3) nanofluid is prepared by using two step method. Al_2O_3 nanoparticle is mixed with double distilled water. But in order to prepare a nanofluid it is essential to determine the weight of Al_2O_3 for different concentrations. The weight of Al_2O_3 can be calculated by using the standard expression as follows:-

$$f_v = V_{np} / V_{nf}$$

Where, $V_{np} = W_{np} / \rho_{np}$

$V_{nf} = V_{np} + V_{bf}$ and

$V_{bf} = W_{bf} / \rho_{bf}$

Expression in modified form:

$$f_v = \frac{V_{np}}{V_{np} + V_{bf}} = \frac{W_{np} / \rho_{np}}{W_{np} / \rho_{np} + V_{nf}}$$

where, V_{np} is the quantity of nanoparticle, V_{bf} is the quantity of base fluid, V_{nf} is the quantity of nanofluid, W_{np} is the weight of nanoparticle, W_{bf} is the weight of nanofluid.

Quantity of base fluid (Water), $V_{bf} = 10$ litres

Density of Al_2O_3 particles, $\rho_{np} = 3.97$ gm/cm^3

Density of water, $\rho_{bf} = 1000$ kg/m^3

Table 4.4: Weight of Al_2O_3 particles to prepare the nanofluid of different concentrations

f_v (%)	W_{np} (gms)	W_{np} (gms)
0.01	0.397 (1 ltr.)	3.97 (10 ltr.)
0.05	1.985 (1 ltr.)	19.85 (10 ltr.)

Firstly weight of nanoparticle in grams by using weighing machine is determined shown in the figure 4.13.

Figure 4.13: Weighing machine

Then make the volume concentrations of 0.01% & 0.05% by stirring 0.397 gm, 1.985 gm of nanoparticles for 30 - 35 minutes in 1000 ml of double distilled water are prepared using a device called magnetic stirrer hot plate. Figure 4.14 shows the picture of magnetic stirrer hot plate & figure 4.15 shows the stirring process of alumina (Al_2O_3) nanofluid carry out on the magnetic stirrer hot plate.

Figure 4.14: Magnetic stirrer hot plate

Figure 4.15: Stirring process of alumina (Al_2O_3) nanofluid on Magnetic stirrer hot plate

This test is repeated 10 times in order to prepare 10 litres of aluminium oxide nanofluid for both concentrations. To make the nanoparticles more stable and remain more dispersed in water, ultra bath sonicator is used.

Sonication of aluminium oxide nanoparticles is necessary before testing any thermo physical property of the nanofluids like viscosity, thermal conductivity, and electrical conductivity. In this experiment sonication is done for 2 hours in an ultra-bath sonicator. By this aluminium oxide nanoparticles become more evenly dispersed in distilled water. After sonication the obtained nanofluid solution is ready for the application. Figure 4.16(a) & (b) shows the aluminium oxide water based (Al_2O_3) nanofluid with 0.01% & 0.05% volume concentration.

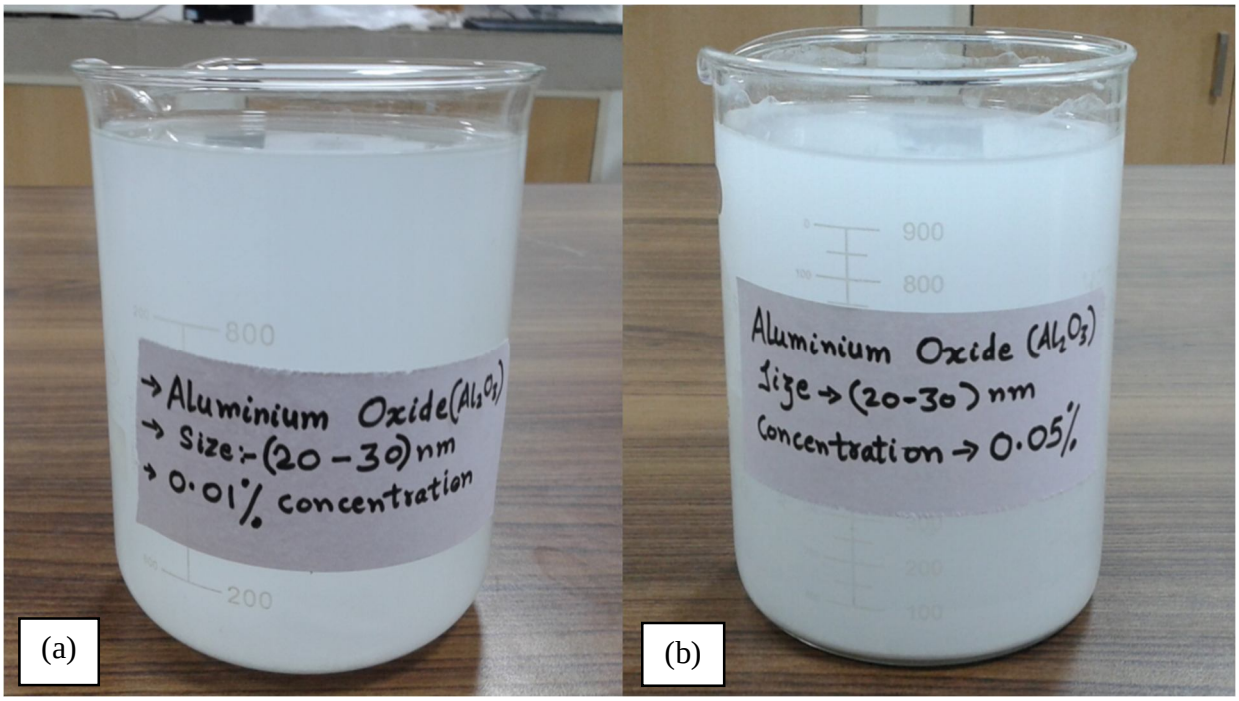

Figure 4.16 (a) & (b): Aluminium oxide water based (Al_2O_3) nanofluid with 0.01% & 0.05% volume concentration

4.4.2 Sonication of copper oxide (CuO) nanoparticles

The copper oxide (CuO) nanofluid is prepared by using two step method. Copper oxide nanoparticle is mixed with double distilled water. But in order to prepare a nanofluid it is essential to determine the weight of Copper oxide for different concentrations. The weight of Copper oxide can be calculated by using same standard expression as discussed for aluminium oxide in the section 4.4.1.

Quantity of Base fluid (Water), V_{bf} = 10 litres

Density of CuO particles, ρ_{np} = 6.40 gm/cm^3

Density of water, ρ_{bf} = 1000 kg/m^3

Table 4.5: Weight of CuO particles to prepare the nanofluid of different concentrations

f_v (%)	W_{np} (gms)	W_{np} (gms)
0.01	0.64 (1 ltr.)	6.40 (10 ltr.)
0.05	3.20 (1 ltr.)	32.0 (10 ltr.)

Firstly weight of nanaoparticle in grams by using weighing machine is determined as shown in the figure 4.13. Then make the volume concentration of 0.01% & 0.05% by stirring 0.64 gm, 3.20 gm of nanoparticles for 30 - 35 minutes in 1000 ml of double distilled water using a device called magnetic stirrer hot plate as shown in the figure 4.14. Figure 4.17 shows the stirring process of copper oxide (CuO) carry out on the magnetic stirrer hot plate.

Figure 4.17: Stirring process of copper oxide (CuO) on the magnetic stirrer hot plate

This test is repeated 10 times in order to prepare 10 litres of copper oxide nanofluid for both concentrations. Figure 4.18 (a) & (b) shows the copper oxide water based (CuO) nanofluid

with 0.01% & 0.05% volume concentration. To make the nanoparticles more stable and remain more dispersed in water, ultra bath sonicator is used.

Figure 4.18 (a) & (b): Copper oxide water based (CuO) nanofluid with 0.01% & 0.05% volume concentration

Sonication of copper oxide nanoparticles is necessary before testing any thermo physical property of the nanofluids like viscosity, thermal conductivity, and electrical conductivity. In this experiment sonication is done for 2 hours in an ultra-bath sonicator. By this copper oxide nanoparticles become more evenly dispersed in distilled water. After sonication the prepared nanofluid solution is ready for the application. Figure 4.19 shows the Bransonic ultra-bath sonicator (CPXH series).

Figure 4.19: Bransonic ultra-bath sonicator (CPXH series)

4.5 Measuring Instruments

4.5.1 Solar power meter

Solar Power meter is an instrument used for the measurement of the solar radiation that is emitted by the sun. The spectrum of solar radiation is close to that of a black body with a temperature of about 5800 K. About half of the radiation is in the visible short-wave part of the electromagnetic spectrum. The other half is mostly in the near-infrared part, with some in the ultraviolet part of the spectrum. The Solar power meter device is shown on figure 4.20.

Figure 4.20: Solar power meter

Table 4.6: specifications of solar power meter

Display: 3½ digits, 2000 readings	**Range:** 2000 W/m^2, 634 BTU / (ft2xh)
Resolution: 0.1 W/m^2, 0.1 BTU/ (ft2xh)	**Angular accuracy:** Cosine corrected
Over-input: Display "OL"	**Drift:** < +/- 2% per year
Accuracy: Typically within +/- 10 W/m^2 or +/- 5% whichever is greater in sunlight, Temperature included error +/- 0.38 W/m^2 / ºC deviation from 25 ºC	
Operating Temp. and Humidity: 0C ~ 50ºC below 80% RH	
Power supply: 9V battery x1	**Sampling time:** 0.25 second

4.5.2 Angular magnetic base instrument

The magnetic base angular measuring instrument is used to vary the angle of parabolic collector in accordance with sun's direction. Figure 4.21 shows the magnetic base angular measuring instrument.

Figure 4.21: Angular magnetic base instrument

Features of Angular Magnetic Base Instrument are:-

- Accurate measuring angle range**:** 0-90 degrees in any quadrant.
- Accurate to 0.5.
- Provided with Magnetic base for mounting on steel framing or pipes.
- Simply place angle finder vertically on any surface for instant accurate reading.
- User conversion chart on the back to determine pitch per inch and pitch per foot.
- Magnetically attaches to metal squares for easier reading.
- Provided with permanent high duty ceramic magnet.
- Can be mounted on non-metallic squares with self-threading screws (not included).
- Includes conversion chart for determining pitch per inch and foot.

4.5.3 Digital anemometer AM-4201

The digital anemometer model no. AM-4201 is used in the present experiment to check the air flow velocity in m/sec or in km/hr. The digital anemometer AM-4201 is shown in the figure 4.22.

Figure 4.22: Digital anemometer AM-4201

Table 4.7: specifications of Digital anemometer AM-4201

Display: 18mm (0.7") LCD (Liquid Crystal Display), 3 1/2 digits.	
Resolution: 0.1 m/s, 0.1 km/h, 10 ft/min., 0.1 knots	
Operating temperature: 0℃ to 50℃	**Operating humidity:** Less than 80 % RH.
Air velocity measurement range: 0.4-30.0 m/s, 1.4-108.0 km/hr, 80-5910 ft/min., 0.8-58.3 knots	
Applications: To check air conditioning & heating systems, measure air velocities, wind speeds, temperature.	
Power supply: DC 9V 006P, MN1604 (PP3) km/hr, battery (Heavy Duty Type) or equivalent.	

4.5.4 Thermometer

Figure 4.23: Thermometer

Figure 4.23 shows the mercury-in glass thermometer used in the experiment. The inlet & outlet temperature of the working fluid i.e. water, water based alumina (Al_2O_3) & water-based copper oxide (CuO) nanofluid is measured with the help of a mercury-in glass thermometer. The temperature range of this thermometer is from 0°C to 110°C.

CHAPTER-5

RESULTS AND DISCUSSIONS

This chapter mainly deals with the results in form of plots/graphs which are obtained by the experimental work on nanofluid based concentrating parabolic solar collector (NCPSC) by using water based alumina (Al_2O_3) & copper oxide (CuO) nanofluids as working fluid.

5.1 Efficiency Calculations for Parabolic Solar Collector

These all calculations are determined for water, water based alumina (Al_2O_3) & copper oxide (CuO) nanofluid for 20, 40 & 60 l/hr given in the appendix in tabular form.

1) Absorbed Flux

$$S = G_T R_b (\alpha\tau) \beta\Upsilon$$

where

G_T is solar intensity in W/m^2, R_b is bond resistance, α is absorptivity of the receiver tube, τ is glass cover transmissivity for solar radiation, β is specular reflectivity & Υ is intercept factor.

2) Convective Heat Transfer Coefficient

Average velocity, V

$$V = \frac{4\,\dot{m}}{\pi D_i^{\,2} \rho}$$

where $\dot{m}$ is mass flow rate in kg/sec, D_i is the inner diameter of receiver tube, ρ is the density of water or nanofluid in kg/m^3, respectively.

Reynolds number, R_e

$$R_e = \frac{V D_i}{\nu}$$

where

V is the average velocity & ν is the viscosity of water or nanofluid in m^2/s, D_i is the inner diameter of receiver tube respectively.

Prandtl number, P_r

$$P_r = \frac{c_p \nu \rho}{k}$$

where c_p is the specific heat in J/kg K, v is viscosity in m^2/s, ρ is density in kg/m^3, k is the thermal conductivity in W/m-K of water or nanofluid respectively.

Nusselt number, N_u

$$N_u = 0.023 \times R_e^{0.8} \times P_r^{0.4}$$

where N_u, R_e, & P_r are the nusselt number, reynolds number & prandtl number of water or nanofluids respectively.

- **Convective heat transfer coefficient**, h_f

$$h_f = N_u \times \frac{k}{D_i}$$

where N_u, k are the nusselt number and thermal conductivity of water or nanofluid & D_i is the inner diameter of receiver tube respectively.

3) Collector Heat Removal Factor

Assume $U_l = 13.28\ W/m^2K$

- **Collector efficiency factor,** F'

$$F' = \frac{D_i h_f}{D_i h_f + D_0 U_l}$$

where D_0 & D_i is the outer and inner diameter of receiver tube, h_f is the convective heat transfer coefficient, U_l is the overall loss coefficient.

- **Value of x**

$$x = \frac{\dot{m} c_p}{\pi L D_0 U_l}$$

- **Heat removal factor,** F_R

$$F_R = \frac{\dot{m} c_p}{\pi L D_0 U_l}\left[1 - \exp\left(\frac{-\pi D_0 U_l L F'}{\dot{m} c_p}\right)\right]$$

where F_R is the heat removal factor, $F'$is the collector efficiency factor, L is the length of collector, ṁ is the mass flow rate, U_l is the overall loss coefficient. D_0 is the outer diameter of receiver tube , c_p is the specific heat in J/kg K of water or nanofluid respectively.

4) Concentration Ratio C_r

$$C_r = \frac{\text{Aperture area}}{\text{Absorber area}}$$

$$C_r = \frac{(W - D_{co})}{\pi D_0}$$

where W is the width of collector & D_{co} is the outer diameter of glass cover tube respectively. The value of concentration ratio is same.

5) Optical Efficiency , η_{opt} = 70.6% (Sukhatme, 1984)

$$\beta \Upsilon (\tau\alpha) \frac{(W - D_{co})}{W} + (\tau\alpha) \times \frac{D_{co}}{W}$$

where α is absorptivity of the receiver tube, τ is glass cover transmissivity for solar radiation, β is specular reflectivity & Υ is intercept factor, D_{co} is the outer diameter of glass cover tube, W is the width of collector. The value of optical efficiency remains constant for all calculations.

6) Useful Heat Gain

$$q_u = \dot{m}\, c_p\, (T_{out} - T_{in})$$

where $\dot{m}$ is the mass flow rate in kg/sec, c_p is the specific heat in J/kg K of water or nanofluid respectively, T_{out} & T_{in} are the outlet & inlet temperatures.

7) Instantaneous Efficiency, η_i

$$\frac{\dot{m}\, c_p\, (T_{out} - T_{in})}{G_T R_b\, W\, L}$$

where $\dot{m}$ is the mass flow rate in kg/sec , c_p is the specific heat in J/kg K of water or nanofluid respectively, T_{out} & T_{in} are the outlet & inlet temperatures, G_T is solar intensity in W/m^2, R_b is bond resistance, W is the width of collector, L is the length of collector respectively.

8) Thermal Efficiency η_{th} (per half an hour)

$$\frac{m\, c_p\, (T_{out} - T_{in})}{A_{aper.}\, G_T\, t}$$

where m is the mass of water or nanofluid in kg taken as 10 kg , c_p is the specific heat in J/kg K of water or nanofluid, T_{out} & T_{in} are the outlet & inlet temperatures, G_T is solar intensity in W/m^2, $A_{aper.}$ is the aperture area taken as 1.0188 m^2 respectively.

9) Overall Thermal Efficiency (average) η_{ov}

$$\frac{m\, c_p\, (T_{max} - T_{min})}{A_{aper.}\, G_{avg.}}$$

where m is the mass of water or nanofluid in kg taken as 10 kg , c_p is the specific heat in J/kg K of water or nanofluid, T_{max} & T_{min} are the maximum and minimum temperatures, $A_{aper.}$ is the aperture area taken as 1.0188 m^2 & $G_{avg.}$ is the average solar intensity in W/m^2 respectively.

Note:

- The calculated values of parameters such as absorbed heat flux in W/m^2, useful heat gain in W, instantaneous efficiency, thermal efficiency, overall efficiency for water given in appendix A, for alumina water-based nanofluid (Al_2O_3) given in appendix B (0.01% concentration) & appendix C (0.05% concentration), for copper oxide (CuO) water-based nanofluid given in appendix D (0.01% concentration) & appendix E (0.05% concentration).
- The calculated values of reynolds number R_e, prandtl number P_r, nusselt number N_u, convective heat transfer coefficient h_f , collector efficiency factor F', heat removal factor F_R for water ,for alumina water-based nanofluid (Al_2O_3) & copper oxide (CuO) water-based nanofluid with 0.01% concentration & 0.05% concentration given in appendix F.

5.2 Calculations for Nanofluids

1. Density of nanofluids (Khullar et al., (2012b))

$$\rho_{nf} = f_v\, \rho_{np} + (1 - f_v)\, \rho_{bf}$$

where f_v is the volume fraction of the nanoparticles, ρ_{nf} , ρ_{np} , ρ_{bf} are the densities of the nanofluid in kg/m^3, nanoparticles and the base fluids, respectively.

2. Specific heat of nanofluids (Yousefi et al., (2012b))

$$c_{pnf} = \frac{[(1 - f_v)\,\rho_{bf}\,c_{bf} + f_v\,\rho_{np}\,c_{np}\,]}{\rho_{nf}}$$

where c_{pnf} , c_{bf} , c_{np} are the specific heats of nanofluid, base fluids and nanoparticles, respectively.

3. Thermal conductivity of nanofluids (Javadi et al., 2013)

$$k_{nf} = \left[\frac{k_{np} + 2k_{bf} + 2f_v\,(k_{np} - k_{bf})}{k_{np} + 2k_{bf} - f_v(k_{np} - k_{bf})}\right] k_{bf}$$

where k_{nf} , k_{bf} , k_{np} , are the thermal conductivities of nanofluid, base fluids and nanoparticles in W/m-K, respectively, & f_v is the volume fraction of the nanoparticles.

4. Dynamic viscosity of nanofluids (Javadi et al., 2013)

$$\mu_{nf} = \frac{1}{(1 - f_v)^{2.5}}\,\mu_{bf}$$

where μ_{nf} , μ_{bf} are the dynamic viscosities of nanofluids and base fluids in m^2/s , & f_v is the volume fraction of the nanoparticles respectively.

5. Thermal conductivity ratio for nanofluids (Lee et al., 1999)

$$\frac{k_{nf}}{k_{bf}} = y$$

where k_{nf} , k_{bf} , are the thermal conductivities of nanofluid, base fluids in W/m-K, respectively

Note: The calculated values of. density ρ_{nf} , specific heat c_{pnf} , thermal conductivity k_{nf}, dynamic viscosity μ_{nf} of alumina water-based nanofluid (Al_2O_3) & copper oxide (CuO) water-based nanofluid with 0.01% & 0.05% volume concentration given in appendix G.

5.3 Experimental Results

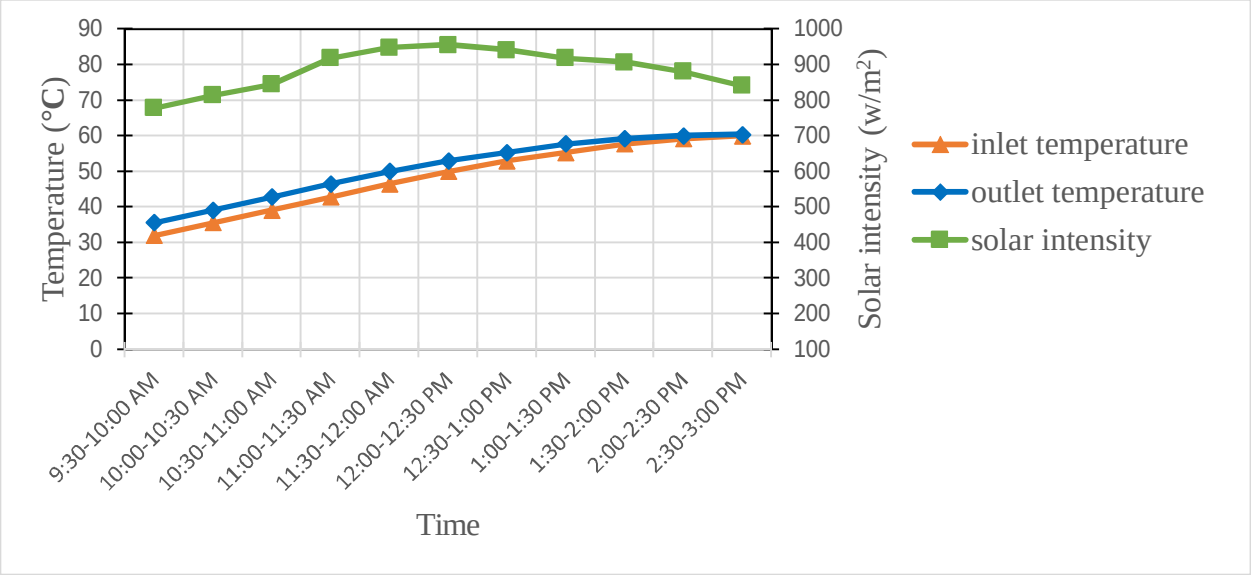

Figure 5.1: Variation of outlet temperature, inlet temperature and solar intensity of water for a mass flow rate of 20 l/hr

Figure 5.1 shows the variation of outlet temperature, inlet temperature and solar intensity for water having mass flow rate of 20 l/hr. This experiment is performed on 26th April 2014. From the graph it is observed that the inlet and outlet temperature is minimum at 9:30-10:00 AM i.e. 32°C & 35.6°C which increases gradually with time and reaches its maximum value 60°C & 60.3°C at 2:30-3:00 PM. On the other hand, solar intensity (solar radiations coming from sun) is minimum at 9:30-10:00 AM i.e. 778 W/m^2 which increases gradually with time and reaches to its maximum value 955 W/m^2 at 12:00-12:30 PM and after this period of time it starts decreases gradually up to 3:00 PM.

Figure 5.2 shows the variation of outlet temperature, inlet temperature and solar intensity for water having mass flow rate of 40 l/hr. This experiment is performed on 28th April 2014. From the graph it is observed that the inlet and outlet temperature is minimum at 9:30-10:00 AM i.e. 32.5°C & 36.1°C which increases gradually with time and reaches its maximum value 60.8 °C & 61°C at 2:30-3:00 PM.

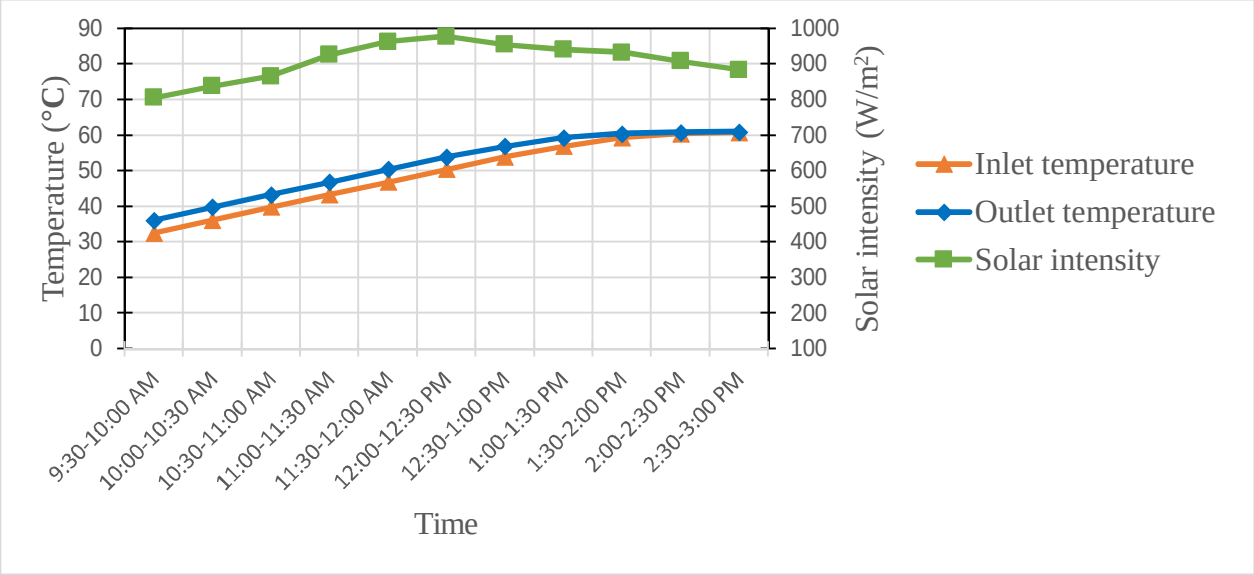

Figure 5.2: Variation of outlet temperature, inlet temperature and solar intensity of water for a mass flow rate of 40 l/hr

On the other hand, the value of solar intensity is minimum at 9:30-10:00 AM i.e. 806 W/m^2 which increases gradually with time and reaches to its maximum value 978 W/m^2 at 12:00-12:30 PM and after this period of time it starts decreases gradually up to 3:00 PM.

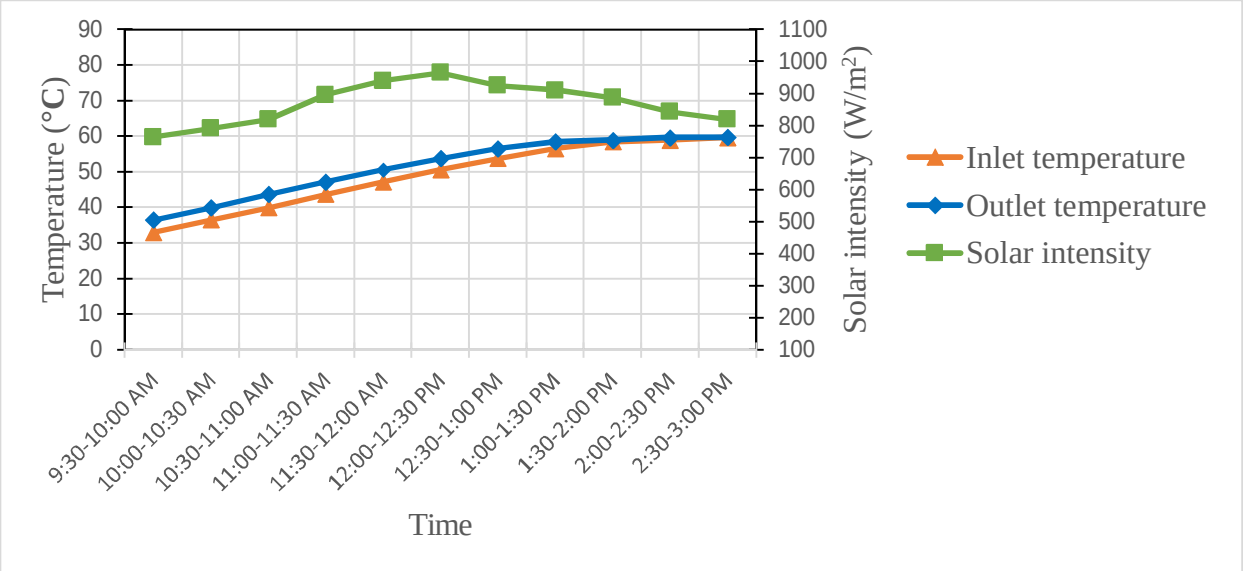

Figure 5.3: Variation of outlet temperature, inlet temperature and solar intensity of water for a mass flow rate of 60 l/hr

Figure 5.3 shows the variation of outlet temperature, inlet temperature and solar intensity for water having mass flow rate of 60 l/hr. This experiment is performed on 29th April 2014. From the graph it is observed that the inlet and outlet temperature is minimum at 9:30-10:00 AM i.e. 33°C & 36.5°C which increases gradually with time and reaches its maximum value 59.6 °C

& 59.7°C at 2:30-3:00 PM. On the other hand, the value solar intensity is minimum at 9:30-10:00 AM i.e. 765 W/m^2 which increases gradually with time and reaches to its maximum value 966 W/m^2 at 12:00-12:30 PM and after this period of time it starts decreases gradually up to 3:00 PM.

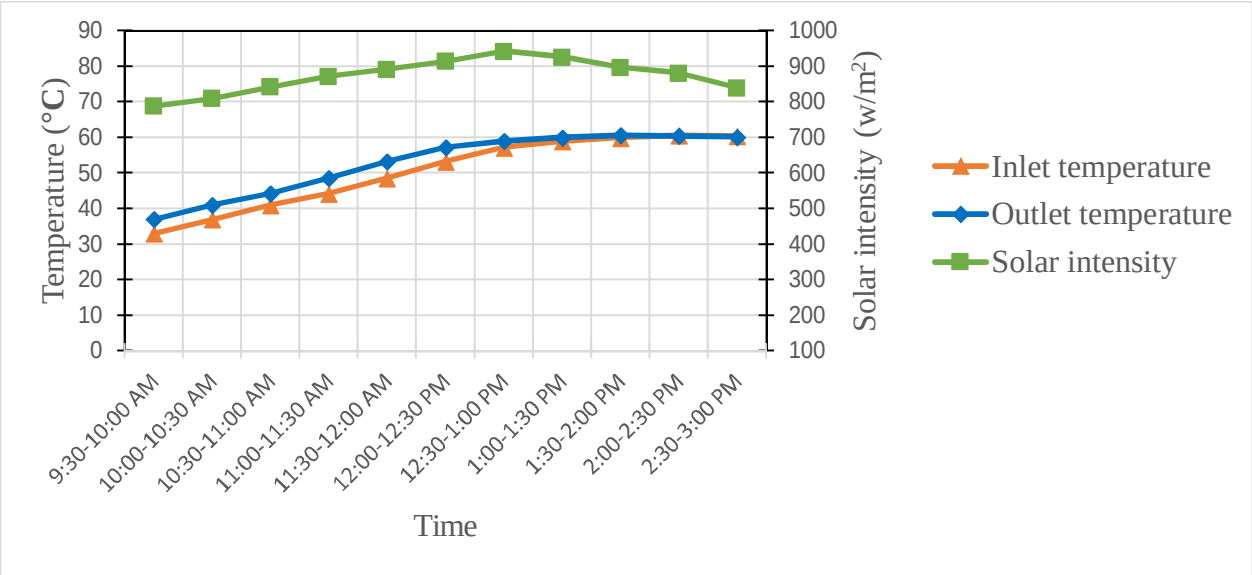

Figure 5.4: Variation of outlet temperature, inlet temperature and solar intensity for water based alumina (0.01%) nanofluid for mass flow rate of 20 l/hr

Figure 5.4 shows the variation of outlet temperature, inlet temperature and solar intensity for water based alumina nanofluid with 0.01% volume concentration having mass flow rate of 20 l/hr. This experiment is performed on 19th May 2014. From the graph it is observed that the inlet and outlet temperature is minimum at 9:30-10:00 AM i.e. 33°C & 37°C which increases gradually with time and reaches its maximum value 60.4°C & 60.1°C at 2:30-3:00 PM. A little drop is observed also in the value of outlet temperature at 2:00-3:00 PM. On the other hand, the value solar intensity is minimum at 9:30-10:00 AM i.e. 788 W/m^2 which increases gradually with time and reaches to its maximum value 942 W/m^2 at 12:30-1:00 PM and after this period of time it starts decreases gradually up to 3:00 PM.

Figure 5.5 shows the variation of outlet temperature, inlet temperature and solar intensity for water based alumina nanofluid with 0.01% volume concentration having mass flow rate of 40 l/hr. This experiment is performed on 20th May 2014.

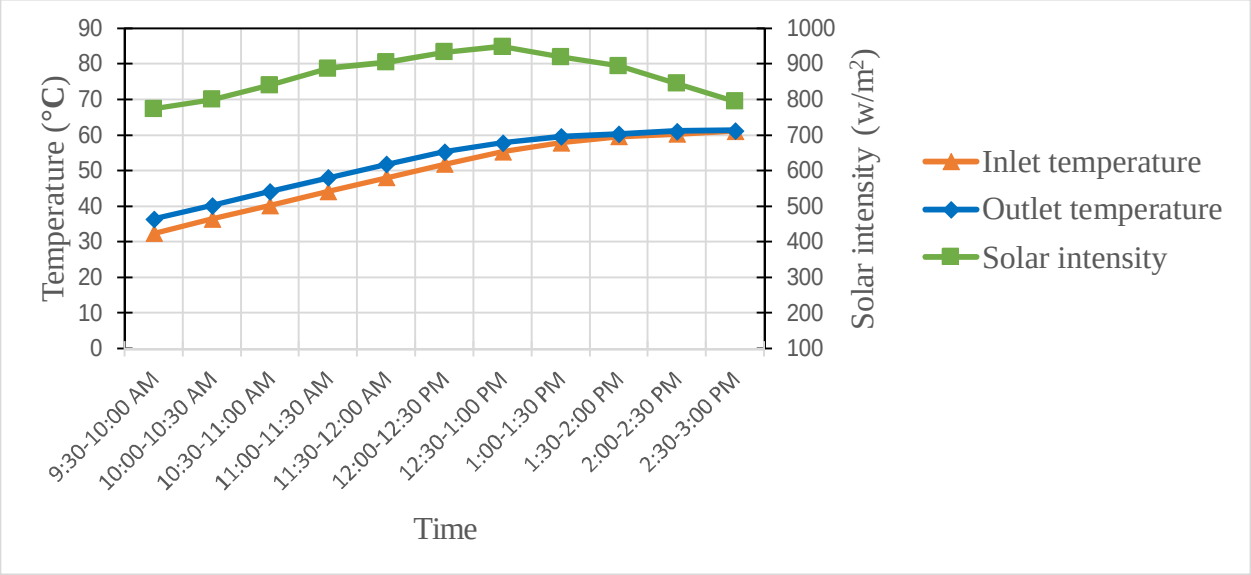

Figure 5.5: Variation of outlet temperature, inlet temperature and solar intensity for water based alumina (0.01%) nanofluid for mass flow rate of 40 l/hr

From the graph it is observed that the inlet and outlet temperature is minimum at 9:30-10:00 AM i.e. 32.4°C & 36.5°C which increases gradually with time and reaches its maximum value 61.1°C & 61.3°C at 2:30-3:00 PM. On the other hand, the value solar intensity is minimum at 9:30-10:00 AM i.e.774 W/m^2 which increases gradually with time and reaches to its maximum value 949 W/m^2 at 12:30-1:00 PM and after this period of time it starts decreases gradually up to 3:00 PM.

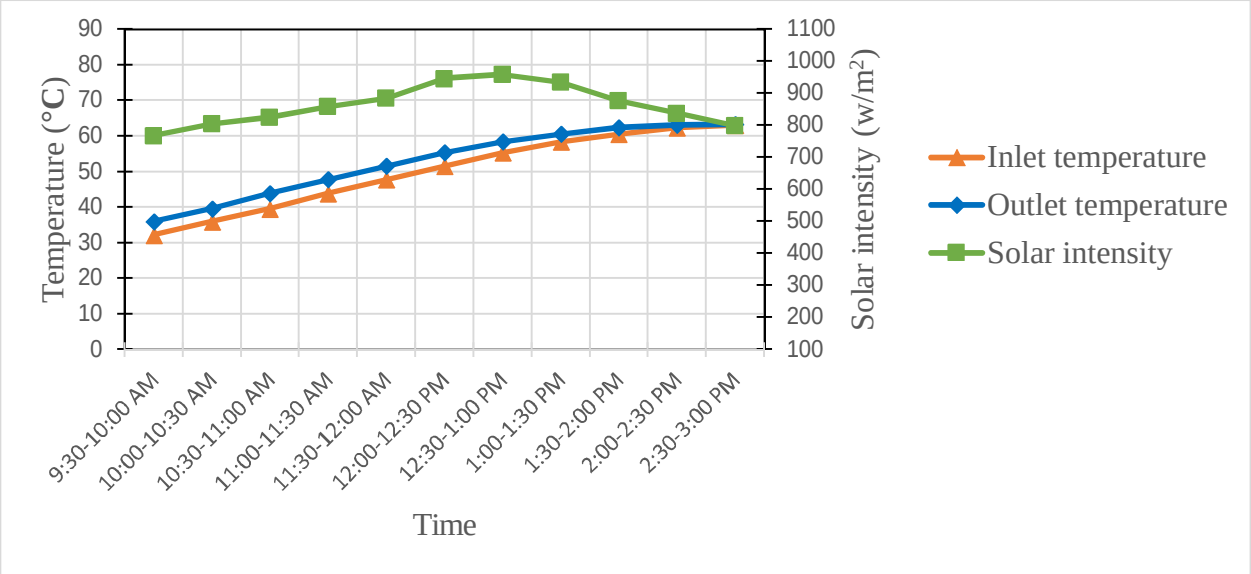

Figure 5.6: Variation of outlet temperature, inlet temperature and solar intensity for water based alumina (0.01%) nanofluid for mass flow rate of 60 l/hr

Figure 5.6 shows the variation of outlet temperature, inlet temperature and solar intensity for water based alumina nanofluid with 0.01% volume concentration having mass flow rate of 60 l/hr. This experiment is performed on 21st May 2014. From the graph it is observed that the inlet and outlet temperature is minimum at 9:30-10:00 AM i.e. 32.2°C & 36°C which increases gradually with time and reaches its maximum value 63.1°C & 63.3°C at 2:30-3:00 PM. On the other hand, the value solar intensity is minimum at 9:30-10:00 AM i.e.768 W/m^2 which increases gradually with time and reaches to its maximum value 959 W/m^2 at 12:30-1:00 PM and after this period of time it starts decreases gradually up to 3:00 PM.

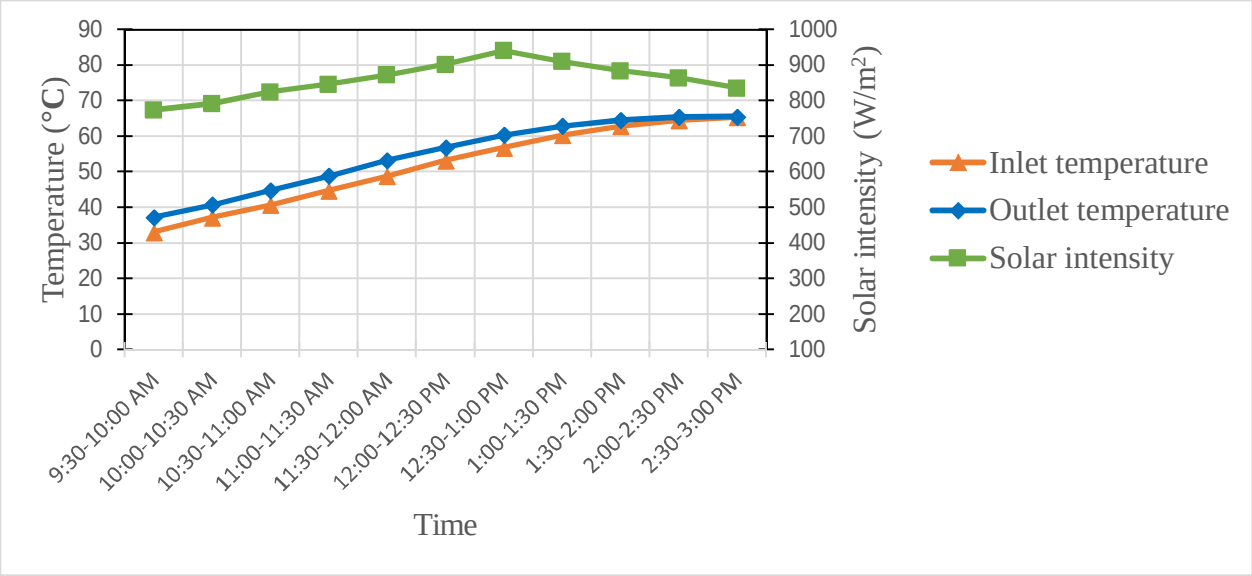

Figure 5.7: Variation of outlet temperature, inlet temperature and solar intensity for water based alumina (0.05%) nanofluid for mass flow rate of 20 l/hr

Figure 5.7 shows the variation of outlet temperature, inlet temperature and solar intensity for water based alumina nanofluid with 0.05% volume concentration having mass flow rate of 20 l/hr. This experiment is performed on 22nd May 2014. From the graph it is observed that the inlet and outlet temperature is minimum at 9:30-10:00 AM i.e. 33.1°C & 37.3°C which increases gradually with time and reaches its maximum value 65.4°C & 65.5°C at 2:30-3:00 PM. On the other hand, the value solar intensity is minimum at 9:30-10:00 AM i.e.774 W/m^2 which increases gradually with time and reaches to its maximum value 941 W/m^2 at 12:30-1:00 PM and after this period of time it starts decreases gradually up to 3:00 PM.

Figure 5.8 shows the variation of outlet temperature, inlet temperature and solar intensity for water based alumina nanofluid with 0.05% volume concentration having mass flow rate of 40 l/hr. This experiment is performed on 24th May 2014.

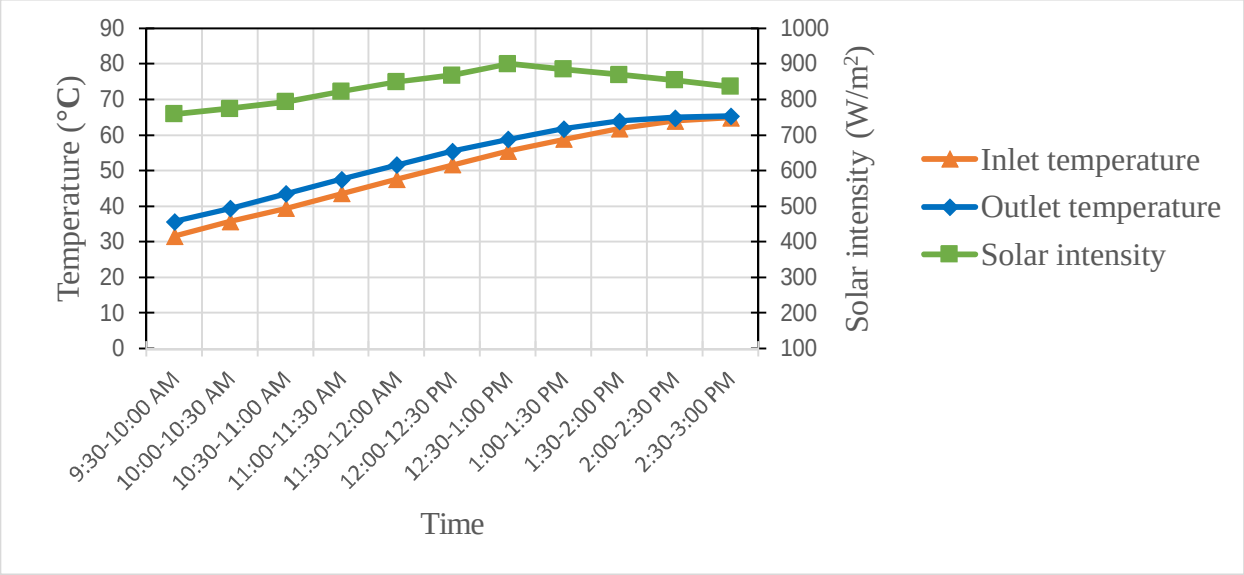

Figure 5.8: Variation of outlet temperature, inlet temperature and solar intensity for water based alumina (0.05%) nanofluid for mass flow rate of 40 l/hr

From the graph it is observed that the inlet and outlet temperature is minimum at 9:30-10:00 AM i.e. 31.6°C & 35.8°C which increases gradually with time and reaches its maximum value 64.9°C & 65.4°C at 2:30-3:00 PM. On the other hand, the value solar intensity is minimum at 9:30-10:00 AM i.e.759 W/m^2 which increases gradually with time and reaches to its maximum value 900 W/m^2 at 12:30-1:00 PM and after this period of time it starts decreases gradually up to 3:00 PM.

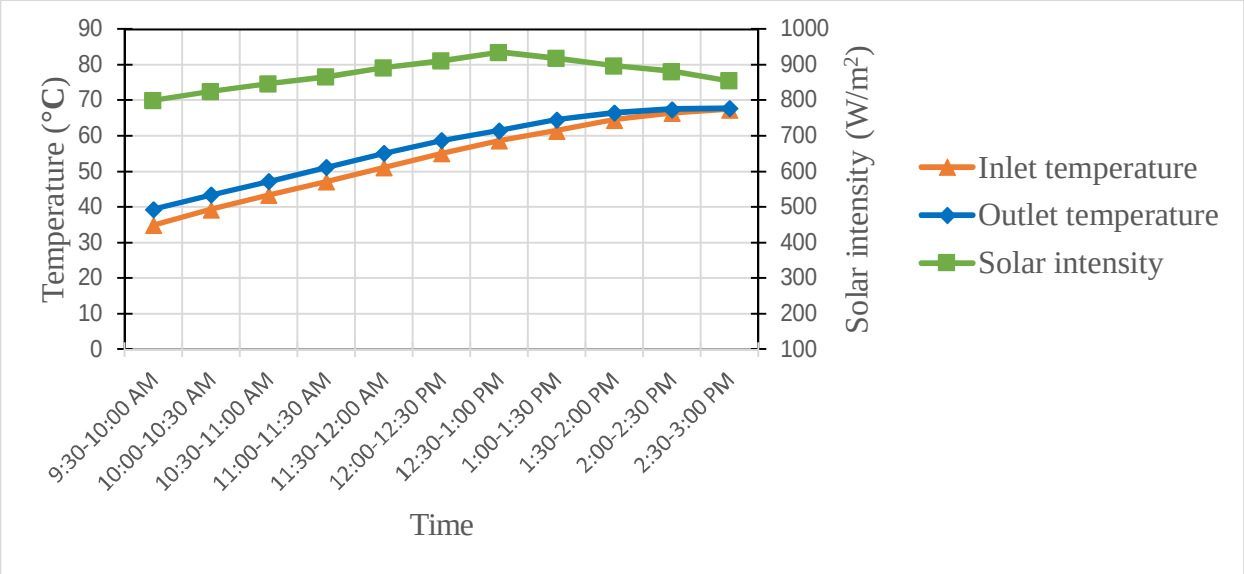

Figure 5.9: Variation of outlet temperature, inlet temperature and solar intensity for water based alumina (0.05%) nanofluid for mass flow rate of 60 l/hr

Figure 5.9 shows the variation of outlet temperature, inlet temperature and solar intensity for water based alumina nanofluid with 0.05% volume concentration having mass flow rate of 60 l/hr. This experiment is performed on 25th May 2014. From the graph it is observed that the inlet and outlet temperature is minimum at 9:30-10:00 AM i.e. 35°C & 39.4°C which increases gradually with time and reaches its maximum value 67.5°C & 67.8°C at 2:30-3:00 PM. On the other hand, the value solar intensity is minimum at 9:30-10:00 AM i.e.800 W/m^2 which increases gradually with time and reaches to its maximum value 935 W/m^2 at 12:30-1:00 PM and after this period of time it starts decreases gradually up to 3:00 PM.

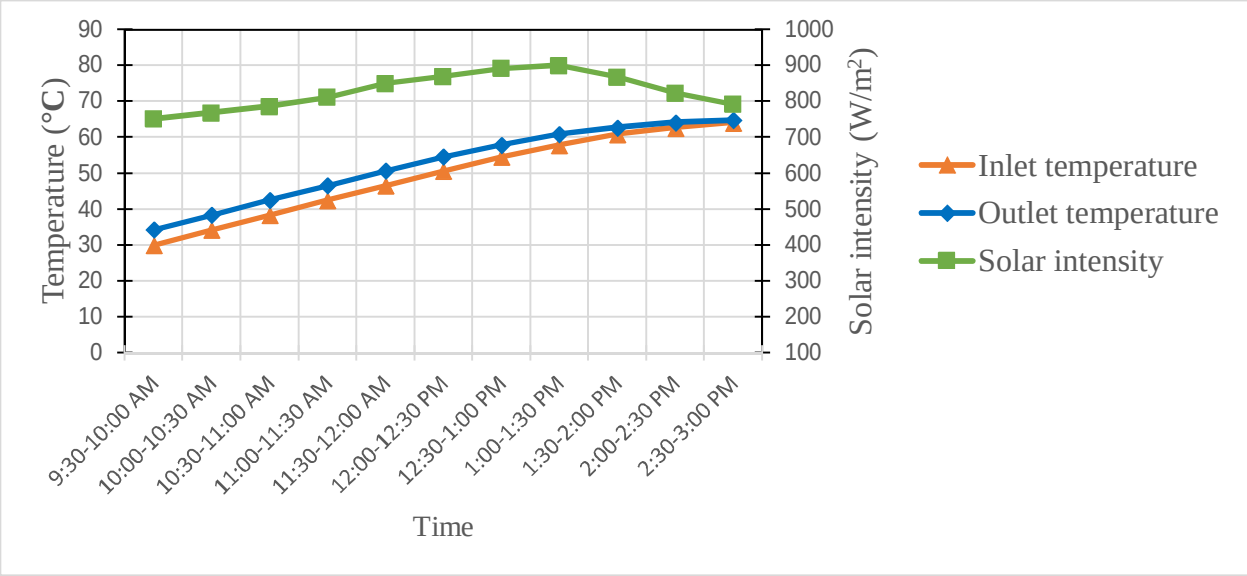

Figure 5.10: Variation of outlet temperature, inlet temperature and solar intensity for water based CuO (0.01%) nanofluid for mass flow rate of 20 l/hr

Figure 5.10 shows the variation of outlet temperature, inlet temperature and solar intensity for water based CuO nanofluid with 0.01% volume concentration having mass flow rate of 20 l/hr. This experiment is performed on 26th May 2014. From the graph it is observed that the inlet and outlet temperature is minimum at 9:30-10:00 AM i.e. 30°C & 34.3°C which increases gradually with time and reaches its maximum value 64.1°C & 64.8°C at 2:30-3:00 PM. On the other hand, the value solar intensity is minimum at 9:30-10:00 AM i.e.751 W/m^2 which increases gradually with time and reaches to its maximum value 900 W/m^2 at 1:00-1:30 PM and after this period of time it starts decreases gradually up to 3:00 PM.

Figure 5.11 shows the variation of outlet temperature, inlet temperature and solar intensity for water based CuO nanofluid with 0.01% volume concentration having mass flow rate of 40 l/hr. This experiment is performed on 28th May 2014.

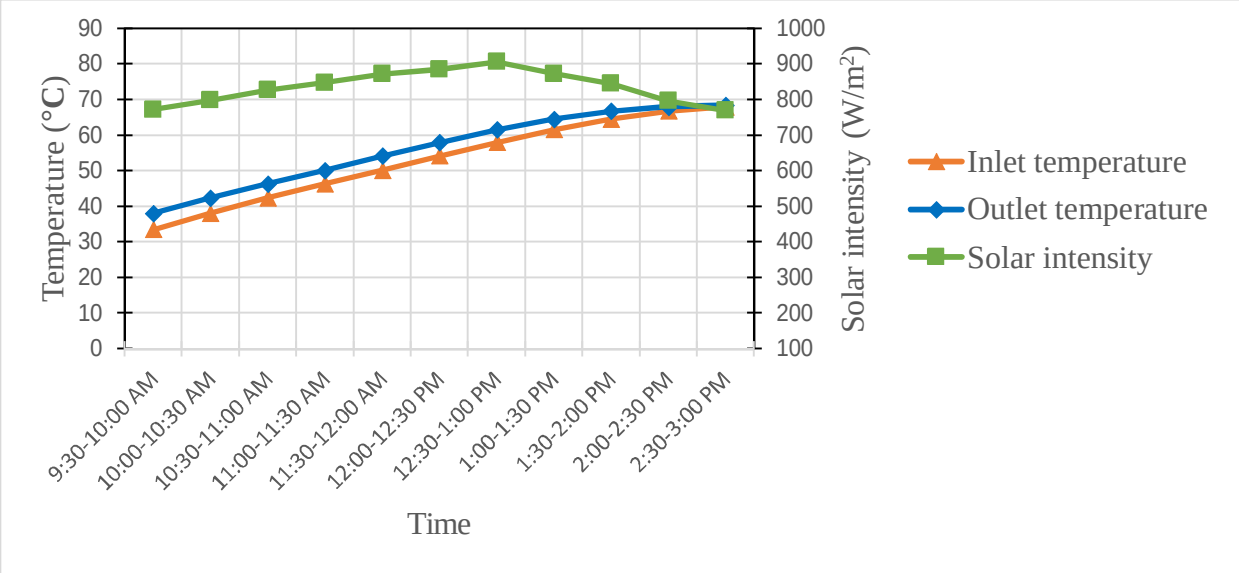

Figure 5.11: Variation of outlet temperature, inlet temperature and solar intensity for water based CuO (0.01%) nanofluid for mass flow rate of 40 l/hr

From the graph it is observed that the inlet and outlet temperature is minimum at 9:30-10:00 AM i.e. 33.5°C & 38.1°C which increases gradually with time and reaches its maximum value 68°C & 68.4°C at 2:30-3:00 PM. On the other hand, the value solar intensity is minimum at 9:30-10:00 AM i.e.773 W/m^2 which increases gradually with time and reaches to its maximum value 907 W/m^2 at 12:30-1:00 PM and after this period of time it starts decreases gradually up to 3:00 PM.

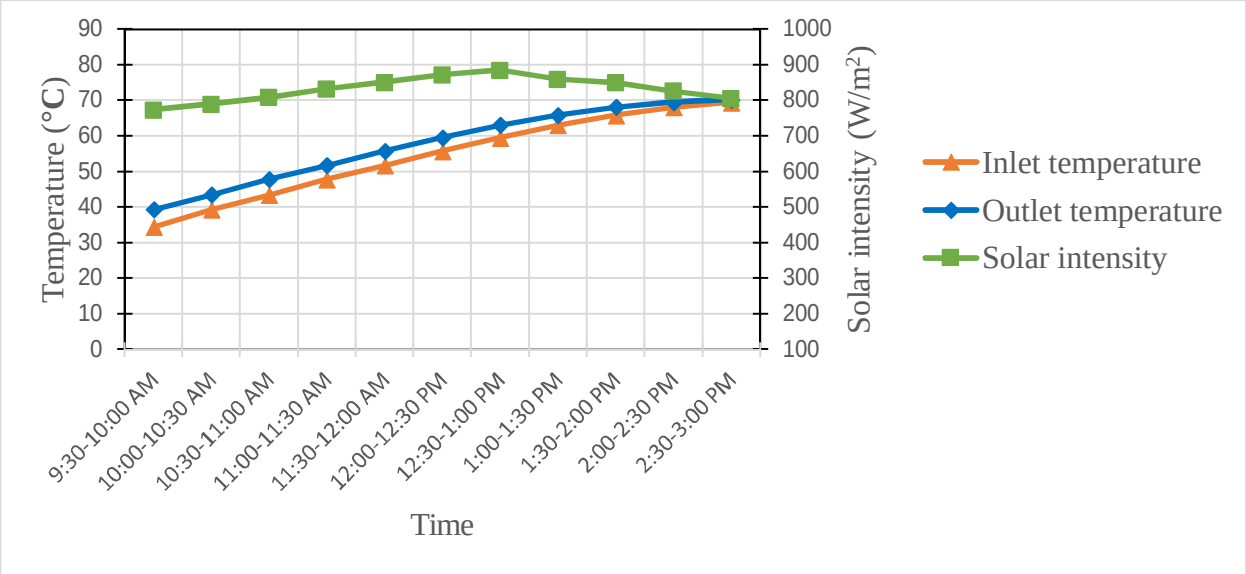

Figure 5.12: Variation of outlet temperature, inlet temperature and solar intensity for water based CuO (0.01%) nanofluid for mass flow rate of 60 l/hr

Figure 5.12 shows the variation of outlet temperature, inlet temperature and solar intensity for water based CuO nanofluid with 0.01% volume concentration having mass flow rate of 60 l/hr. This experiment is performed on 29th May 2014. From the graph it is observed that the inlet and outlet temperature is minimum at 9:30-10:00 AM i.e. 34.5°C & 39.3°C which increases gradually with time and reaches its maximum value 69.5°C & 70.2°C at 2:30-3:00 PM. On the other hand, the value solar intensity is minimum at 9:30-10:00 AM i.e.773 W/m^2 which increases gradually with time and reaches to its maximum value 885 W/m^2 at 12:30-1:00 PM and after this period of time it starts decreases gradually up to 3:00 PM.

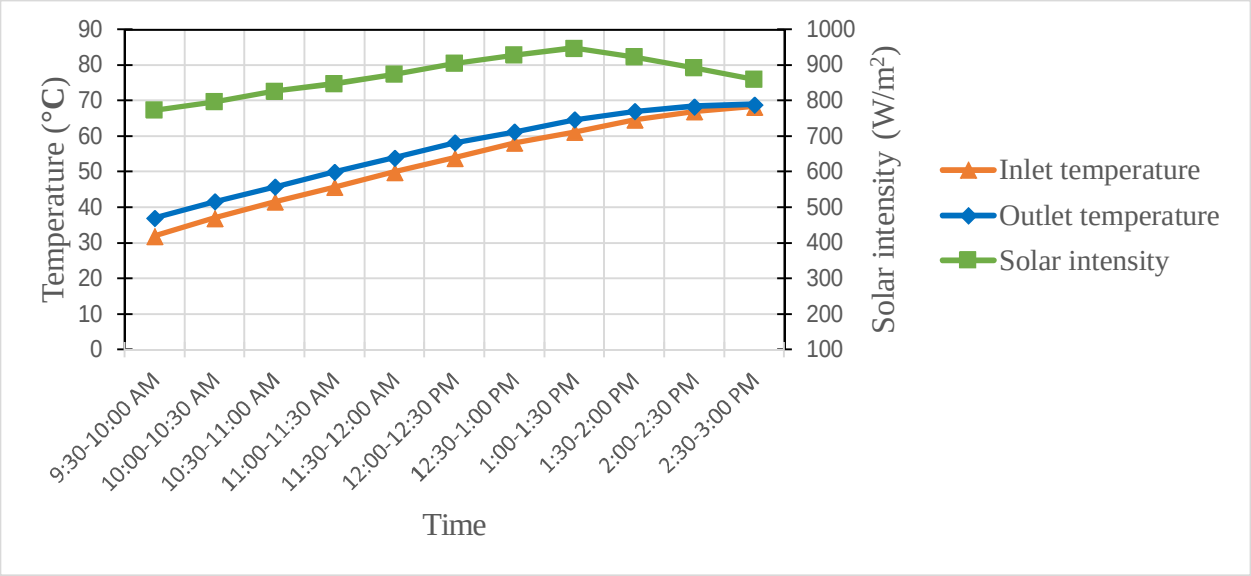

Figure 5.13: Variation of outlet temperature, inlet temperature and solar intensity for water based CuO (0.05%) nanofluid for mass flow rate of 20 l/hr

Figure 5.13 shows the variation of outlet temperature, inlet temperature and solar intensity for water based CuO nanofluid with 0.05% volume concentration having mass flow rate of 20 l/hr. This experiment is performed on 2nd June 2014. From the graph it is observed that the inlet and outlet temperature is minimum at 9:30-10:00 AM i.e. 32°C & 37.1°C which increases gradually with time and reaches its maximum value 68.4°C & 68.9°C at 2:30-3:00 PM. On the other hand, the value solar intensity is minimum at 9:30-10:00 AM i.e.774 W/m^2 which increases gradually with time and reaches to its maximum value 948 W/m^2 at 1:00-1:30 PM and after this period of time it starts decreases gradually up to 3:00 PM.

Figure 5.14 shows the variation of outlet temperature, inlet temperature and solar intensity for water based CuO nanofluid with 0.05% volume concentration having mass flow rate of 40 l/hr. This experiment is performed on 3rd June 2014.

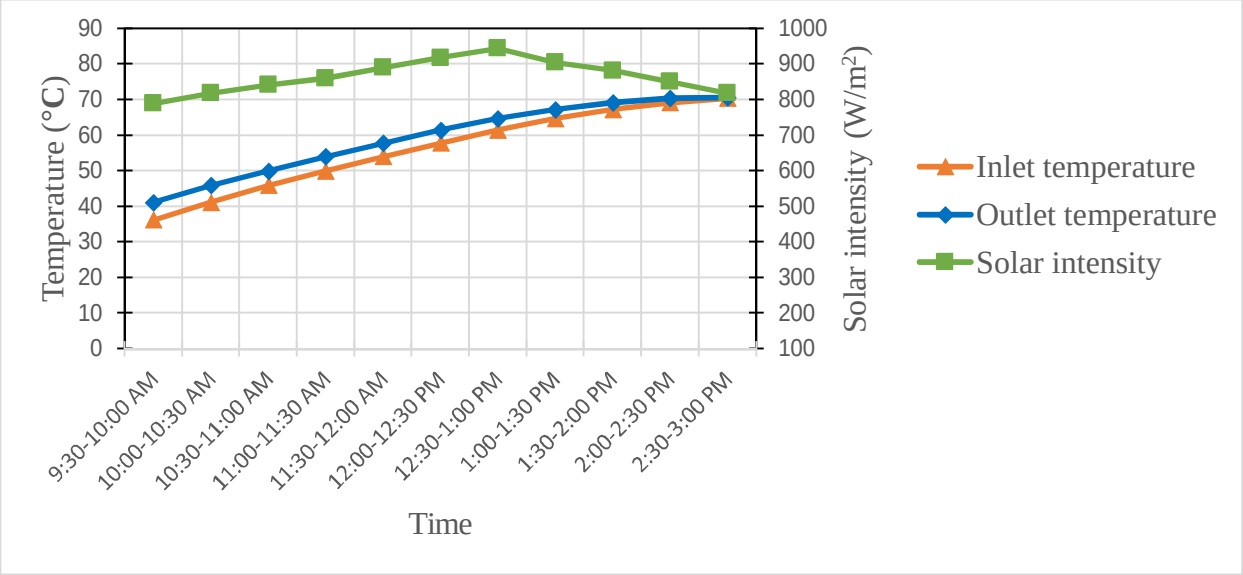

Figure 5.14: Variation of outlet temperature, inlet temperature and solar intensity for water based CuO (0.05%) nanofluid for mass flow rate of 40 l/hr

From the graph it is observed that the inlet and outlet temperature is minimum at 9:30-10:00 AM i.e. 36.2°C & 41.2°C which increases gradually with time and reaches its maximum value 70.4°C & 70.6°C at 2:30-3:00 PM. On the other hand, the value solar intensity is minimum at 9:30-10:00 AM i.e.790 W/m^2 which increases gradually with time and reaches to its maximum value 944 W/m^2 at 12:30-1:00 PM and after this period of time it starts decreases gradually up to 3:00 PM.

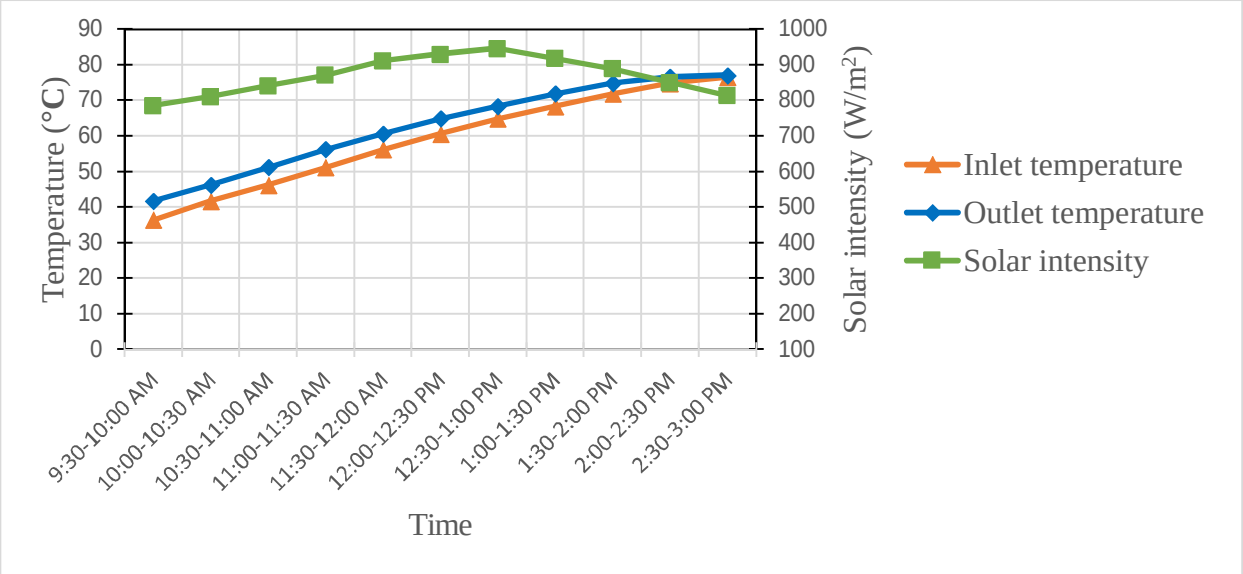

Figure 5.15: Variation of outlet temperature, inlet temperature and solar intensity for water based CuO (0.05%) nanofluid for mass flow rate of 60 l/hr

Figure 5.15 shows the variation of outlet temperature, inlet temperature and solar intensity for water based CuO nanofluid with 0.05% volume concentration having mass flow rate of 60 l/hr. This experiment is performed on 4th June 2014. From the graph it is observed that the inlet and outlet temperature is minimum at 9:30-10:00 AM i.e. 36.5°C & 41.8°C which increases gradually with time and reaches its maximum value 76.6°C & 77°C at 2:30-3:00 PM. On the other hand, the value solar intensity is minimum at 9:30-10:00 AM i.e.786 W/m^2 which increases gradually with time and reaches to its maximum value 946 W/m^2 at 12:30-1:00 PM and after this period of time it starts decreases gradually up to 3:00 PM.

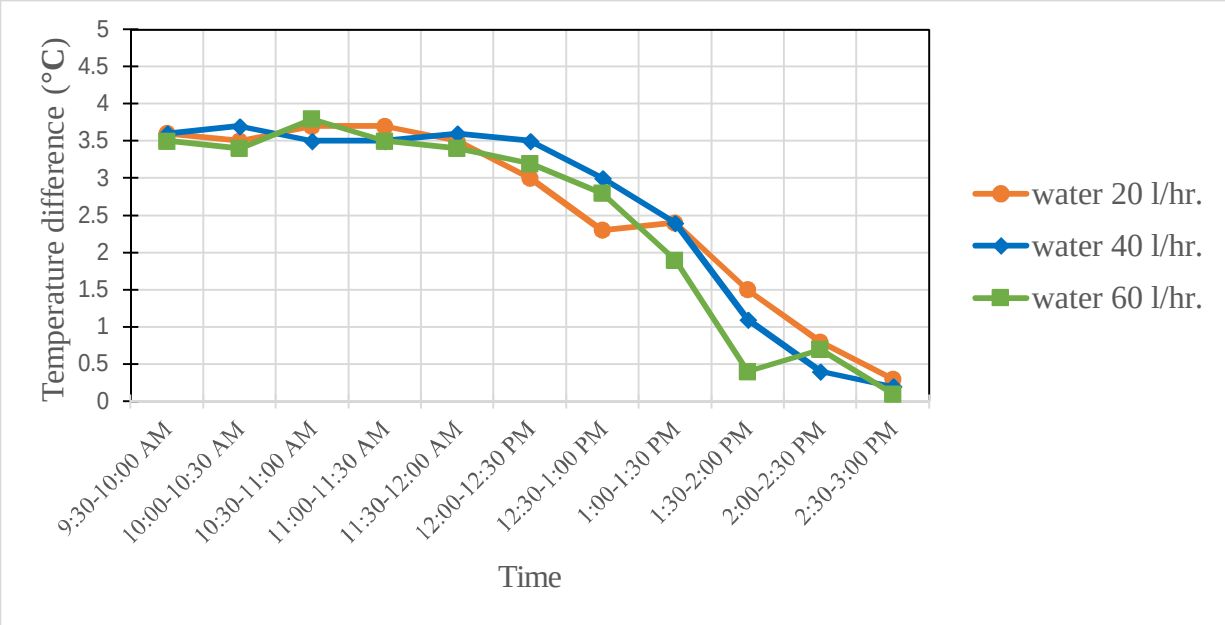

Figure 5.16: Variation in temperature difference w.r.t. time for water at different mass flow rates

Figure 5.16 shows the variation in temperature difference w.r.t. time for water at three different mass flow rates (20, 40, and 60) l/hr. From the graph it has been observed that for all three mass flow rates the value of temperature difference is almost equal at 9:30-10:00 AM. The maximum value of temperature difference is obtained at a mass flow rate of 60 l/hr at 10:30-11:00 AM, for 40 l/hr at 10:00-10:30 AM & for 20 l/hr at 10:30-11:30 AM. It is also noted that the temperature difference has higher values for 40 l/hr from 11:30 AM to 1:00 PM as compare to other mass flow rates. On the other hand the temperature difference shows higher values for 20 l/hr from 1:00 to 3:00 PM as compare to other mass flow rates. Therefore, very mixed results are obtained regarding temperature difference of water. Above all it can be concluded that inspite of different mass flow rates variation in temperature difference is same for water.

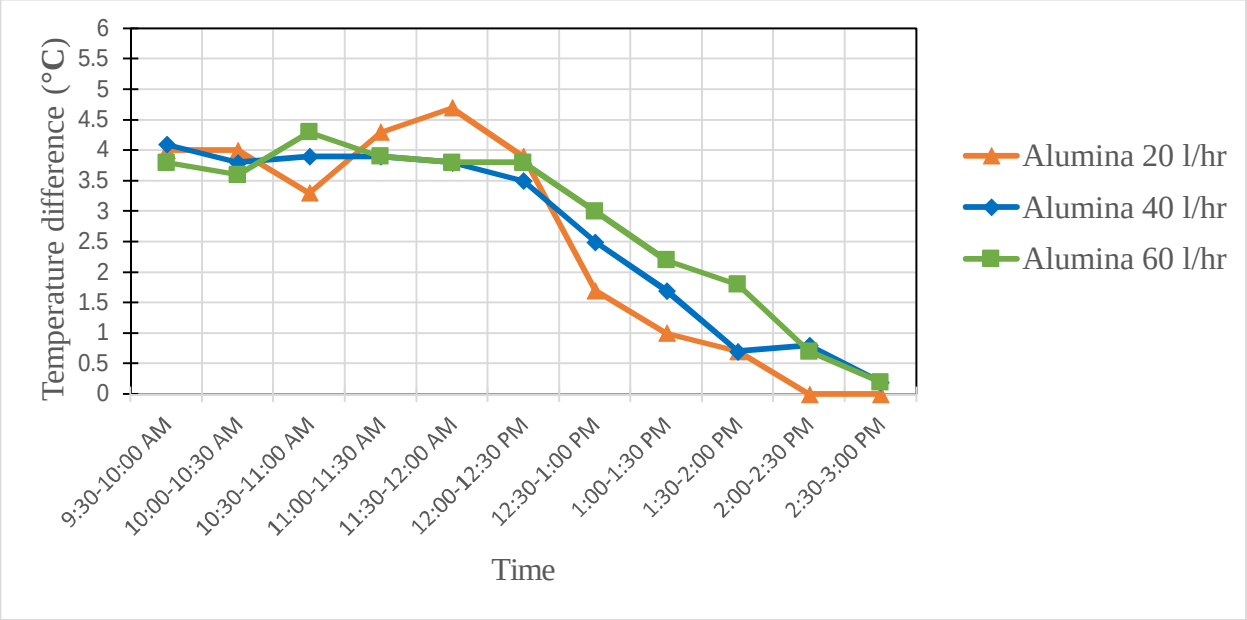

Figure 5.17: Variation in temperature difference w.r.t. time for water based alumina (0.01%) nanofluid at different mass flow rates

Figure 5.17 shows the variation in temperature difference w.r.t. time for water based alumina nanofluid (0.01% concentration) at different mass flow rates. From the graph it is observed that 20 l/hr mass flow rate shows the highest peak value of temperature difference at 11:30-12:00 PM. On the other hand, 60 l/hr mass flow rate shows the highest peak value of temperature difference at 10:30-11:00 AM and shows maximum value from 12:30 to 2:00 PM as compare to other mass flow rates. Hence, with 0.01% concentration mixed results are obtained.

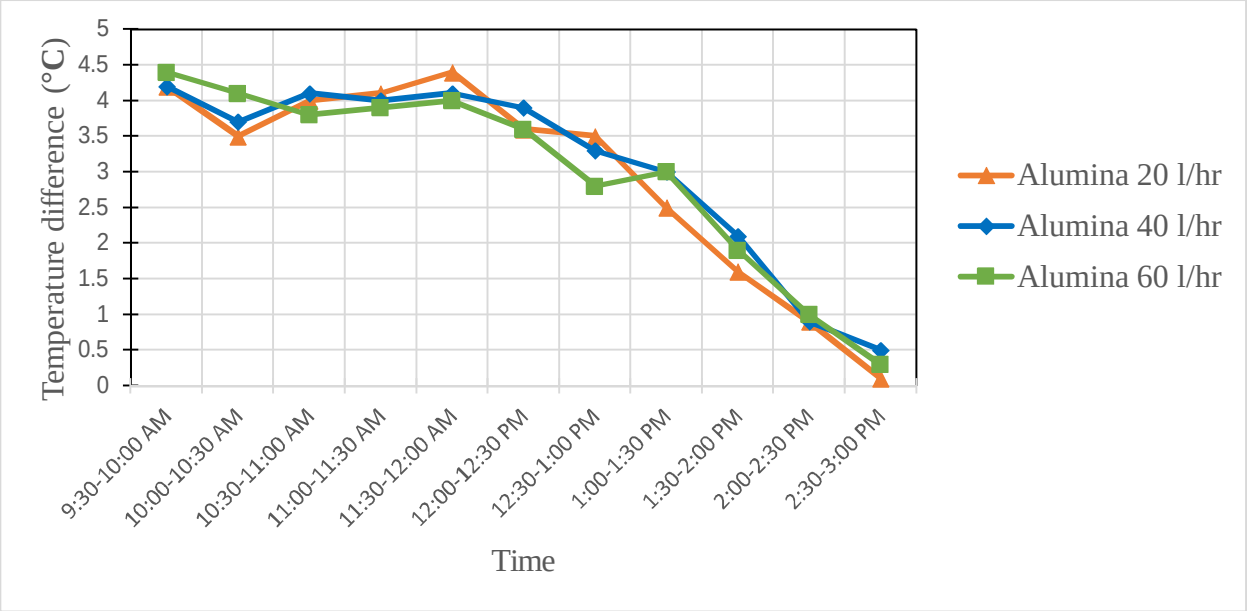

Figure 5.18: Variation in temperature difference w.r.t. time for water based alumina (0.05%) nanofluid at different mass flow rates

Figure 5.18 shows the variation in temperature difference w.r.t. time for water based alumina nanofluid with 0.05% volume concentration at different mass flow rates. From the graph it is clear that for 0.05% concentration 20 l/hr mass flow rate shows the highest value of temperature difference from 11:00 to 12:00 PM and at 12:30-1:00 PM. While on the other hand, 60 l/hr mass flow rate shows the highest value of temperature difference from 9:30-10:30 AM.

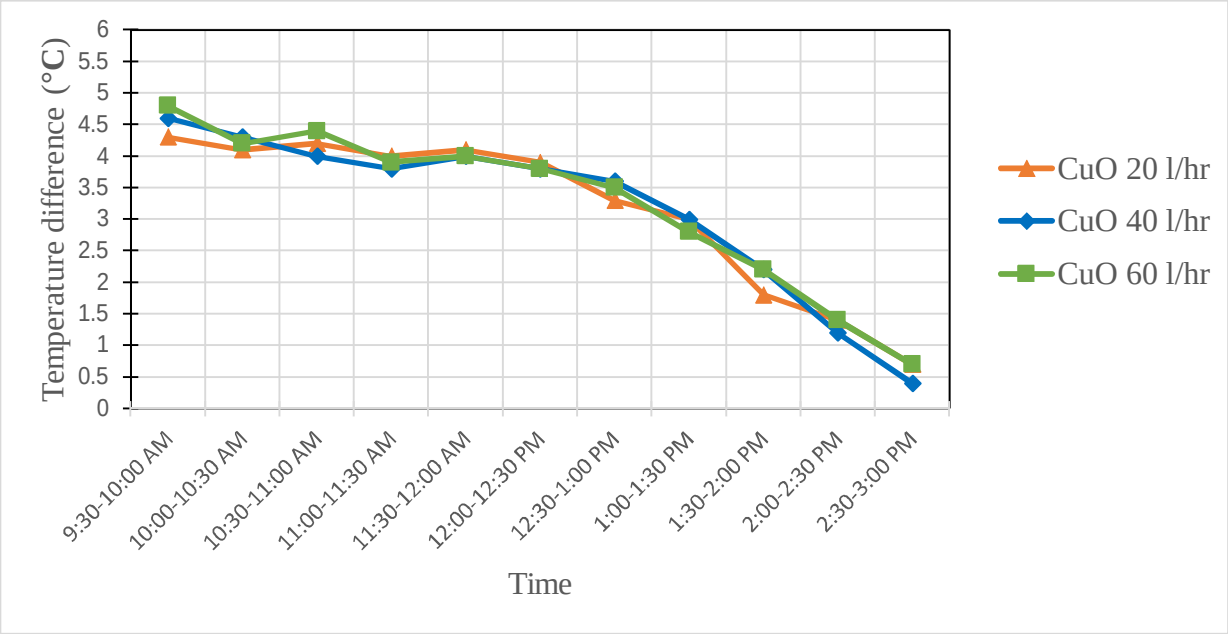

Figure 5.19: Variation in temperature difference w.r.t. time for water based CuO (0.01%) nanofluid at different mass flow rates

Figure 5.19 shows the variation in temperature difference w.r.t. time for water based CuO nanofluid with 0.01% volume concentration at different mass flow rates. From the graph it observed that for 60 l/hr the maximum value of temperature difference is obtained at 9:30-10:00 AM & 10:30-11:00 AM in comparison with other mass flow rates.

Figure 5.20 shows the variation in temperature difference w.r.t. time for water based CuO nanofluid with 0.05% volume concentration at different mass flow rates. From the graph it is clear that for 0.05% concentration 60 l/hr mass flow rate shows the maximum value of temperature difference at 9:30-10:00 AM, from 10:30 AM to 12:00 PM, and from 12:30 to 2:30 PM.

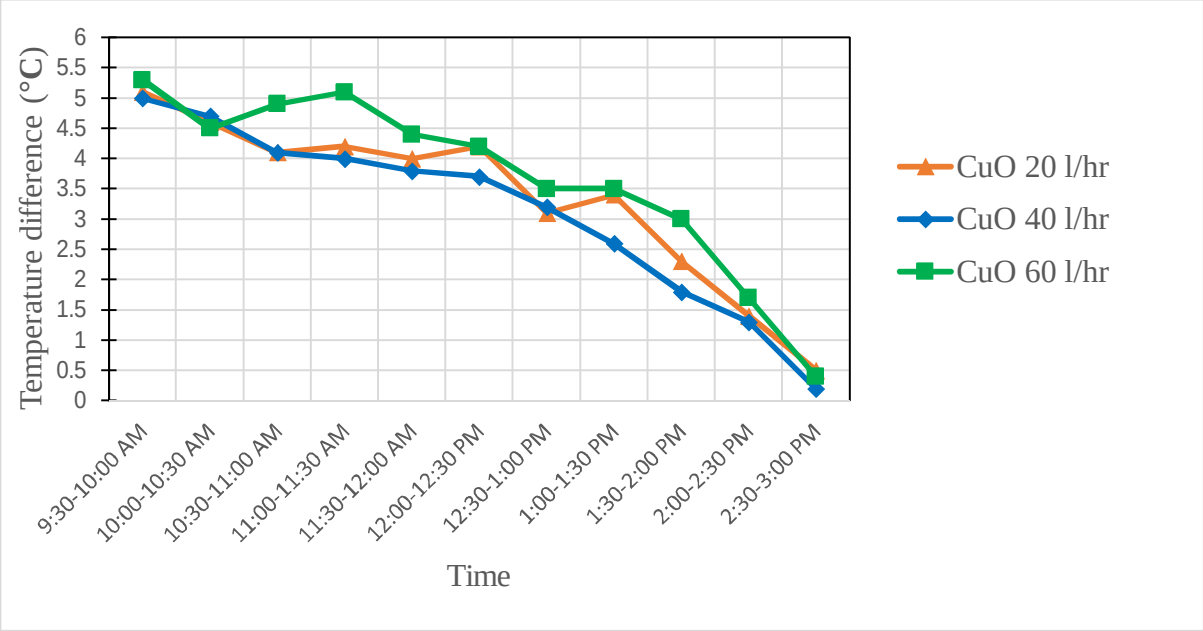

Figure 5.20: Variation in temperature difference w.r.t. time for water based CuO (0.05%) nanofluid at different mass flow rates

Hence, somewhat positive results are obtained increasing mass flow rate. So we can say that for 0.05 % volume concentration the temperature difference increases with increasing mass flow rate as it is not so much true for the cases discussed above.

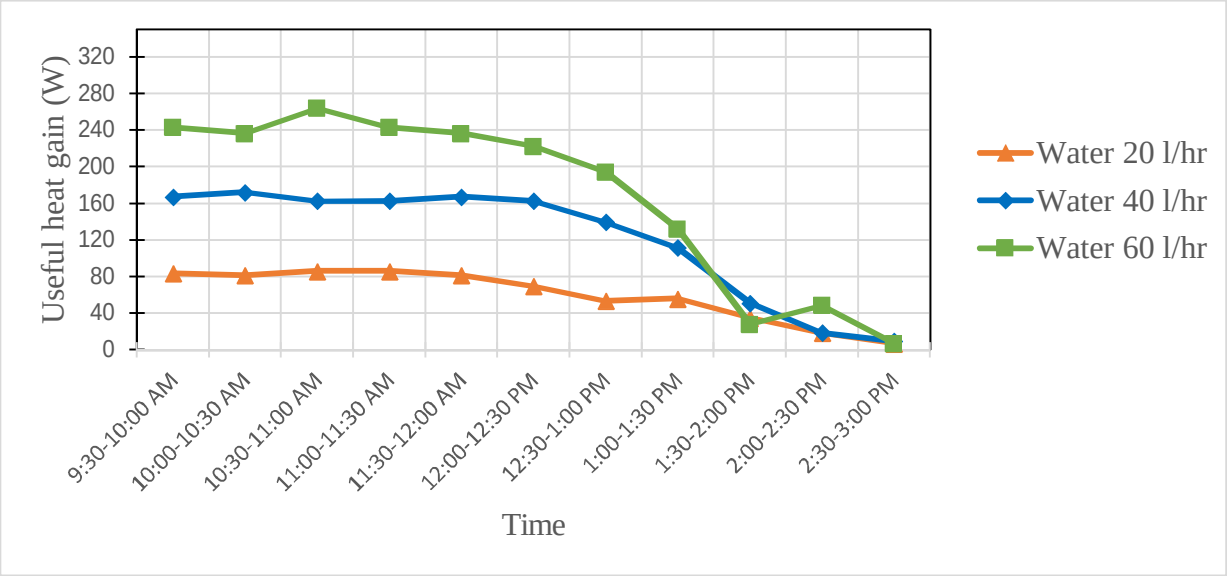

Figure 5.21: Variation in useful heat gain w.r.t. time for water at different mass flow rates

Figure 5.21 shows the variation in useful heat gain w.r.t. time for water at different mass flow rates (20, 40, and 60) l/hr. From the graph it is observed that with increasing mass flow rate the useful heat gain increases. For the mass flow rate of 60 l/hr the highest peak value of useful

heat gain is obtained as 264.16 W at 10:30-11:00 AM. For 60 l/hr a little drop in the temperature difference is also observed at 1:30-2:00 PM in the value of useful heat gain, because useful heat gain directly depends upon the temperature difference. That why at this time period the value of useful heat gain suddenly drops.

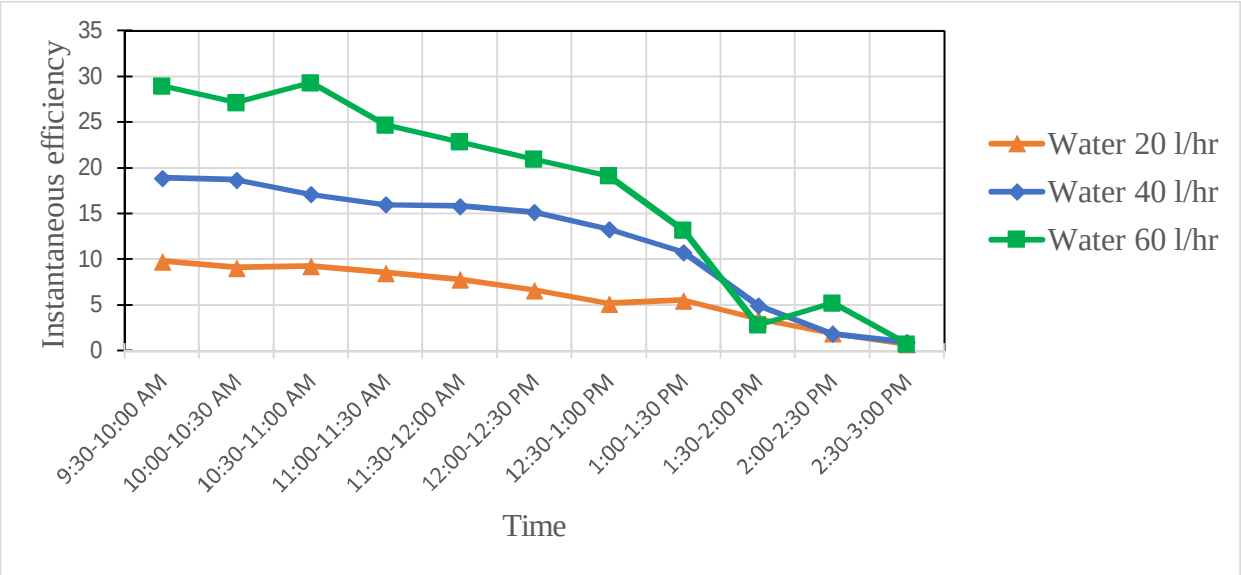

Figure 5.22: Variation in instantaneous efficiency w.r.t. time for water at different mass flow rates

Figure 5.22 shows the variation in instantaneous efficiency w.r.t. time for water at different mass flow rates (20, 40, and 60) l/hr. From the graph it is observed that with increasing mass flow rate the instantaneous efficiency increases. For 60 l/hr mass flow rate the efficiency reaches to the maximum value of 29.34% at 10:30-11:00 AM. A sudden drop is also observed in the value of instantaneous efficiency at 1:30-2:00 PM, because of the same reason as discussed for useful heat gain that is lower temperature difference at this time period.

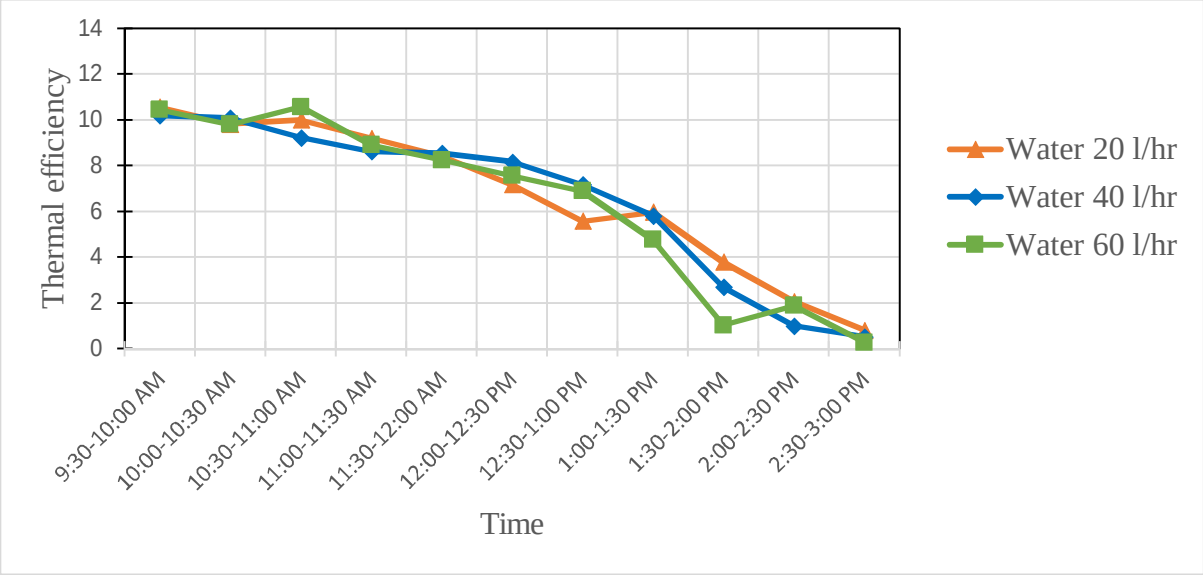

Figure 5.23: Variation in thermal efficiency w.r.t. time for water at different mass flow rates

Figure 5.23 shows the variation in thermal efficiency w.r.t. time for water at different mass flow rates (20, 40, and 60) l/hr. From the graph it is observed that 20 l/hr mass flow rate shows higher thermal efficiency at 11:00-11:30 AM & from 1:00-3:00 PM. For 40 l/hr higher thermal efficiency is observed at 10:00-10:30 AM and from 11:30 AM to 1:00 PM. For 60 l/hr higher thermal efficiency is observed at 10:30-11:00 AM that is 10.58% which is maximum in comparison to other mass flow rates.

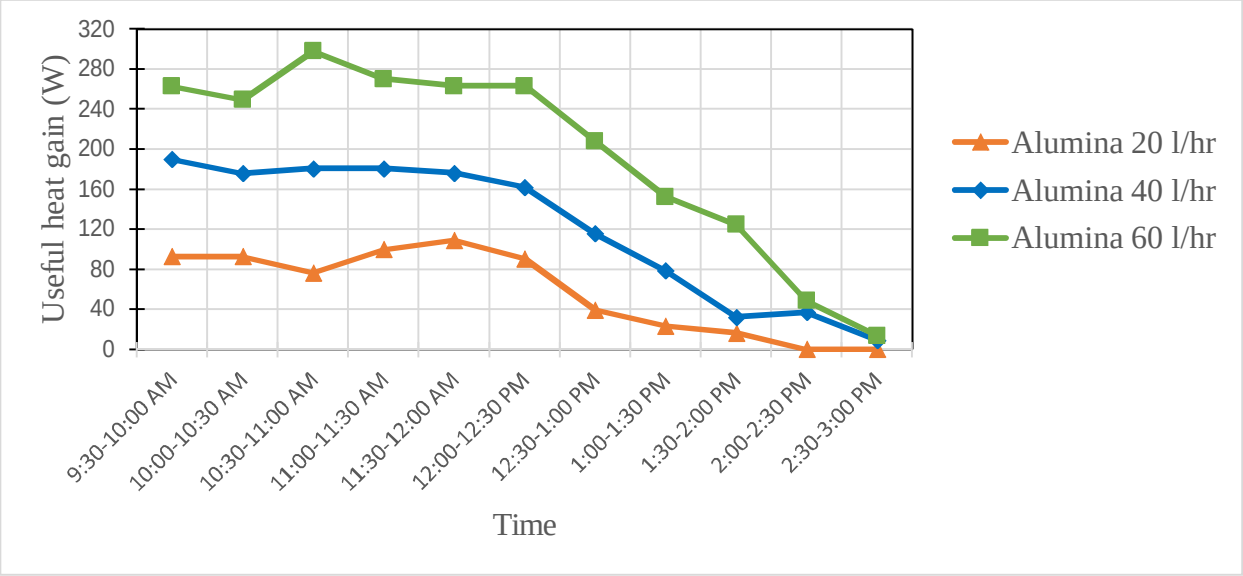

Figure 5.24: Variation in useful heat gain w.r.t. time for water based alumina (0.01%) nanofluid at different mass flow rates

Figure 5.24 shows the variation in useful heat gain w.r.t. time for water based alumina nanofluid with 0.01% volume concentration at different mass flow rates. From the graph it is

observed that for water based aluminium oxide nanofluid useful heat gain increases with increasing mass flow rates. For the mass flow rate of 60 l/hr the highest peak value of useful heat gain is obtained as 298 W at 10:30-11:00 AM. This trend of increasing useful heat gain for 60 l/hr as compare to other mass flow rates continues up to 3:00 PM. It is noted that the useful heat gain for aluminium oxide nanofluid decreases gradually for 20 l/hr from 11:30 AM to 3:00 PM, for 40 l/hr & 60 l/hr from 10:30 AM to 3:00 PM. From the graph it is clear that the trend of increasing useful heat gain continues with increasing mass flow rates from 9:30 AM onwards up to 3:00 PM.

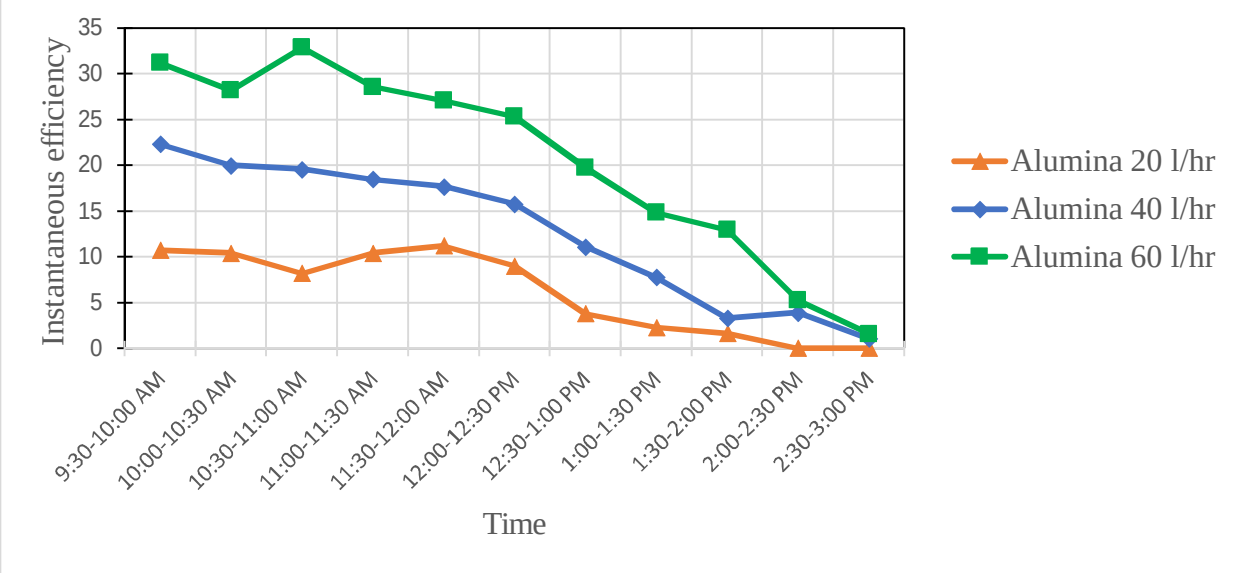

Figure 5.25: Variation in instantaneous efficiency w.r.t. time for water based alumina (0.01%) nanofluid at different mass flow rates

Figure 5.25 shows the variation in instantaneous efficiency w.r.t. time for water based alumina nanofluid with 0.01% volume concentration at different mass flow rates. From the graph it is observed that the instantaneous efficiency increases with increasing mass flow rates. For 60 l/hr mass flow rate the efficiency reaches its highest peak value of 32.9% at 10:30-11:00 AM. For 20 l/hr mass flow rate the efficiency gradually decreases from 11:30 AM to 3:00 PM, for 40 l/hr from 9:30 AM to 3:00 PM, & for 60 l/hr from 10:30 AM to 3:00 PM. From the graph it is clear that the trend of increasing instantaneous efficiency continues with increasing mass flow rates from 9:30 AM onwards up to 3:00 PM.

Figure 5.26 shows the variation in thermal efficiency w.r.t. time for water based alumina nanofluid with 0.01% volume concentration at different mass flow rates.

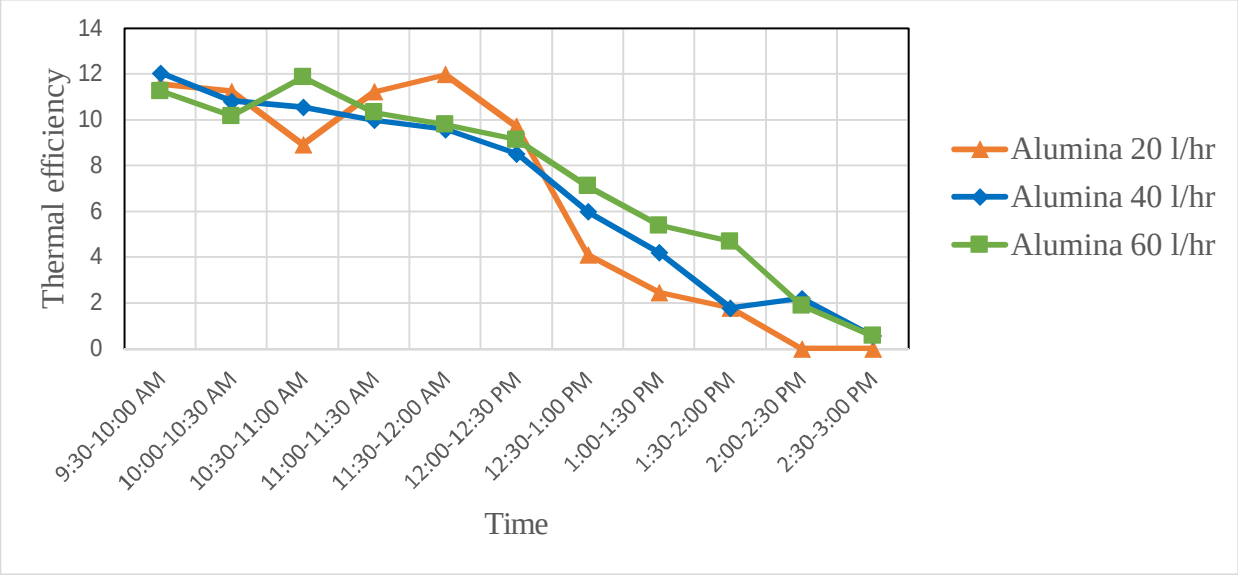

Figure 5.26: Variation in thermal efficiency w.r.t. time for water based alumina (0.01%) nanofluid at different mass flow rates

From the graph it is analysed that the thermal efficiency reaches to its maximum value of 12.06% at 9:30-10:00 AM for the mass flow rate of 40 l/hr which is higher in comparison to other mass flow rates at this time period. On the other hand, 20 l/hr mass flow rate shows higher value of efficiency at 10:00-10:30 AM & from 11:00 AM to 12:30 PM and 60 l/hr mass flow rate shows higher value of efficiency at 10:30-11:00-AM & from 12:30-2:00-PM.

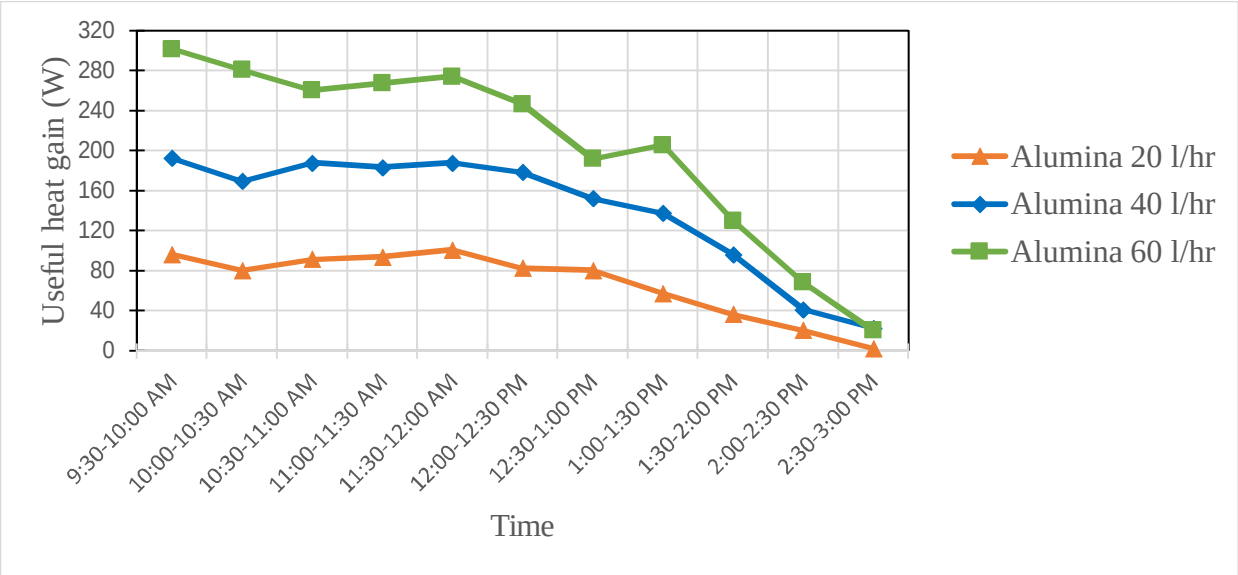

Figure 5.27: Variation in useful heat gain w.r.t. time for water based alumina (0.05%) nanofluid at different mass flow rates

Figure 5.27 shows the variation in useful heat gain w.r.t. time for water based alumina with nanofluid 0.05% volume concentration at different mass flow rates. From the graph it is

observed useful heat gain increases with increasing mass flow rate for water based aluminium oxide nanofluid, therefore a similar trend is observed in useful heat gain as discussed for 0.01% concentration. It is noted that for the mass flow rate of 60 l/hr the highest peak value of useful heat gain is obtained as 301.618 W at 9:30-10:00 AM. This trend of increasing useful heat gain for 60 l/hr as compare to other mass flow rates continues up to 3:00 PM. It is also observed that the useful heat gain decreases gradually for 20 & 40 l/hr mass flow rates from 11:30-3:00 PM & for 60 l/hr from 1:00-3:00 PM. From the graph it is clear that the trend of increasing useful heat gain continues with increasing mass flow rates from 9:30 AM onwards up to 3:00 PM.

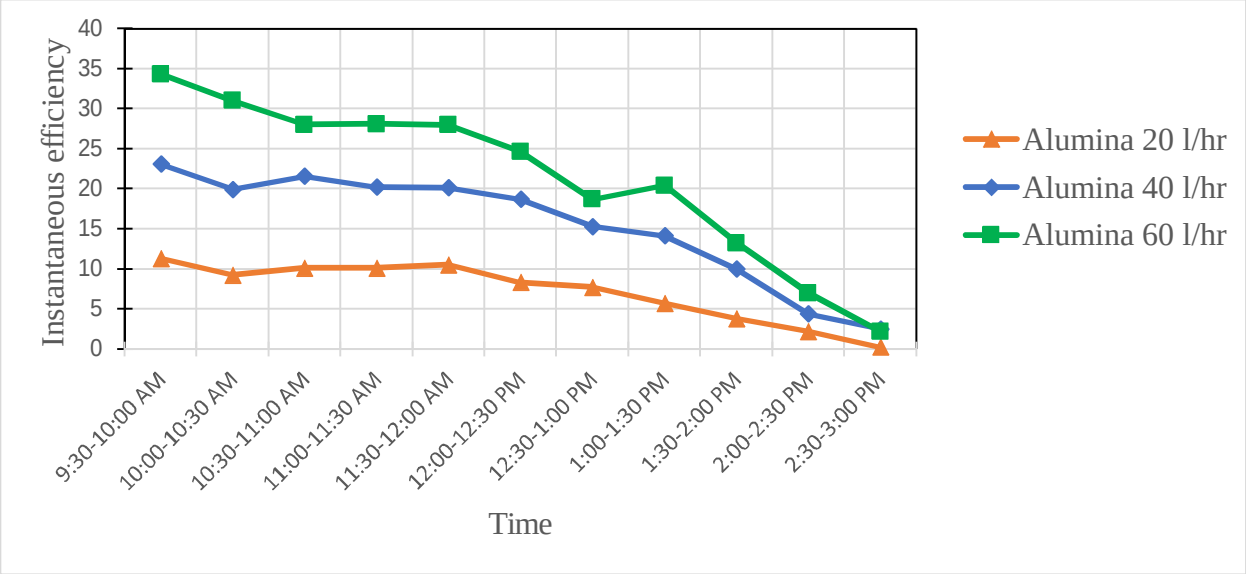

Figure 5.28: Variation in instantaneous efficiency w.r.t. time for water based alumina (0.05%) nanofluid at different mass flow rates

Figure 5.28 shows the variation in instantaneous efficiency w.r.t. time for water based alumina nanofluid with 0.05% volume concentration at different mass flow rates. From the graph it is observed that the instantaneous efficiency increases with increasing mass flow rates. For 60 l/hr mass flow rate the efficiency reaches its highest peak value of 34.33% at 9:30-10:00 AM. For 20 l/hr mass flow rate the efficiency gradually decreases from 11:30 AM to 3:00 PM, for 40 l/hr from 10:30 AM to 3:00 PM, & for 60 l/hr from 1:00-3:00 PM. From the graph it is clear that the trend of increasing instantaneous efficiency continues with increasing mass flow rates from 9:30 AM onwards up to 3:00 PM.

Figure 5.29 shows the variation in thermal efficiency w.r.t. time for water based alumina nanofluid with 0.05% volume concentration at different mass flow rates.

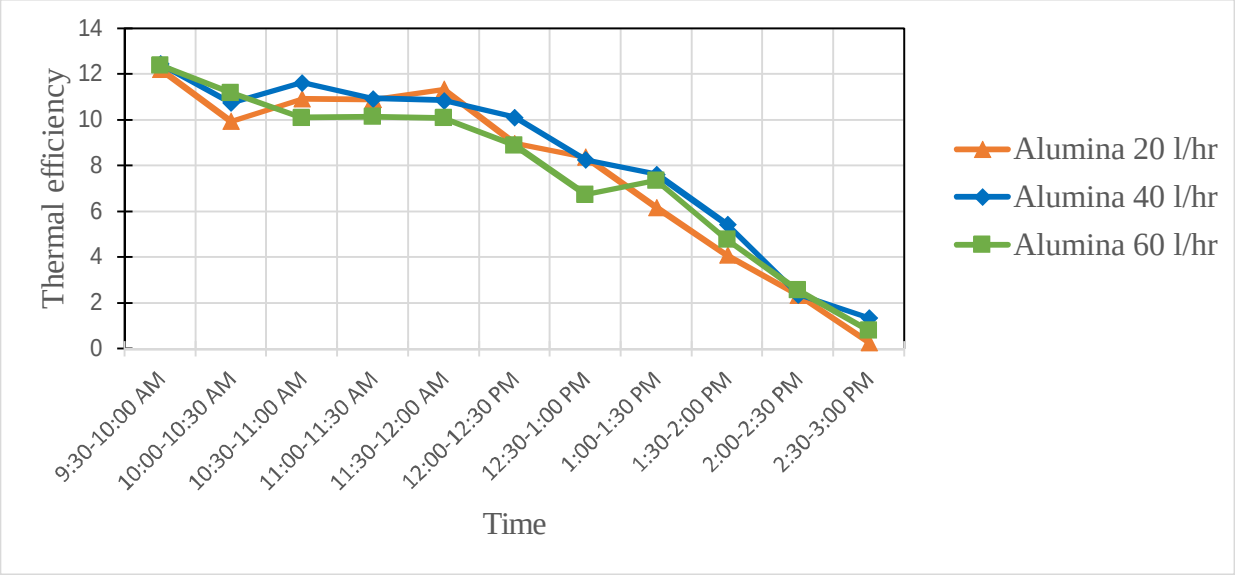

Figure 5.29: Variation in thermal efficiency w.r.t. time for water based alumina (0.05%) nanofluid at different mass flow rates

From the graph it is observed that at 9:30-10:00 AM for 40 l/hr mass flow rate the thermal efficiency increases by 0.24% as compare to 20 l/hr and by 0.07% as compare to 60 l/hr. On the other hand, 20 l/hr mass flow rate shows higher value of efficiency at 11:30-12:00 AM, 40 l/hr mass flow rate shows higher value of efficiency at 10:30-11:30 AM, at 12:00-12:30-PM, at 1:00-2:00 PM, & at 2:30-3:00 PM , 60 l/hr mass flow rate shows higher value of efficiency at 10:00-10:30 AM & at 2:00-2:30 PM

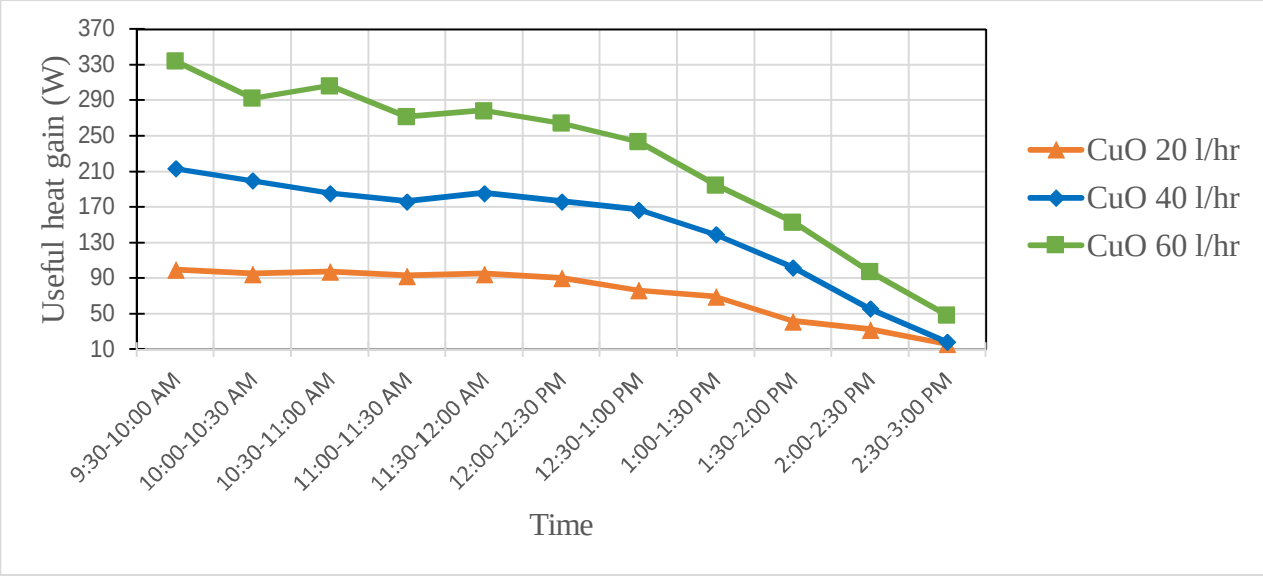

Figure 5.30: Variation in useful heat gain w.r.t. time for water based CuO (0.01%) nanofluid at different mass flow rates

Figure 5.30 shows the variation in useful heat gain w.r.t. time for water based CuO nanofluid with 0.01% volume concentration at different mass flow rates. From the graph it is observed useful heat gain increases with increasing mass flow rate for water based copper oxide nanofluid. It is noted that for the mass flow rate of 60 l/hr the highest peak value of useful heat gain is obtained as 334.33 W at 9:30-10:00 AM. This trend of increasing useful heat gain for 60 l/hr as compare to other mass flow rates continues up to 3:00 PM. It is also observed that the useful heat gain decreases gradually for 20, 40 & 60 l/hr at the same interval from 11:30 AM to 3:00 PM. From the graph it is clear that the trend of increasing useful heat gain continues with increasing mass flow rates from 9:30 AM onwards up to 3:00 PM.

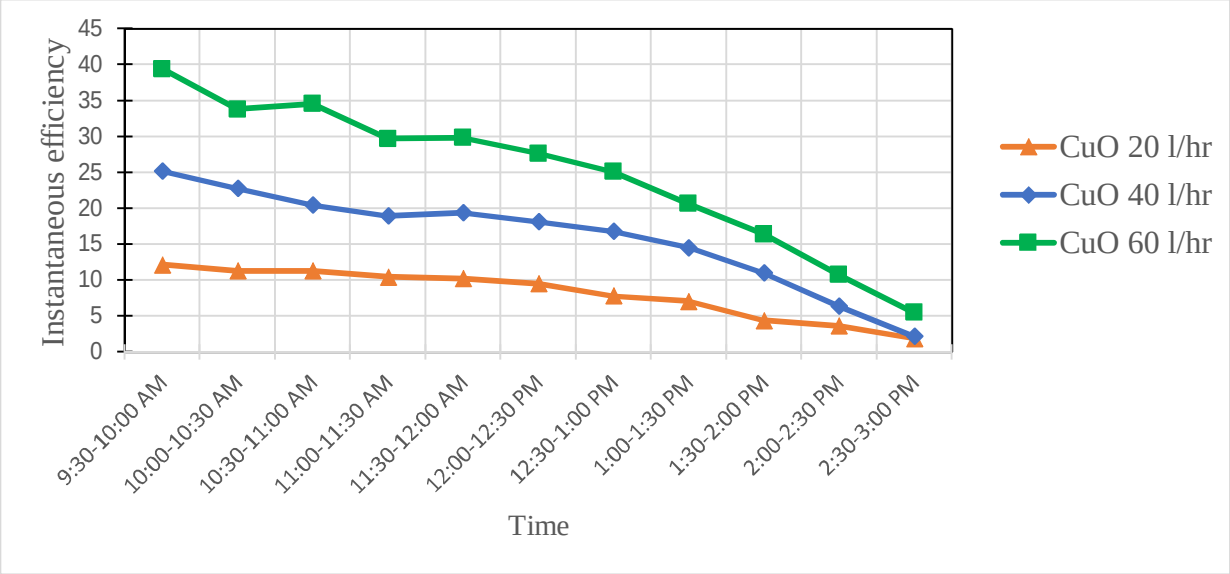

Figure 5.31: Variation in instantaneous efficiency w.r.t. time for water based CuO (0.01%) nanofluid at different mass flow rates

Figure 5.31 shows the variation in instantaneous efficiency w.r.t. time for water based CuO nanofluid with 0.01% volume concentration at different mass flow rates. From the graph it is observed that the instantaneous efficiency increases with increasing mass flow rates. For 60 l/hr mass flow rate the efficiency reaches its highest peak value of 39.39% at 9:30-10:00 AM. On the other hand for 20 l/hr mass flow rate the efficiency gradually decreases from 10:30-3:00 PM, for 40 l/hr from 11:30-3:00 PM, & for 60 l/hr from 11:30-3:00 PM. From the graph it is clear that the trend of increasing instantaneous efficiency continues with increasing mass flow rates from 9:30 AM onwards up to 3:00 PM.

Figure 5.32 shows the variation in thermal efficiency w.r.t. time for water based CuO nanofluid with 0.01% volume concentration at different mass flow rates.

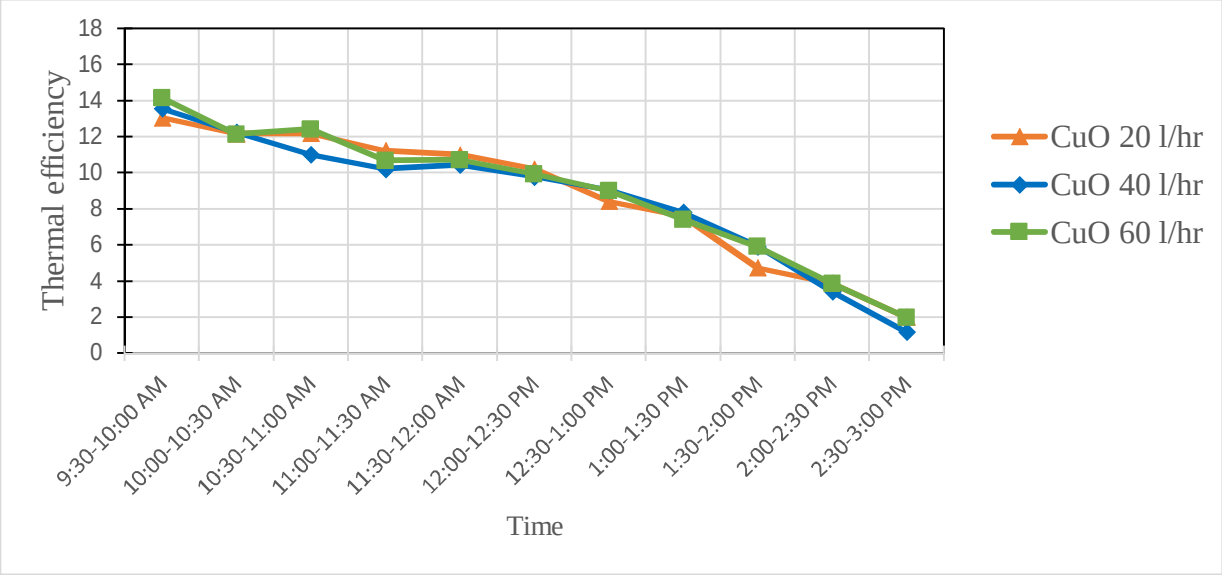

Figure 5.32: Variation in thermal efficiency w.r.t. time for water based CuO (0.01%) nanofluid at different mass flow rates

From the graph it is observed that at 9:30-10:00 AM for 60 l/hr mass flow rate the thermal efficiency increases by 0.59% as compare to 40 l/hr and by 1.1% as compare to 20 l/hr. On the other hand, 20 l/hr mass flow rate shows higher value of efficiency from 11:00 AM to 12:30 PM & from 2:00-3:00 PM, 40 l/hr mass flow rate shows higher value of efficiency at 10:00-10:30 AM & 1:00-1:30 PM, 60 l/hr mass flow rate shows higher value of efficiency at 9:30-10:00 PM & at 10:30-11:00 AM.

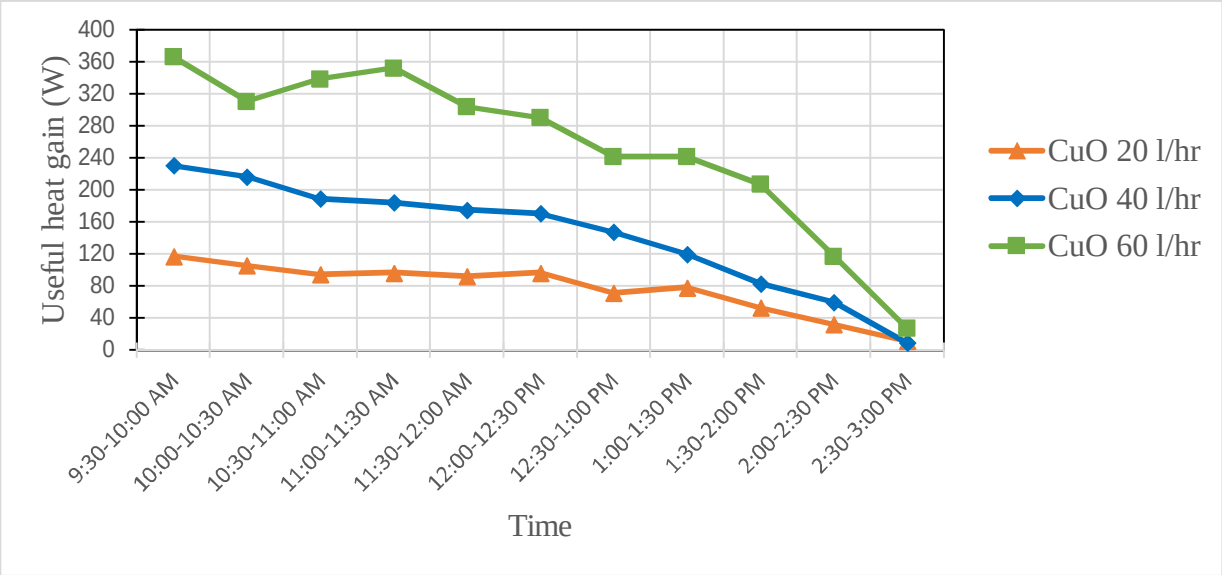

Figure 5.33: Variation in useful heat gain w.r.t. time for water based CuO (0.05%) nanofluid at different mass flow rates

Figure 5.33 shows the variation in useful heat gain w.r.t. time for water based CuO nanofluid with 0.05% volume concentration at different mass flow rates. From the graph it is observed useful heat gain increases with increasing mass flow rate for water based copper oxide nanofluid. It is noted that for the mass flow rate of 60 l/hr the highest peak value of useful heat gain is obtained as 366.39W at 9:30-10:00 AM. This trend of increasing useful heat gain for 60 l/hr as compare to other mass flow rates continues up to 3:00 PM. It is also observed that the useful heat gain decreases gradually for 20 l/hr from 1:00 to 3:00 PM, for 40 l/hr from 9:30 to 3:00 PM & for 60 l/hr from 11:00 AM to 3:00PM. From the graph it is clear that the trend of increasing useful heat gain continues with increasing mass flow rates from 9:30 AM onwards up to 3:00 PM.

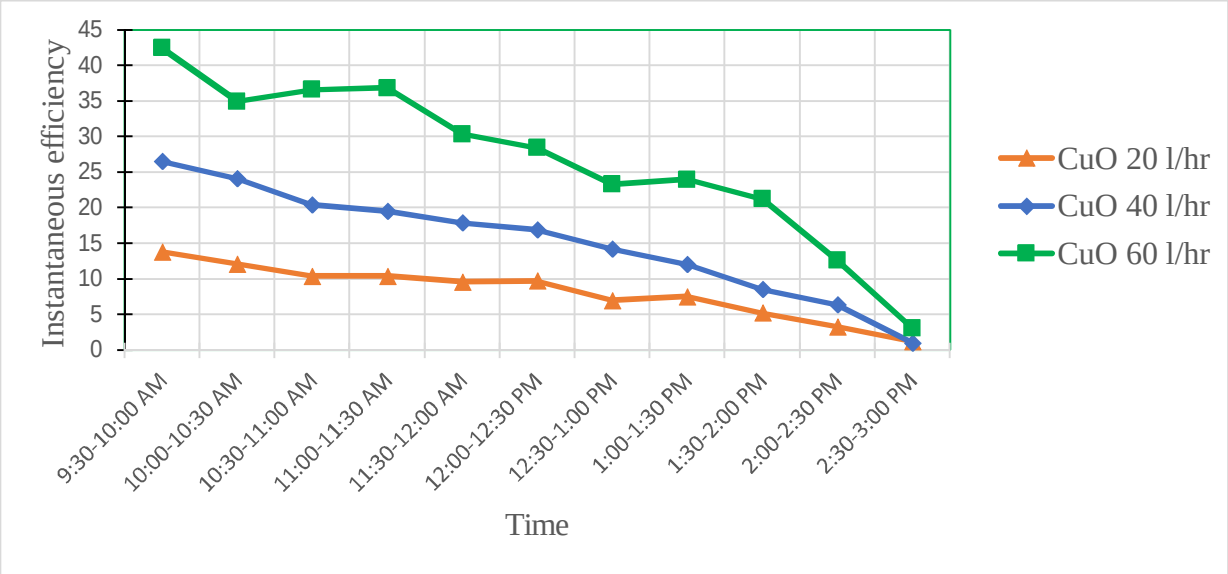

Figure 5.34: Variation in instantaneous efficiency w.r.t. time for water based CuO (0.05%) nanofluid at different mass flow rates

Figure 5.34 shows the variation in instantaneous efficiency w.r.t. time for water based CuO nanofluid with 0.05% volume concentration at different mass flow rates. From the graph it is observed that the instantaneous efficiency increases with increasing mass flow rates. For 60 l/hr mass flow rate the instantaneous efficiency reaches its highest peak value of 42.45% at 9:30-10:00 AM. On the other hand for 20 l/hr mass flow rate the efficiency gradually decreases from 1:00-3:00 PM, for 40 l/hr from 9:30-3:00 PM, & for 60 l/hr from 1:00-3:00 PM. From the graph it is clear that the trend of increasing instantaneous efficiency continues with increasing mass flow rates from 9:30 AM onwards up to 3:00 PM.

Figure 5.35 shows the variation in thermal efficiency w.r.t. time for water based CuO nanofluid with 0.05% volume concentration at different mass flow rates.

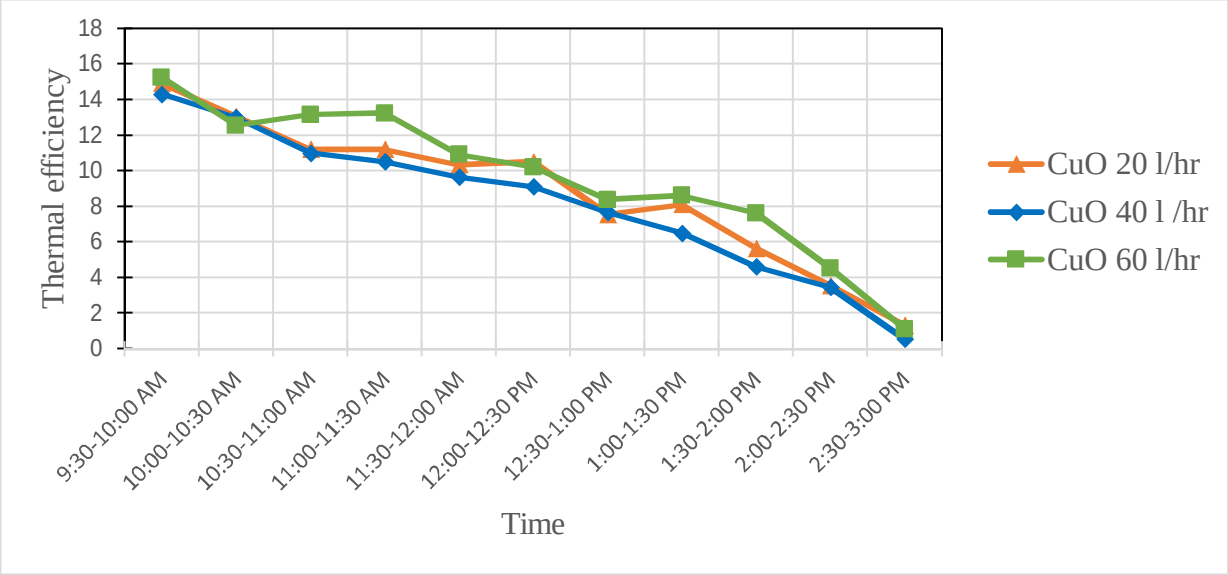

Figure 5.35: Variation in thermal efficiency w.r.t. time for water based CuO (0.05%) nanofluid at different mass flow rates

From the graph it is observed that at 9:30-10:00 AM for 60 l/hr mass flow rate the thermal efficiency increases by 0.93% as compare to 40 l/hr and by 0.35% as compare to 20 l/hr. On the other hand, 20 l/hr mass flow rate shows higher value of efficiency at 12:00-12:30 AM, 40 l/hr mass flow rate shows higher value of efficiency at 10:00-10:30 AM, 60 l/hr mass flow rate shows higher value of efficiency from 10:30 to 12:00 PM & from 12:30 to 2:30 PM. Lastly, we can say that the maximum increasing trend of thermal efficiency value is observed at higher mass flow rates.

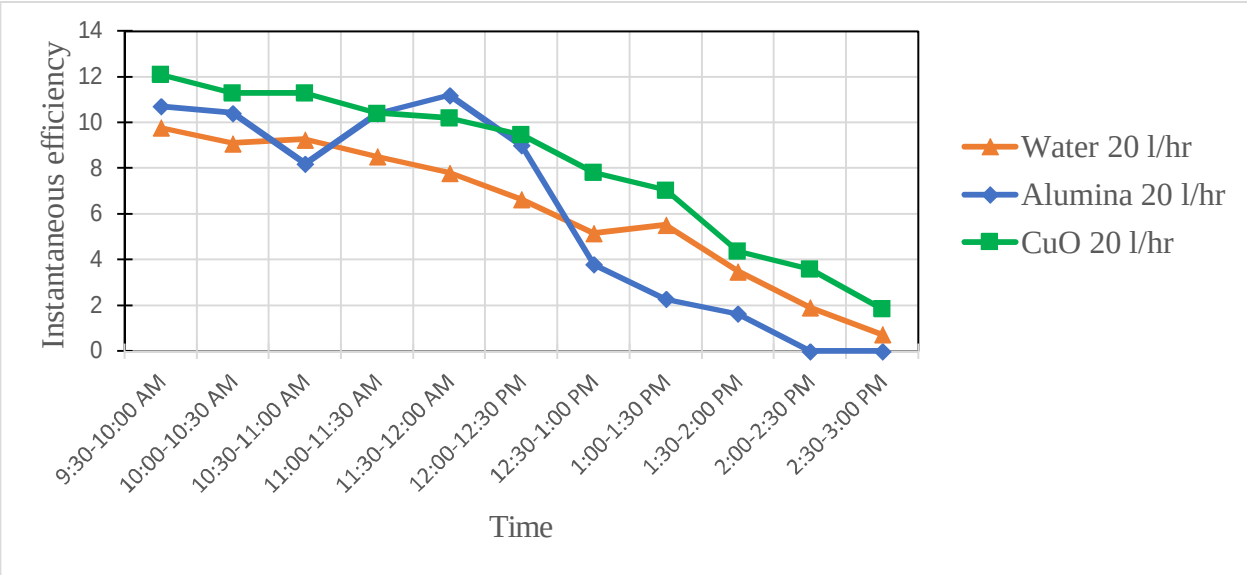

Figure 5.36: Comparison of instantaneous efficiency w.r.t. time for water & water based alumina and CuO (0.01%) nanofluid at 20 l/hr mass flow rate

Figure 5.36 shows the comparison of instantaneous efficiency w.r.t. time for water & water based alumina and CuO nanofluid with 0.01% volume concentration at 20 l/hr mass flow rate. From the graph it is observed that the copper oxide nanofluid shows higher efficiency from 9:30-11:30 AM & from 12:00-3:00 PM in comparison with alumina nanofluid & water. If we talk about alumina nanofluid, it shows higher efficiency than water from 9:30 to 10:30 AM & from 11:00 AM to 12:30 PM because of higher temperature difference & lower intensity of radiations. But there is sudden drop also observes in the instantaneous efficiency of alumina at 10:30-11:00 AM than water because of the higher specific heat of water, as instantaneous efficiency directly depends upon specific heat. If specific heat increases efficiency increases. From 12:30-3:00 PM water has higher efficiency because of the higher specific heat & faster variation in temperature difference as compare to alumina nanofluid. The overall maximum value of instantaneous efficiency for CuO is 12.11% at 9:30-10:00 AM, for alumina is 11.2% at 11:30-12:00 PM & with water is 9.79% at 9:30-10:00 AM. It is noted that at the time interval from 11:30 to 12:00 PM the efficiency of alumina is higher than CuO because of its higher specific heat and increased temperature difference as compare to copper oxide nanofluid at this time interval.

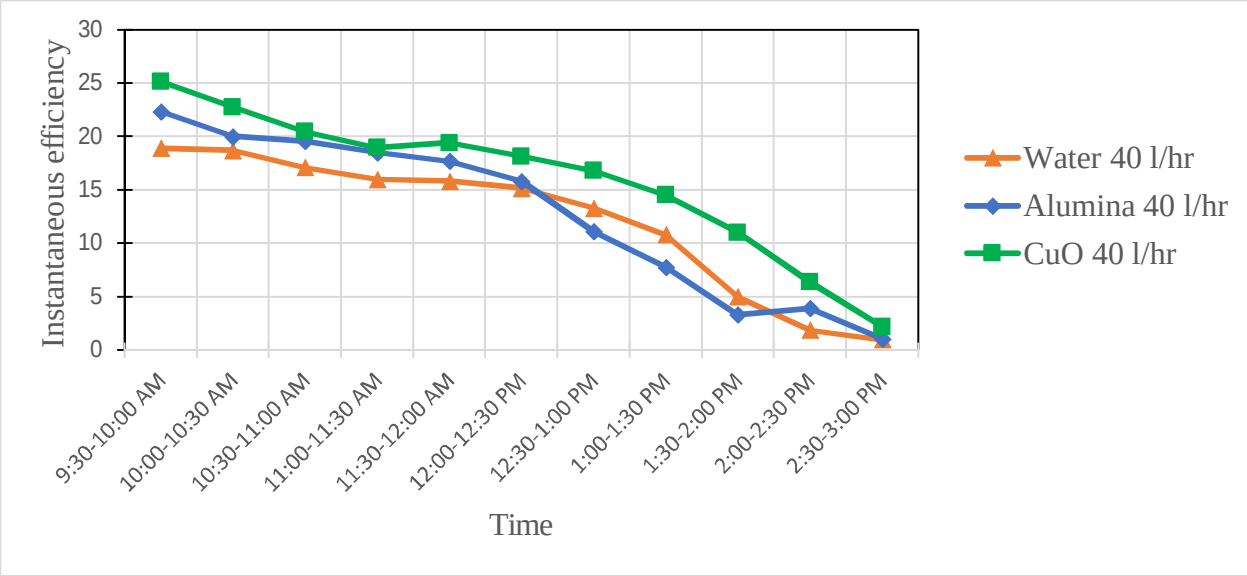

Figure 5.37: Comparison of instantaneous efficiency w.r.t. time for water & water based alumina and CuO (0.01%) nanofluid at 40 l/hr mass flow rate

Figure 5.37 shows the comparison of instantaneous efficiency w.r.t. time for water & water based alumina and CuO nanofluid with 0.01% volume concentration at 40 l/hr mass flow rate. From the graph it is observed that the copper oxide nanofluid shows the higher efficiency at the time interval from 9:30 AM to 3:00 PM in comparison with water & alumina nanofluid.

On the other hand, alumina nanofluid shows higher efficiency from 9:30 to 12:30 PM & at 2:00 to 3:00 PM in comparison with water because of higher temperature difference & lower intensity of radiations. Water shows higher efficiency as compare to alumina nanofluid from 12:30 to 2:00 PM because of its higher specific heat value. The overall maximum value of instantaneous efficiency for CuO is 25.17%, for alumina is 22.35% & for water is 18.91% at 9:30-10:00 AM.

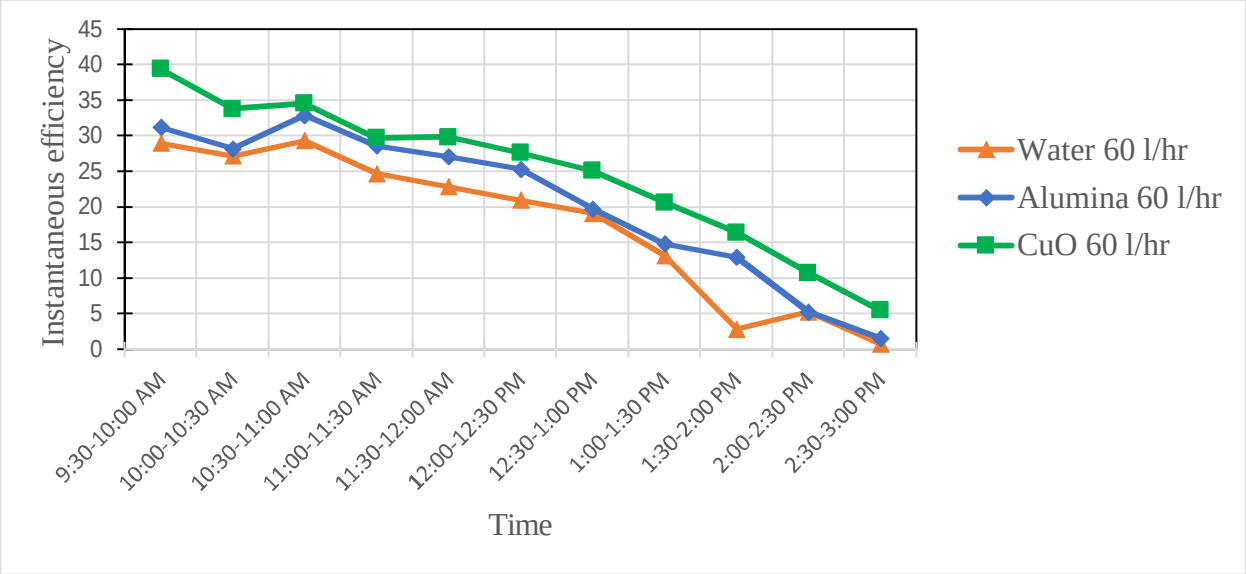

Figure 5.38: Comparison of instantaneous efficiency w.r.t. time for water & water based alumina and CuO (0.01%) nanofluid at 60 l/hr mass flow rate

Figure 5.38 shows the comparison of instantaneous efficiency w.r.t. time for water & water based alumina and CuO nanofluid with 0.01% concentration at 60 l/hr mass flow rate. From the graph it is observed that copper oxide nanofluid shows the higher efficiency at the time interval from 9:30 AM to 3:00 PM because of faster variation in temperature difference. Hence, similar trend of increasing efficiency is observed as discussed above for 40 l/hr mass flow rate. On the other hand, alumina nanofluid shows higher efficiency as compare to water at the time interval from 9:30 AM to 3:00 PM because of higher temperature difference than water. The overall maximum value of instantaneous efficiency for CuO is 39.39% at 9:30-10:00 AM, for alumina is 32.9% at 10:30-11:00 AM & for water is 29.34% at 10:30-11:00 AM.

Figure 5.39 shows the comparison of instantaneous efficiency w.r.t. time for water & water based alumina and CuO nanofluid with 0.05% volume concentration at 20 l/hr mass flow rate. From the graph it is observed that the copper oxide nanofluid shows higher efficiency at 9:30-11:30 AM, at 12:00-12:30 PM & from 1:00-3:00 PM in comparison with water and alumina nanofluid.

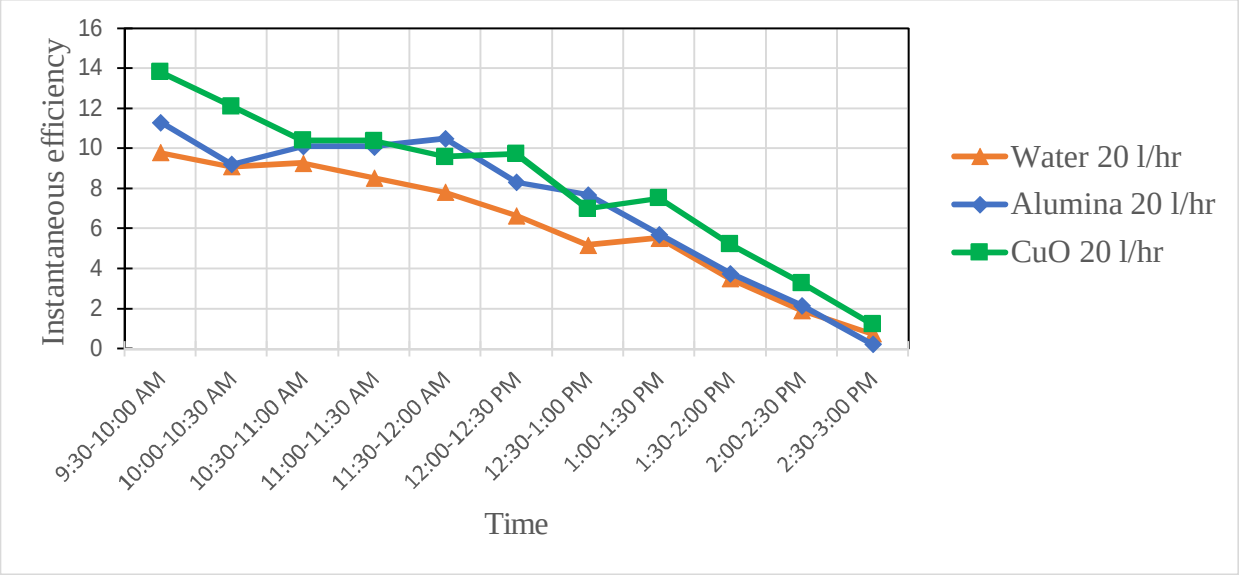

Figure 5.39: Comparison of instantaneous efficiency w.r.t. time for water & water based alumina and CuO (0.05%) nanofluid at 20 l/hr mass flow rate

On the other hand, alumina nanofluid shows higher efficiency from 9:30 AM to 2:30 PM as compare to water because of the lower intemsity of radiations. CuO nanofluid shows the reverse trend in the efficiency at 11:30-12:00 PM & at 12:30-1:00 PM because of the lower specific heat than water and alumina nanofluid. The overall maximum value of instantaneous efficiency for CuO is 13.83%, for alumina is 11.32% & for water is 9.79% at the same interval from 9:30-10:00 AM.

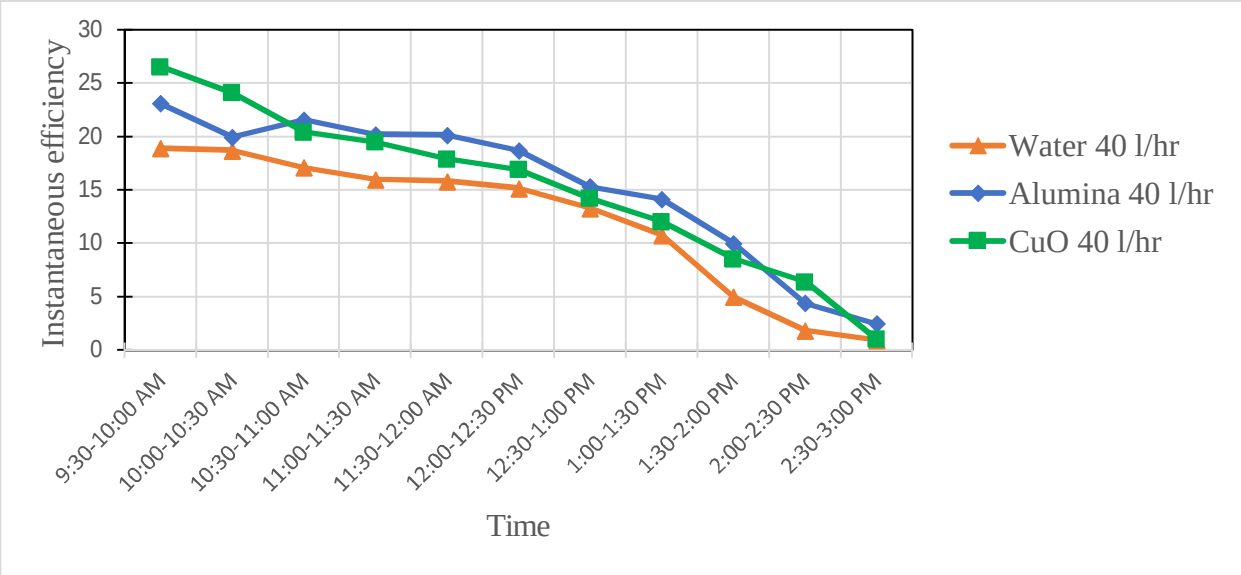

Figure 5.40: Comparison of instantaneous efficiency w.r.t. time for water & water based alumina and CuO (0.05%) nanofluid at 40 l/hr mass flow rate

Figure 5.40 shows the comparison of instantaneous efficiency w.r.t. time for water & water based alumina and CuO nanofluid with 0.05% volume concentration at 40 l/hr mass flow rate. From the graph it is observed that the alumina nanofluid shows the higher efficiency from 10:30-2:00 PM & at 2:30-3:00 PM in comparison with water and copper oxide nanofluid. As instantaneous efficiency is inversely proportional to solar intensity that is if the solar intensity decreases the efficiency increases. The efficiency of alumina nanofluid shows higher efficiency because of the lower values of solar intensity and slower variation in temperature difference at all above mentioned time intervals. It is also observed that CuO nanofluid shows higher efficiency from 9:30-10:30 AM & at 2:00-2:30 PM in comparison with water & alumina nanofluid because of higher temperature difference. The overall maximum value of instantaneous efficiency for CuO is 26.56%, for alumina is 23.1% & for water is 18.91% at the same interval at 9:30-10:00 AM.

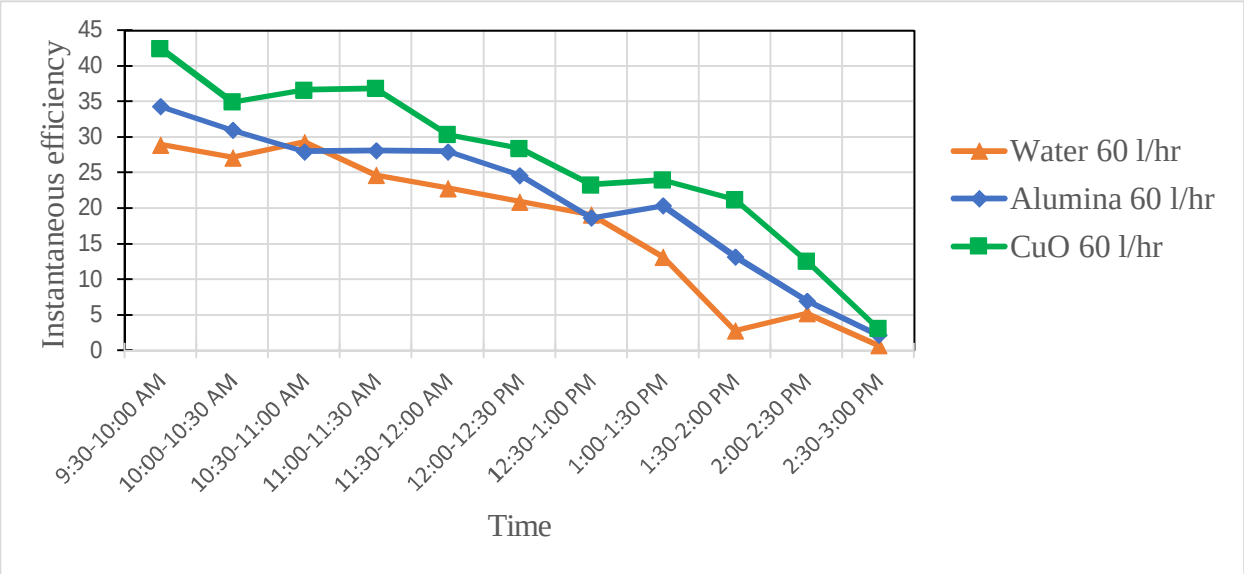

Figure 5.41: Comparison of instantaneous efficiency w.r.t. time for water & water based alumina and CuO (0.05%) nanofluid at 60 l/hr mass flow rate

Figure 5.41 shows the comparison of instantaneous efficiency w.r.t. time for water & water based alumina and CuO nanofluid with 0.05% volume concentration at 60 l/hr mass flow rate. From the graph it is observed that the CuO nanofluid shows the higher efficiency from 9:30 AM to 3:00 PM in comparison with water & alumina nanofluid because of faster variation in temperature difference at these time periods. On the other hand, alumina nanofluid shows the higher efficiency at 9:30-10:30 AM, from 11:00-12:30 PM & from 1:00-3:00 PM because of the faster variation in the temperature difference as compare to water. Water shows maximum value of efficiency at 10:30-11:00 AM & at 12:30-1:00 PM as compare to alumina nanofluid

because of higher specific heat value. The overall maximum value of instantaneous efficiency for CuO is 42.45%, for alumina is 34.33% at 9:30-10:00 AM & for water is 29.34% at 10:30-11:00 AM.

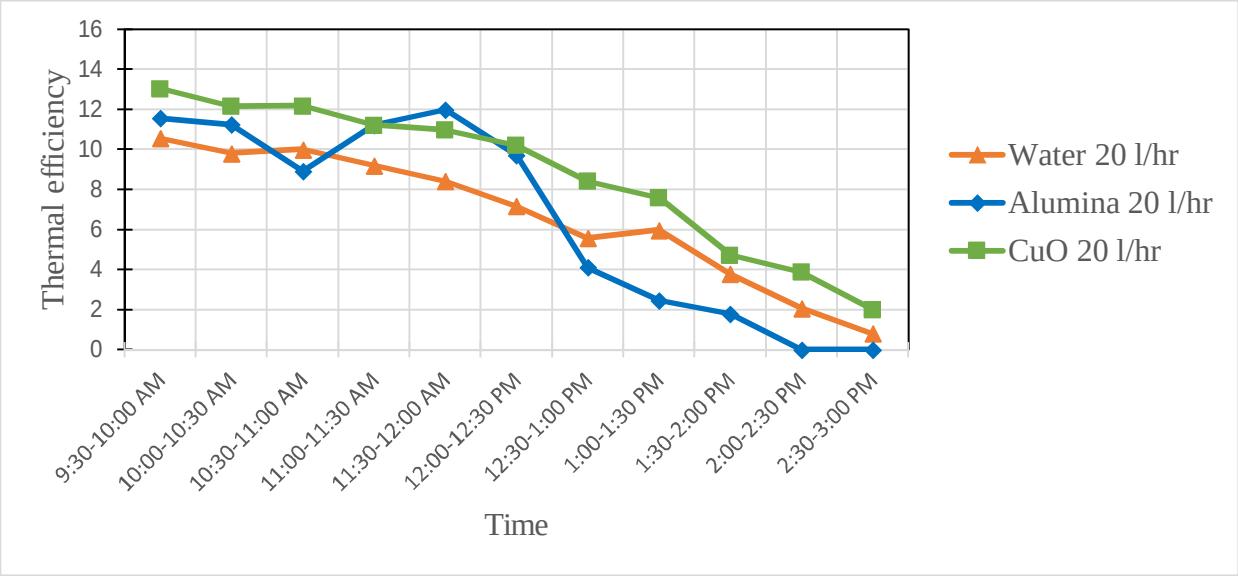

Figure 5.42: Comparison of thermal efficiency w.r.t. time for water & water based alumina and CuO (0.01%) nanofluid at 20 l/hr mass flow rate

Figure 5.42 shows the comparison of thermal efficiency w.r.t. time for water & water based alumina and CuO nanofluid with 0.01% volume concentration at 20 l/hr mass flow rate. From the graph it is analysed that the CuO nanofluid shows the higher efficiency from 9:30-11:30 AM & from 12:00-3:00 PM because of the faster variation in the temperature difference in comparison with water & alumina naniofluid. On the other hand, alumina nanofluid shows the higher efficiency from 9:30-10:30 AM & from 11:00-12:30 PM in comparison with water because of faster variation in the temperature difference and lower intensity of radiation. From the graph it is also noted that the alumina nanofluid shows the higher peak value of efficiency at 11:30-12:00 PM in as compare to CuO nanofluid because of higher value of specific heat by the amount 90.02 J/kgK and higher temperature difference. The overall maximum value of instantaneous efficiency for CuO is 13.05% and for water is 10.56% at 9:30-10:00 AM & for alumina is 11.99% at 11:30-12:00 PM.

Figure 5.43 shows the comparison of thermal efficiency w.r.t. time for water & water based alumina and CuO nanofluid with 0.01% volume concentration at 40 l/hr mass flow rate. From the graph it is observed that the CuO nanofluid shows the higher efficiency continuously from 9:30 AM to 3:00 PM in comparison water & alumina naniofluid because of higher temperature difference.

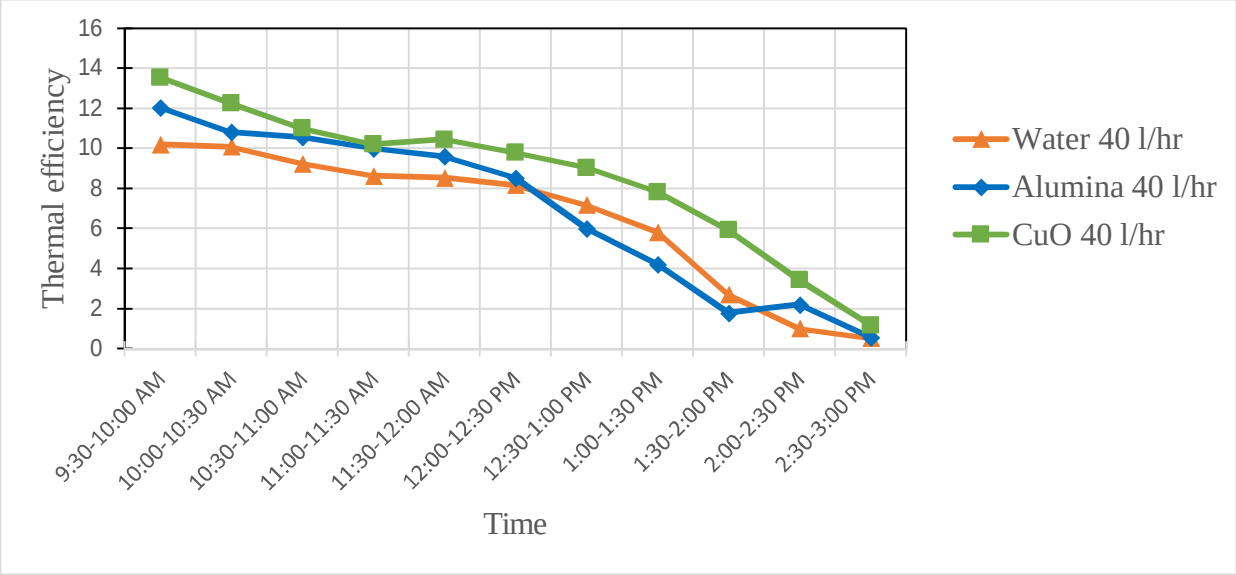

Figure 5.43: Comparison of thermal efficiency w.r.t. time for water & water based alumina and CuO (0.01%) nanofluid at 40 l/hr mass flow rate

It is also observed that the alumina nanofluid shows the higher efficiency from 9:30-12:30 PM & from 2:00-3:00 PM as compare to water because of lower solar intensity and faster variation in temperature difference while on the other hand, water shows higher efficiency from 12:30-2:00 PM as compare to alumina nanofluid because of higher specific heat value & higher temperature difference at these time periods. The overall maximum value of instantaneous efficiency for CuO is 13.56%, for alumina is 12.06% &.for water is 10.20% at the same interval of 9:30-10:00 AM.

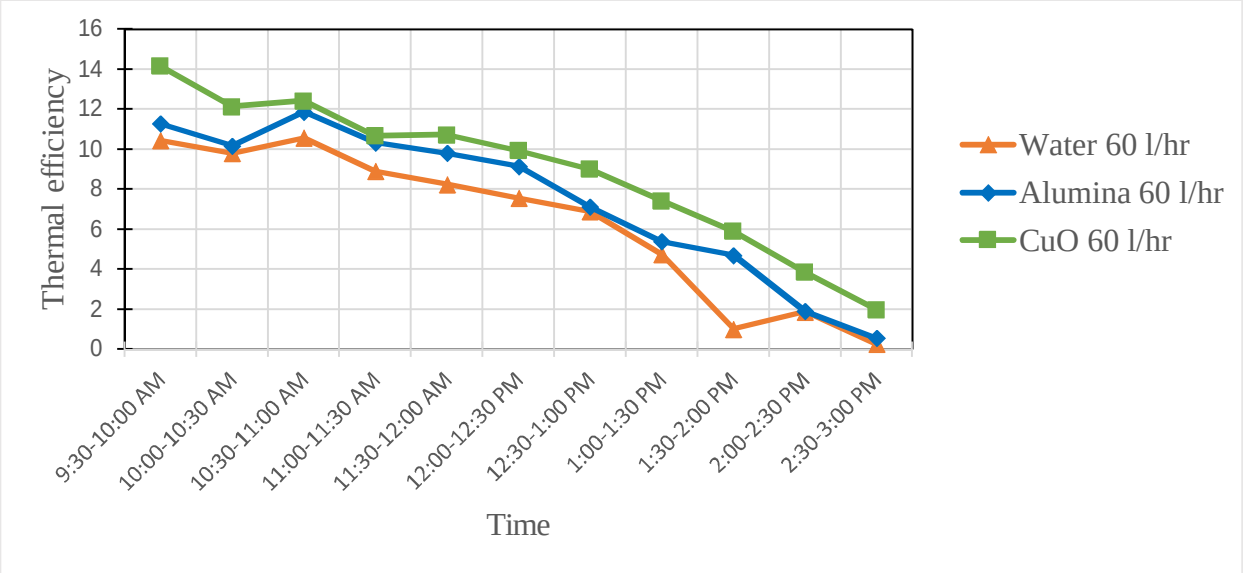

Figure 5.44: Comparison of thermal efficiency w.r.t. time for water & water based alumina and CuO (0.01%) nanofluid at 60 l/hr mass flow rate

Figure 5.44 shows the comparison of thermal efficiency w.r.t. time for water & water based alumina and CuO nanofluid with 0.01% volume concentration at 60 l/hr mass flow rate. From the graph it is observed that the CuO nanofluid shows the higher efficiency at regular intervals from 9:30 AM to 3:00 PM because of faster variation in temperature difference in comparison water & alumina nanofluid. On the other hand it is also observed that the alumina nanofluid shows higher efficiency from 9:30-3:00 PM as compare to water because of lower solar intensity & higher temperature difference. The overall maximum value of instantaneous efficiency for CuO is 14.15% at 9:30-10:00 AM, for alumina is 11.87% &.for water is 10.58% at the same interval of 10:30-11:00AM.

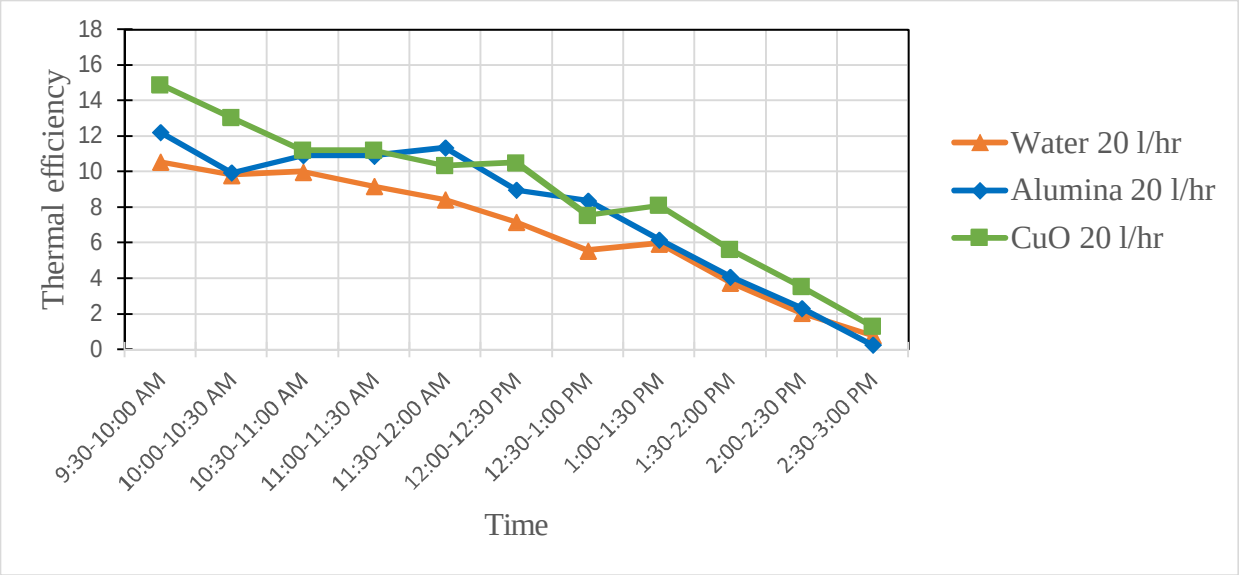

Figure 5.45: Comparison of thermal efficiency w.r.t. time for water & water based alumina and CuO (0.05%) nanofluid at 20 l/hr mass flow rate

Figure 5.45 shows the comparison of thermal efficiency w.r.t. time for water & water based alumina and CuO nanofluid with 0.05% volume concentration at 20 l/hr mass flow rate. From the graph it is observed that the CuO nanofluid shows the higher efficiency from 9:30 to 11:30 AM, at 12:00-12:30 PM & from 1:00 to 3:00 PM because of the faster variation in temperature difference in comparison water & alumina nanofluid. On the other hand alumina nanofluid shows then higher efficiency as compare to water at regular intervals from 9:30 to 2:30 PM because of lower solar intensity & higher temperature difference. If we compare alumina with copper oxide nanofluid we see that the efficiency of alumina nanofluid increases at 11:30-12:00 PM & at 12:30-1:00 PM because of the higher specific heat, higher temperature difference & lower solar intensity. The overall maximum value of thermal efficiency for CuO is 14.9% at

9:30-10:00 AM, for alumina is 12.22% &.for water is 10.56% at the same interval of 9:30-10:00 AM.

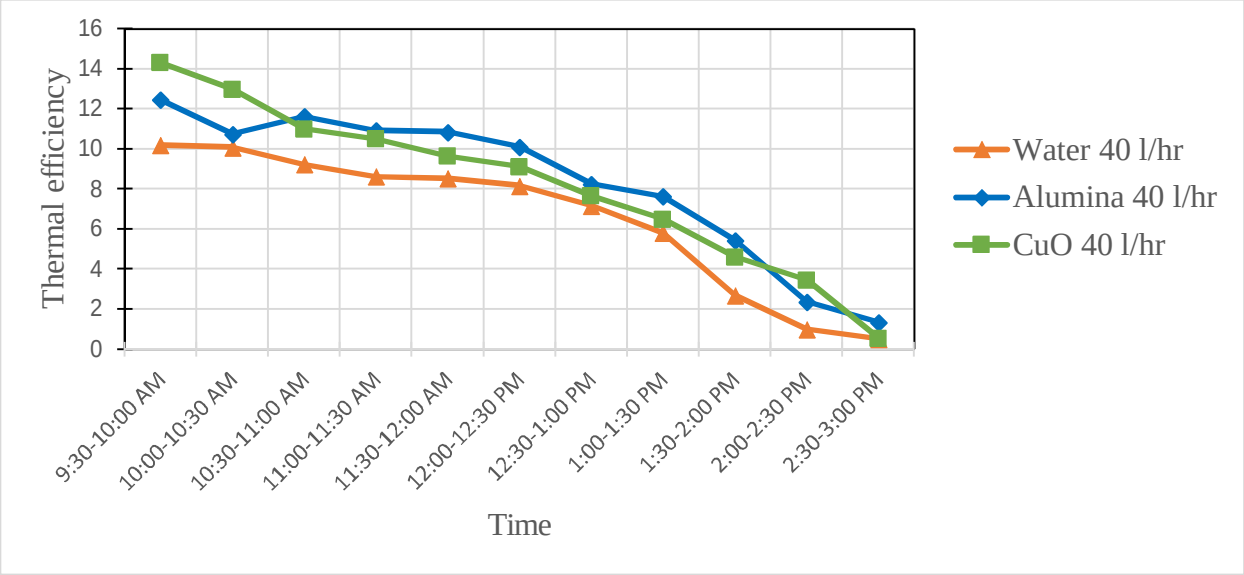

Figure 5.46: Comparison of thermal efficiency w.r.t. time for water & water based alumina and CuO (0.05%) nanofluid at 40 l/hr mass flow rate

Figure 5.46 shows the comparison of thermal efficiency w.r.t. time for water & water based alumina and CuO nanofluid with 0.05% volume concentration at 40 l/hr mass flow rate. From the graph it is observed that the alumina nanofluid shows the higher efficiency from 10:30 to 2:00 PM in comparison with CuO nanofluid & water because of lower values of solar intensity and slower variation in temperature difference at all mentioned time intervals. The CuO nanofluid shows higher efficiency at 9:30-10:30 AM & at 2:00-2:30 PM because of faster variation in temperature difference in comparison with water & alumina nanofluid. If we compare alumina nanofluid with CuO nanofluid we see that for 0.05% concentration efficiency of CuO nanofluid is lowered from 10:30 AM to 2:00 PM & at 2:30-3:00 PM because of its lower value of specific heat value & higher solar intensity. The overall maximum value of thermal efficiency for CuO is 14.32% at 9:30-10:00 AM, for alumina is 12.46% &.for water is 10.2% at the same interval of 9:30-10:00AM.

Figure 5.47 shows the comparison of thermal efficiency w.r.t. time for water & water based alumina and CuO nanofluid with 0.05% volume concentration at 60 l/hr mass flow rate. From the graph it is observed that the CuO nanofluid shows the higher efficiency at regular intervals from 9:30 AM to 3:00 PM in comparison water & alumina nanofluid because of higher temperature difference & higher intensity of radiations.

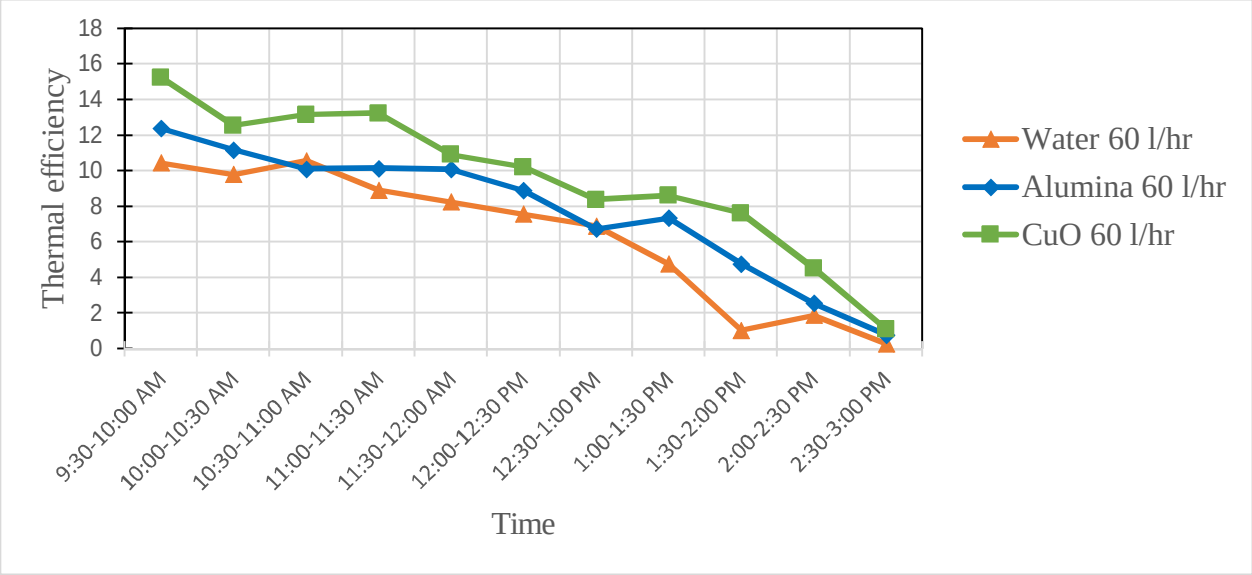

Figure 5.47: Comparison of thermal efficiency w.r.t. time for water & water based alumina and CuO (0.05%) nanofluid at 60 l/hr mass flow rate

On the other hand, alumina nanofluid shows higher efficiency as compare to water from 9:30 to 10:30 AM, 11:00 to 12:30 PM & 1:00 to 3:00 PM only because of the faster variation in temperature difference and lower intensity of radiations at these time intervals. Whereas, on the other hand, water shows higher efficiency at 10:30-11:00 AM as compare to alumina nanofluid because of higher specific heat value, lower value of solar intensity. The overall maximum value of thermal efficiency for CuO is 15.25% at 9:30-10:00 AM, for alumina is 12.39% at the same interval of 9:30-10:00AM. &.for water is 10.58% at 10:30-11:00 PM.

CHAPTER-6

CONCLUSIONS

The purpose of this thesis work is to check the performance of parabolic concentrating solar collector by using water, water based aluminium oxide (Al_2O_3) & copper oxide (CuO) nanofluid as the working fluids. Two volume concentrations (0.01% & 0.05%) of nanoparticles have been used to prepare nanofluids.

- It is concluded that the higher outlet temperatures are obtained by using copper oxide as a working fluid as compare to water & aluminium oxide nanofluid at both concentrations that is 0.01 & 0.05 in percent. On the other side, if we talk about aluminium oxide nanofluid it shows higher outlet temperatures at both concentrations as mentioned above in comparison with water.

6.1 Comparison Results of CuO Nanofluid vs. Water

By using copper oxide (CuO) nanofluid as a working fluid with 0.01% concentration:-

- Collector's instantaneous efficiency is improved from 0.88 to 2.83%, 1.24 to 6.26%, and 4.74 to 13.57% for 20, 40 & 60 l/hr mass flow rates.
- Collector's thermal efficiency is improved from 0.95 to 3.05%, 0.66 to 3.36%, and 1.7 to 4.87% for 20, 40 & 60 l/hr mass flow rates.

By using copper oxide (CuO) nanofluid as a working fluid with 0.05% concentration:-

- Collector's instantaneous efficiency is improved from 0.47 to 4.04%, 0.07 to 7.65%, and 2.32 to 18.4% for 20, 40 & 60 l/hr mass flow rates.
- Collector's thermal efficiency is improved from 0.51 to 4.34%, 0.03 to 4.12%, and 0.83 to 6.6% for 20, 40 & 60 l/hr mass flow rates.

6.2 Comparison Results of CuO Nanofluid vs. Alumina Nanofluid

By using copper oxide (CuO) nanofluid as a working fluid with 0.01% concentration:-

- Collector's instantaneous efficiency is improved from 0.02 to 4.77%, 0.45 to 7.71%, and 1.1 to 8.16% for 20, 40 & 60 l/hr mass flow rates.
- Collector's thermal efficiency is improved from 0.5 to 5.14%, 0.21 to 4.15%, and 0.33 to 2.88% for 20, 40 & 60 l/hr mass flow rates.

By using copper oxide (CuO) nanofluid as a working fluid with 0.05% concentration:-

- Collector's instantaneous efficiency is improved from 0.28 to 2.89%, 2.02 to 4.17%, and 0.9 to 8.75% for 20, 40 & 60 l/hr mass flow rates.
- Collector's thermal efficiency is improved from 0.29 to 2.68%, 1.09 to 2.24%, and 0.32 to 3.06% for 20, 40 & 60 l/hr mass flow rates.

6.3 Comparison Results of Alumina Nanofluid vs. Water

By using alumina (Al_2O_3) nanofluid as a working fluid with 0.01% concentration:-

- Collector's instantaneous efficiency is enhanced from 0.92 to 3.39%, 0.1 to 3.44%, and 0.02 to 10.1% for 20, 40 & 60 l/hr mass flow rates.
- Collector's thermal efficiency is enhanced from 1 to 2.55%, 0.05 to 1.86%, and 0.01 to 3.67% for 20, 40 & 60 l/hr mass flow rates.

By using alumina (Al_2O_3) nanofluid as a working fluid with 0.05% concentration

- Collector's instantaneous efficiency is enhanced from 0.12 to 2.69%, 1.26 to 5.01%, and 1.42 to 10.37% for 20, 40 & 60 l/hr mass flow rates.
- Collector's thermal efficiency is enhanced from 0.13 to 2.92%, 0.68 to 2.75%, and 0.51 to 3.74% for 20, 40 & 60 l/hr mass flow rates.

6.4 Comparison Results of Alumina Nanofluid vs CuO Nanofluid

By using alumina (Al_2O_3) nanofluid as a working fluid with 0.05% concentration

- Collector's instantaneous efficiency is enhanced from 0.68 to 2.21%, for 40 l/hr mass flow rates because of lower intensity of radiations & slower variation in temperature difference from 10:30 AM to 2:00 PM.
- Collector's thermal efficiency is enhanced from 0.42 to 1.2%, for 40 l/hr mass flow rates because of lower intensity of radiations & slower variation in temperature difference from 10:30 AM to 2:00 PM.

CHAPTER-7

FUTURE & SCOPE

There is a lot of scope in the field of solar energy harvesting using nanofluid-based concentrating parabolic solar collector (NCPSC) system. In the present experimental work we took fixed dimensions & same material of receiver tube, glass cover tube, and parabolic collector & take only one size of nanoparticles. In addition, thermophysical properties (density, specific heat, viscosity & thermal conductivity) are taken at standard temperature.

In the future various investigations will be carried out to check out the performance of parabolic collectors are given as follows:-

1. By varying the dimensions (length, diameter) of the receiver tube and glass cover tube.
2. By varying the dimensions (length, height) of parabolic collector.
3. By changing the material of receiver tube & glass cover tube such as quartz or Pyrex glass.
4. By changing the material of reflector such as stainless steel sheet, aluminium sheet or aluminium sheet.
5. By changing the size of nanoparticle and try with different concentrations with different base fluids other than water like with ethanol or therminol-VP1.
6. Calculate thermophysical properties (density, specific heat, viscosity & thermal conductivity of nanofluid at varying temperatures.
7. By using air as a working medium instead of using nanofluids with the help of blower.
8. By using automatic tracking system in place of manual tracking system.

REFERENCES

Barlev D., Vidu R. , Stroeve P., (2011), Innovation in concentrated solar power, *"Solar Energy Materials & Solar Cells"*, vol. 95, issue 10, pp. 2703–2725.

Chaji H., Ajabshirchi Y., Esmaeilzadeh E., Heris Saeid Z., Hedayatizadeh M. , Kahani M., (2013), Experimental study on thermal efficiency of flat plate solar collector using TiO_2/Water nanofluid, *"Modern Applied Science"* published by Canadian Centre of Science and Education, vol. 7, issue 10,pp.60-69.

Chougule Sandesh S., Pise Ashok T., Madane Pravin A.,(2012), Performance of nanofluid-charged solar water heater by solar tracking system, *In: Proceedings of "IEEE-International Conference On Advances In Engineering, Science And Management (ICAESM -2012)" March 30, 31,2012*,pp.247-253.

Chow T.T. (2009), A review on photovoltaic/thermal hybrid solar technology, *"Applied Energy"*, vol. 87, issue 2, pp.365-379.

De Risi A., Milanese M., Laforgia D.,(2013), Modelling and optimization of transparent parabolic trough collector based on gas-phase nanofluids, *"Renewable Energy"*,vol. 58,pp.134-139.

Dr. Kumar D.S., Heat and Mass Transfer, (2009), 7th revised edition, *"S. K. Kataria & Sons publication"*, page 819.

Han D., Meng Z., Wu D., Zhang C., Zhu H.,(2011), Thermal properties of carbon black aqueous nanofluids for solar absorption,*"Nanoscale Research Letters"*,vol. 6,pp.1-7.

Javadi F.S., Sadeghipour S., Saidur R., BoroumandJazi G., Rahmati B., Elias M.M., Sohel M.R.,(2013), The effects of nanofluid on thermophysical properties and heat transfer characteristics of a plate heat exchanger, *"International Communications in Heat and Mass Transfer"*, vol. 44, pp.58-63.

Khullar V., Tyagi H.,(2010), Application of nanofluids as the working fluid in concentrating parabolic solar collectors, *"37th National & 4th International Conference on Fluid Mechanics & Fluid Power"*, IIT Madras, Chennai, India, Dec. 16–18, Paper No. FMFP2010-179.

Khullar V., Tyagi H., (2012a), A study on environmental impact of nanofluid based concentrating solar water heating system, *"International Journal of Environmental Studies"*, vol. 69, issue 2, pp. 220–232.

Khullar V., Tyagi H., Phelan P.E., Otanicar T.P., Singh H., Taylor R.A.,(2012b), Solar energy harvesting using nanofluids-based concentrating solar collector, *"Journal of Nanotechnology in Engineering and Medicine"*, vol. 3 ,pp. 031003-1 to 9.

Lee S., Choi S. U.-S., Li S., Eastman J. A., (1999), Measuring Thermal Conductivity of Fluids Containing Oxide Nanoparticles, *"Journal of Heat Transfer"*,vol. 121, issue 2, pp.280-289.

Maddah H., Rezazadeh M., Maghsoudi M., NasiriKokhdan S., (2013), The effect of silver and aluminium oxide nanoparticles on thermophysical properties of nanofluids, *"Journal of Nanostructure in Chemistry"*, vol. 3, pp.1-6.

Mahian O., Kianifar A. , Kalogirou S. A., Pop I. , Wongwises S., (2013), A review of the applications of nanofluids in solar energy, *"International Journal of Heat and Mass Transfer"*, vol. 57, Issue 2, pp. 582–594.

Mercatelli L., Sani E., Fontani D., Zaccanti G., Martelli F., Di Ninni P.,(2011), Scattering and absorption properties of carbon nanohorn-based nanofluids for solar energy applications, *"Journal of the European Optical Society-Rapid Publications"*, vol. 6, pp.11025-1 to 5.

Natarajan E. & Sathish R., (2009), Role of nanofluids in solar water heater, *"Int J Adv Manuf. Technol."*, special issue, doi 10.1007/s00170-008-1876-8.

Otanicar T.P., Phelan P.E., Prasher R.S., Rosengarten G., and Taylor R.A., (2010), Nanofluid-based direct absorption solar collector, *"Journal of Renewable and Sustainable Energy"*, vol. 2, issue 3,pp. 033102-1 to 13.

Philip John, Shima P.D., (2012), Thermal properties of nanofluids, *"Advances in Colloid and Interface Science"*, vol. 183–184, pp. 30–45.

Reddy K.S., Kumar K. R., (2012), Solar collector field design and viability analysis of standalone parabolic trough power plants for Indian conditions, *"Energy for Sustainable Development"*, vol. 16, Issue 4, pp. 456–470.

Saidur R., Leong K.Y., Mohammad H.A.,(2011), A review on applications and challenges of nanofluids, *"Renewable and Sustainable Energy Reviews"*, vol. 15, Issue 3, pp. 1646–1668.

Saidur R., Meng T.C., Said Z., Hasanuzzaman M., Kamyar A., (2012), Evaluation of the effect of nanofluid-based absorbers on direct solar collector, *"International Journal of Heat and Mass Transfer"*, vol. 55, issues 21–22,pp. 5899–5907.

Sani E., Mercatelli L., Barison S, Pagura C. , Agresti F., Colla L., Sansoni P.,(2011), Potential of carbon nanohorn-based suspensions for solar thermal collectors, *"Solar Energy Materials & Solar Cells"*, vol. 95, Issue 11, pp. 2994–3000.

Sani E., Barison S., Pagura C., Mercatelli L., Sansoni P., Fontani D., Jafrancesco D. and Francini F., (2010), Carbon nanohorns-based nanofluids as direct sunlight absorbers, *"journal optic express"*, vol. 18, issue. 5, pp.1-9.

Sridhara V., Narayan Satapathy L., (2011), Al_2O_3-based nanofluids: a review, *"Nanoscale Research Letters"*, vol. 6, pp.1-16.

Sukhatme S. P., (1984), Solar Energy: Principles of Thermal Collection and Storage, *"Tata McGraw-Hill publication"*, pp.158-180.

Taylor R.A., Phelan P.E., Otanicar T.P., Walker C.A., Nguyen M., Trimble S., and Prasher R., (2011a), Applicability of nanofluids in high flux solar collectors, *"Journal of Renewable and Sustainable Energy"*, vol. 3, issue 2, pp. 023104-1 to 15.

Taylor R.A., Phelan P.E., Otanicar T.P., Adrian R., Prasher R.P., (2011b), Nanofluid optical property characterization: towards efficient direct absorption solar collectors, *"Nanoscale Research Letters"*, vol. 6, issue 1, pp. 225.

Thirugnanasambandam M., Iniyan S., Goic R., (2010), A review of solar thermal technologies, *"Renewable Sustainable Energy Reviews."*, vol. 14, Issue 1, pp. 312–322.

Tian Y., Zhao C.Y., (2013), A review of solar collectors and thermal energy storage in solar thermal applications, *"Applied Energy"*, vol. 104, pp..538–553.

Tiwari A. K., Ghosh P., Sarkar J., (2013), Solar water heating using nanofluids-a comprehensive overview and environmental impact analysis,*"International Journal of Emerging Technology and Advanced Engineering"*, vol. 3, Issue 3:ICERTSD 2013, pp. 221-224.

Tyagi H., Phelan P., Prasher R., (2009), Predicted efficiency of a low-temperature nanofluid – based direct absorption solar collector, *"Journal of Solar Energy Engineering"*, vol. 131, pp. 041004-1 to 7.

Wong K. V., De Leon O., (2010), Applications of nanofluids: current and future, *"Advances in Mechanical Engineering"*, vol. 2010, Article ID 519659, pp.1-11 doi:10.1155/2010/519659.

Yadav A, Kumar M., Balram, (2013), Experimental Study and Analysis of Parabolic trough Collector with Various Reflectors, *"International Journal of Physical, Nuclear Science and Engineering"* vol. 7,issue12, pp.281-285.

Yahya S.M. Turbines, Compressors and Fans, (2012) (fourth edition), Tata McGraw Hill Publication, pp. 694-729.

Yousefi T., Veisy F., Shojaeizadeh E., Zinadini S., (2012a), An experimental investigation on the effect of Al_2O_3-H_2O nanofluid on the efficiency of flat-plate solar collectors, "*Renewable Energy*",vol. 39, pp. 293-298.

Yousefi T., Veisy F., Shojaeizadeh E., Zinadini S., (2012b), An experimental investigation on the effect of MWCNT-H_2O nanofluid on the efficiency of flat plate solar collectors, "*Experimental Thermal and Fluid Science*",vol. 39, pp. 207–212.

Yousefi T., Shojaeizadeh E., Veysi F., Zinadini S., (2012c), An experimental investigation on the effect of pH variation of MWCNT–H_2O nanofluid on the efficiency of a flat-plate solar collector, *"Solar Energy"*, vol. 86, Issue 2, pp. 771-779.

Yu W., Xie H., (2012), A Review on Nanofluids: Preparation, Stability Mechanisms and Applications, *"Journal of Nanomaterials"*, vol. 2012, Article ID 435873, 17 pages, doi: 10.1155/2012/435873.

Zhang X., Gu H., Fujii M., (2007), Effective thermal conductivity and thermal diffusivity of nanofluids containing spherical and cylindrical nanoparticles, *"Experimental Thermal and Fluid Science"*, vol. 31, Issue 6, pp. 593–599.

APPENDIX: A

(For water)

Table A.1: Experimental readings for 20 l/hr mass flow rate using water as a working fluid

Experiment date: 26/04/2014					
Time	Inlet temperature (°C)	Outlet temperature (°C)	Temperature difference (°C)	Solar intensity (W/m^2)	wind speed (m/sec)
9:30-10:00 AM	32	35.6	3.6	778	3.88
10:00-10:30 AM	35.6	39.1	3.5	814	3.88
10:30-11:00 AM	39.1	42.8	3.7	845	5
11:00-11:30 AM	42.8	46.5	3.7	918	5
11:30-12:00 AM	46.5	50	3.5	948	4.72
12:00-12:30 PM	50	53	3	955	4.72
12:30-1:00 PM	53	55.3	2.3	941	4.44
1:00-1:30 PM	55.3	57.7	2.4	918	4.44
1:30-2:00 PM	57.7	59.2	1.5	907	4.166
2:00-2:30 PM	59.2	60	0.8	881	4.166
2:30-3:00 PM	60	60.3	0.3	841	4.166

Table A.2: Calculations for various parameters for 20 l/hr mass flow rate using water

Time	Absorbed heat flux (W/m^2)	Useful heat gain (W)	Instantaneous efficiency	Thermal efficiency	Overall efficiency
9:30-10:00 AM	544.39	83.66	9.79	10.56	6.63
10:00-10:30 AM	569.58	81.33	9.1	9.82	
10:30-11:00 AM	591.27	85.98	9.27	10	
11:00-11:30 AM	642.35	85.98	8.53	9.2	
11:30-12:00 AM	663.34	81.33	7.81	8.43	
12:00-12:30 PM	668.24	69.71	6.65	7.17	
12:30-1:00 PM	658.44	53.45	5.17	5.58	
1:00-1:30 PM	642.35	55.77	5.53	5.97	

Contd…

1:30-2:00 PM	634.65	34.86	3.5	3.78	
2:00-2:30 PM	616.46	18.59	1.92	2.07	
2:30-3:00 PM	588.474	6.97	0.75	0.81	

Table A.3: Experimental readings for 40 l/hr mass flow rate using water as a working fluid

Experiment date: 28/04/2014					
Time	Inlet temperature (°C)	Outlet temperature (°C)	Temperature difference (°C)	Solar intensity (W/m^2)	Wind speed (m/sec)
9:30-10:00 AM	32.5	36.1	3.6	806	3.333
10:00-10:30 AM	36.1	39.8	3.7	838	3.333
10:30-11:00 AM	39.8	43.3	3.5	866	4.166
11:00-11:30 AM	43.3	46.8	3.5	926	4.166
11:30-12:00 AM	46.8	50.4	3.6	963	4.166
12:00-12:30 PM	50.4	53.9	3.5	978	4.166
12:30-1:00 PM	53.9	56.9	3	955	4.444
1:00-1:30 PM	56.9	59.3	2.4	941	4.444
1:30-2:00 PM	59.3	60.4	1.1	933	4.722
2:00-2:30 PM	60.4	60.8	0.4	908	4.722
2:30-3:00 PM	60.8	61	0.2	884	4.722

Table A.4: Calculations for various parameters for 40 l/hr mass flow rate using water

Time	Absorbed heat flux (W/m^2)	Useful heat gain(W)	Instantaneous efficiency	Thermal efficiency	Overall efficiency
9:30-10:00 AM	563.98	167.31	18.91	10.2	6.51
10:00-10:30 AM	586.37	171.96	18.69	10.08	
10:30-11:00 AM	605.96	162.66	17.11	9.23	
11:00-11:30 AM	647.95	162.66	16	8.63	
11:30-12:00 AM	673.84	167.31	15.82	8.54	
12:00-12:30 PM	684.33	162.66	15.15	8.17	

Contd…

12:30-1:00 PM	668.24	139.43	13.3	7.17	
1:00-1:30 PM	658.44	111.54	10.8	5.82	
1:30-2:00 PM	652.84	51.12	4.99	2.69	
2:00-2:30 PM	635.35	18.59	1.86	1	
2:30-3:00 PM	618.56	9.3	0.96	0.52	

Table A.5: Experimental readings for 60 l/hr mass flow rate using water as a working fluid

Experiment date: 29/04/2014					
Time	Inlet temperature (°C)	Outlet temperature (°C)	Temperature difference (°C)	Solar intensity (W/m^2)	Wind speed (m/sec)
9:30-10:00 AM	33	36.5	3.5	765	2.222
10:00-10:30 AM	36.5	39.9	3.4	792	2.222
10:30-11:00 AM	39.9	43.7	3.8	820	2.777
11:00-11:30 AM	43.7	47.2	3.5	897	2.777
11:30-12:00 AM	47.2	50.6	3.4	941	3.055
12:00-12:30 PM	50.6	53.8	3.2	966	3.055
12:30-1:00 PM	53.8	56.6	2.8	926	3.333
1:00-1:30 PM	56.6	58.5	1.9	911	3.333
1:30-2:00 PM	58.5	58.9	0.4	888	3.611
2:00-2:30 PM	58.9	59.6	0.7	844	3.611
2:30-3:00 PM	59.6	59.7	0.1	820	3.888

Table A.6: Calculations for various parameters for 60 l/hr mass flow rate using water

Time	Absorbed heat flux (W/m^2)	Useful heat gain(W)	Instantaneous efficiency	Thermal efficiency	Overall efficiency
9:30-10:00 AM	535.29	243.26	28.96	10.45	
10:00-10:30 AM	554.18	236.31	27.17	9.8	
10:30-11:00 AM	573.78	264.16	29.34	10.58	
11:00-11:30 AM	627.65	243.26	24.7	8.91	

Contd…

11:30-12:00 AM	658.44	236.31	22.87	8.25	6.37
12:00-12:30 PM	675.94	222.41	20.97	7.56	
12:30-1:00 PM	647.95	194.61	19.14	6.9	
1:00-1:30 PM	637.45	132.06	13.2	4.76	
1:30-2:00 PM	621.36	27.8	2.85	1.03	
2:00-2:30 PM	590.57	48.65	5.25	1.89	
2:30-3:00 PM	573.78	6.95	0.77	0.28	

APPENDIX: B

(For water-based alumina nanofluid with 0.01% concentration)

Table B.1: Experimental readings for 20 l/hr mass flow rate using water-based alumina (Al_2O_3) nanofluid as working fluid

Experiment date: 19/05/2014					
Time	Inlet temperature (°C)	Outlet temperature (°C)	Temperature difference (°C)	Solar intensity (W/m^2)	wind speed m/sec
9:30-10:00 AM	33	37	4	788	1.944
10:00-10:30 AM	37	41	4	810	1.944
10:30-11:00 AM	41	44.3	3.3	842	2.222
11:00-11:30 AM	44.3	48.6	4.3	872	2.222
11:30-12:00 AM	48.6	53.3	4.7	892	2.222
12:00-12:30 PM	53.3	57.2	3.9	914	2.222
12:30-1:00 PM	57.2	58.9	1.7	942	2.5
1:00-1:30 PM	58.9	59.9	1	926	2.5
1:30-2:00 PM	59.9	60.6	0.7	897	2.777
2:00-2:30 PM	60.6	60.4	-0.2	881	2.777
2:30-3:00 PM	60.4	60.1	-0.3	840	3.055

Table B.2: Calculations for various parameters for 20 l/hr mass flow rate using water-based alumina (Al_2O_3) nanofluid

Time	Absorbed heat flux (W/m^2)	Useful heat gain(W)	Instantaneous efficiency	Thermal efficiency	Overall efficiency
9:30-10:00 AM	551.39	92.69	10.71	11.56	
10:00-10:30 AM	566.78	92.69	10.42	11.24	
10:30-11:00 AM	589.17	76.47	8.2	8.92	
11:00-11:30 AM	610.17	99.64	10.4	11.23	
11:30-12:00 AM	624.16	109	11.2	11.99	
12:00-12:30 PM	639.56	90.37	9	9.72	

Contd…

12:30-1:00 PM	659.15	39.39	3.8	4.11	7.97
1:00-1:30 PM	647.95	23.17	2.279	2.46	
1:30-2:00 PM	627.66	16.22	1.64	1.78	
2:00-2:30 PM	616.46	0	0	0	
2:30-3:00 PM	587.77	0	0	0	

Table B.3: Experimental readings for 40 l/hr mass flow rate using water-based alumina (Al_2O_3) nanofluid as working fluid

Experiment date: 20/05/2014					
Time	Inlet temperature (°C)	Outlet temperature (°C)	Temperature difference (°C)	Solar intensity (W/m^2)	wind speed m/sec
9:30-10:00 AM	32.4	36.5	4.1	774	2.777
10:00-10:30 AM	36.5	40.3	3.8	800	2.777
10:30-11:00 AM	40.3	44.2	3.9	841	3.333
11:00-11:30 AM	44.2	48.1	3.9	888	3.333
11:30-12:00 AM	48.1	51.9	3.8	905	3.333
12:00-12:30 PM	51.9	55.4	3.5	934	3.333
12:30-1:00 PM	55.4	57.9	2.5	949	3.333
1:00-1:30 PM	57.9	59.6	1.7	920	3.333
1:30-2:00 PM	59.6	60.3	0.7	895	3.611
2:00-2:30 PM	60.3	61.1	0.8	845	3.611
2:30-3:00 PM	61.1	61.3	0.2	795	3.611

Table B.4: Calculations for various parameters for 40 l/hr mass flow rate using water-based alumina (Al_2O_3) nanofluid

Time	Absorbed heat flux (W/m^2)	Useful heat gain(W)	Instantaneous efficiency	Thermal efficiency	Overall efficiency
9:30-10:00 AM	541.59	190	22.35	12.06	6.8
10:00-10:30 AM	559.79	176	20	10.82	
10:30-11:00 AM	588.47	180.75	19.57	10.56	
11:00-11:30 AM	621.36	180.75	18.5	10	
11:30-12:00 AM	633.26	176.1	17.7	9.6	
12:00-12:30 PM	653.55	162.1	15.81	8.53	
12:30-1:00 PM	664.05	115.8	11.11	6	
1:00-1:30 PM	643.75	78.7	7.79	4.21	
1:30-2:00 PM	626.26	32.4	3.3	1.78	
2:00-2:30 PM	591.27	37	3.9	2.2	
2:30-3:00 PM	556.29	9.2	1.06	0.57	

Table B.5: Experimental readings for 60 l/hr mass flow rate using water-based alumina (Al_2O_3) nanofluid as working fluid

Experiment date: 21/05/2014					
Time	Inlet temperature (°C)	Outlet temperature (°C)	Temperature difference (°C)	Solar intensity (W/m^2)	wind speed m/sec
9:30-10:00 AM	32.2	36	3.8	768	2.777
10:00-10:30 AM	36	39.6	3.6	805	2.777
10:30-11:00 AM	39.6	43.9	4.3	825	3.611
11:00-11:30 AM	43.9	47.8	3.9	859	3.611
11:30-12:00 AM	47.8	51.6	3.8	885	3.611
12:00-12:30 PM	51.6	55.4	3.8	946	3.611
12:30-1:00 PM	55.4	58.4	3	959	3.611
1:00-1:30 PM	58.4	60.6	2.2	935	3.611

Contd…

1:30-2:00 PM	60.6	62.4	1.8	877	3.888
2:00-2:30 PM	62.4	63.1	0.7	838	3.888
2:30-3:00 PM	63.1	63.3	0.2	799	3.888

Table B.6: Calculations for various parameters for 60 l/hr mass flow rate using water-based alumina (Al_2O_3) nanofluid

Time	Absorbed heat flux (W/m^2)	Useful heat gain(W)	Instantaneous efficiency	Thermal efficiency	Overall efficiency
9:30-10:00 AM	537.39	263	31.23	11.27	7.46
10:00-10:30 AM	563.28	249.5	28.23	10.18	
10:30-11:00 AM	577.28	298	32.9	11.87	
11:00-11:30 AM	601.07	270.3	28.6	10.34	
11:30-12:00 AM	619.26	263.3	27.1	9.8	
12:00-12:30 PM	661.95	263.3	25.35	9.15	
12:30-1:00 PM	671.04	208	19.74	7.12	
1:00-1:30 PM	654.25	152.4	14.85	5.4	
1:30-2:00 PM	613.66	124.7	12.95	4.7	
2:00-2:30 PM	586.38	48.5	5.27	1.9	
2:30-3:00 PM	559.09	13.8	1.58	0.57	

APPENDIX: C

(For water-based alumina nanofluid with 0.05% concentration)

Table C.1: Experimental readings for 20 l/hr mass flow rate using water-based alumina (Al_2O_3) nanofluid as working fluid

Experiment date: 22/05/2014					
Time	Inlet temperature (°C)	Outlet temperature (°C)	Temperature difference (°C)	Solar intensity (W/m^2)	wind speed m/sec
9:30-10:00 AM	33.1	37.3	4.2	774	2.222
10:00-10:30 AM	37.3	40.8	3.5	792	2.222
10:30-11:00 AM	40.8	44.8	4	825	2.777
11:00-11:30 AM	44.8	48.9	4.1	847	2.777
11:30-12:00 AM	48.9	53.3	4.4	873	3.055
12:00-12:30 PM	53.3	56.9	3.6	903	3.055
12:30-1:00 PM	56.9	60.4	3.5	941	3.055
1:00-1:30 PM	60.4	62.9	2.5	911	3.055
1:30-2:00 PM	62.9	64.5	1.6	885	3.055
2:00-2:30 PM	64.5	65.4	0.9	865	3.055
2:30-3:00 PM	65.4	65.5	0.1	836	3.055

Table C.2: Calculations for various parameters for 20 l/hr mass flow rate using water-based alumina (Al_2O_3) nanofluid

Time	Absorbed heat flux (W/m^2)	Useful heat gain(W)	Instantaneous efficiency	Thermal efficiency	Overall efficiency
9:30-10:00 AM	541.59	96.25	11.32	12.22	
10:00-10:30 AM	554.19	80.2	9.22	9.95	
10:30-11:00 AM	577.28	91.67	10.12	10.92	
11:00-11:30 AM	592.67	93.9	10.1	10.9	
11:30-12:00 AM	610.87	100.8	10.5	11.35	
12:00-12:30 PM	631.86	82.5	8.32	8.98	

Contd…

12:30-1:00 PM	658.45	80.2	7.7	8.38	7.62
1:00-1:30 PM	637.46	57.2	5.72	6.18	
1:30-2:00 PM	619.26	36.6	3.77	4.1	
2:00-2:30 PM	605.27	20.62	2.17	2.34	
2:30-3:00 PM	584.98	2.291	0.24	0.27	

Table C.3: Experimental readings for 40 l/hr mass flow rate using water-based alumina (Al_2O_3) nanofluid as working fluid

Experiment date: 24/05/2014					
Time	Inlet temperature (°C)	Outlet temperature (°C)	Temperature difference (°C)	Solar intensity (W/m^2)	wind speed m/sec
9:30-10:00 AM	31.6	35.8	4.2	759	2.5
10:00-10:30 AM	35.8	39.5	3.7	774	2.5
10:30-11:00 AM	39.5	43.6	4.1	793	2.777
11:00-11:30 AM	43.6	47.6	4	823	2.777
11:30-12:00 AM	47.6	51.7	4.1	850	2.222
12:00-12:30 PM	51.7	55.6	3.9	868	2.222
12:30-1:00 PM	55.6	58.9	3.3	900	1.388
1:00-1:30 PM	58.9	61.9	3	885	1.388
1:30-2:00 PM	61.9	64	2.1	870	0.833
2:00-2:30 PM	64	64.9	0.9	854	0.833
2:30-3:00 PM	64.9	65.4	0.5	836	1.111

Table C.4: Calculations for various parameters for 40 l/hr mass flow rate using water-based alumina (Al_2O_3) nanofluid as working fluid

Time	Absorbed heat flux (W/m^2)	Useful heat gain(W)	Instantaneous efficiency	Thermal efficiency	Overall efficiency
9:30-10:00 AM	531.1	192.5	23.1	12.46	8.16
10:00-10:30 AM	541.59	169.5	19.95	10.76	
10:30-11:00 AM	554.89	187.9	21.58	11.64	
11:00-11:30 AM	575.88	183.34	20.2	10.94	
11:30-12:00 AM	594.77	187.9	20.13	10.86	
12:00-12:30 PM	607.37	178.7	18.7	10.12	
12:30-1:00 PM	629.76	152.2	15.3	8.26	
1:00-1:30 PM	619.26	137.5	14.15	7.63	
1:30-2:00 PM	608.77	96.2	10	5.44	
2:00-2:30 PM	597.57	41.25	4.39	2.37	
2:30-3:00 PM	584.98	22.9	2.49	1.35	

Table C.5: Experimental readings for 60 l/hr mass flow rate using water-based alumina (Al_2O_3) nanofluid as working fluid

Experiment date: 25/05/2014					
Time	Inlet temperature (°C)	Outlet temperature (°C)	Temperature difference (°C)	Solar intensity (W/m^2)	wind speed m/sec
9:30-10:00 AM	35	39.4	4.4	800	3.333
10:00-10:30 AM	39.4	43.5	4.1	825	3.333
10:30-11:00 AM	43.5	47.3	3.8	847	3.333
11:00-11:30 AM	47.3	51.2	3.9	866	3.333
11:30-12:00 AM	51.2	55.2	4	892	2.5
12:00-12:30 PM	55.2	58.8	3.6	911	2.5
12:30-1:00 PM	58.8	61.6	2.8	935	1.666
1:00-1:30 PM	61.6	64.6	3	918	1.666

Contd…

1:30-2:00 PM	64.6	66.5	1.9	897	0.833
2:00-2:30 PM	66.5	67.5	1	881	0.833
2:30-3:00 PM	67.5	67.8	0.3	855	1.111

Table C.6: Calculations for various parameters for 60 l/hr mass flow rate using water-based alumina (Al_2O_3) nanofluid as working fluid

Time	Absorbed heat flux (W/m^2)	Useful heat gain(W)	Instantaneous efficiency	Thermal efficiency	Overall efficiency
9:30-10:00 AM	559.79	301.618	34.33	12.39	7.44
10:00-10:30 AM	577.28	281	31	11.19	
10:30-11:00 AM	592.67	260.48	28	10.1	
11:00-11:30 AM	605.97	267.34	28.11	10.14	
11:30-12:00 AM	624.16	274.19	27.99	10.09	
12:00-12:30 PM	637.46	246.7	24.67	8.9	
12:30-1:00 PM	654.25	192	18.69	6.74	
1:00-1:30 PM	642.35	205.6	20.4	7.36	
1:30-2:00 PM	627.66	130.2	13.22	4.77	
2:00-2:30 PM	616.46	68.54	7	2.56	
2:30-3:00 PM	598.27	20.56	2.19	0.79	

APPENDIX: D

(For water-based copper oxide nanofluid with 0.01% concentration)

Table D.1: Experimental readings for 20 l/hr mass flow rate using water-based copper oxide (CuO) nanofluid as working fluid

Experiment date: 26/05/2014					
Time	Inlet temperature (°C)	Outlet temperature (°C)	Temperature difference (°C)	Solar intensity (W/m^2)	wind speed m/sec
9:30-10:00 AM	30	34.3	4.3	751	1.667
10:00-10:30 AM	34.3	38.4	4.1	768	1.667
10:30-11:00 AM	38.4	42.6	4.2	786	1.388
11:00-11:30 AM	42.6	46.6	4	812	1.388
11:30-12:00 AM	46.6	50.7	4.1	850	1.667
12:00-12:30 PM	50.7	54.6	3.9	870	1.667
12:30-1:00 PM	54.6	57.9	3.3	892	1.667
1:00-1:30 PM	57.9	60.9	3	900	1.667
1:30-2:00 PM	60.9	62.7	1.8	868	1.944
2:00-2:30 PM	62.7	64.1	1.4	823	1.944
2:30-3:00 PM	64.1	64.8	0.7	792	2.222

Table D.2: Calculations for various parameters for 20 l/hr mass flow rate using water-based copper oxide (CuO) nanofluid as working fluid

Time	Absorbed heat flux (W/m^2)	Useful heat gain(W)	Instantaneous efficiency	Thermal efficiency	Overall efficiency
9:30-10:00 AM	525.5	99.84	12.11	13.05	
10:00-10:30 AM	537.39	95.19	11.29	12.17	
10:30-11:00 AM	550	97.51	11.3	12.18	
11:00-11:30 AM	568.18	92.87	10.42	11.23	
11:30-12:00 AM	594.77	95.19	10.2	10.99	
12:00-12:30 PM	608.77	90.55	9.48	10.22	

Contd…

12:30-1:00 PM	624.16	76.62	7.82	8.43	8.7
1:00-1:30 PM	629.76	69.65	7.05	7.6	
1:30-2:00 PM	607.37	41.79	4.38	4.73	
2:00-2:30 PM	575.88	32.5	3.6	3.88	
2:30-3:00 PM	554.2	16.25	1.87	2.01	

Table D.3: Experimental readings for 40 l/hr mass flow rate using water-based copper oxide (CuO) nanofluid as working fluid

Experiment date: 28/05/2014					
Time	Inlet temperature (°C)	Outlet temperature (°C)	Temperature difference (°C)	Solar intensity (W/m^2)	wind speed m/sec
9:30-10:00 AM	33.5	38.1	4.6	773	1.666
10:00-10:30 AM	38.1	42.4	4.3	799	1.666
10:30-11:00 AM	42.4	46.4	4	827	2.222
11:00-11:30 AM	46.4	50.2	3.8	848	2.222
11:30-12:00 AM	50.2	54.2	4	872	2.777
12:00-12:30 PM	54.2	58	3.8	885	2.777
12:30-1:00 PM	58	61.6	3.6	907	3.888
1:00-1:30 PM	61.6	64.6	3	873	3.888
1:30-2:00 PM	64.6	66.8	2.2	845	4.722
2:00-2:30 PM	66.8	68	1.2	797	4.722
2:30-3:00 PM	68	68.4	0.4	770	5

Table D.4: Calculations for various parameters for 40 l/hr mass flow rate using water-based copper oxide (CuO) nanofluid as working fluid

Time	Absorbed heat flux (W/m^2)	Useful heat gain(W)	Instantaneous efficiency	Thermal efficiency	Overall efficiency
9:30-10:00 AM	540.89	213.6	25.17	13.56	8.65
10:00-10:30 AM	559.09	199.67	22.76	12.26	
10:30-11:00 AM	578.68	185.74	20.45	11.02	
11:00-11:30 AM	593.37	176.45	18.95	10.21	
11:30-12:00 AM	610.17	185.74	19.4	10.45	
12:00-12:30 PM	619.26	176.45	18.16	9.79	
12:30-1:00 PM	634.66	167.17	16.79	9.05	
1:00-1:30 PM	610.87	139.31	14.53	7.83	
1:30-2:00 PM	591.27	102.16	11.01	5.93	
2:00-2:30 PM	557.69	55.72	6.37	3.43	
2:30-3:00 PM	538.79	18.57	2.2	1.18	

Table D.5: Experimental readings for 60 l/hr mass flow rate using water-based copper oxide (CuO) nanofluid as working fluid

Experiment date: 29/05/2014					
Time	Inlet temperature (°C)	Outlet temperature (°C)	Temperature difference (°C)	Solar intensity (W/m^2)	wind speed m/sec
9:30-10:00 AM	34.5	39.3	4.8	773	0.8333
10:00-10:30 AM	39.3	43.5	4.2	789	0.8333
10:30-11:00 AM	43.5	47.9	4.4	808	0.8333
11:00-11:30 AM	47.9	51.8	3.9	833	0.8333
11:30-12:00 AM	51.8	55.8	4	851	1.388
12:00-12:30 PM	55.8	59.6	3.8	872	1.388
12:30-1:00 PM	59.6	63.1	3.5	885	1.944
1:00-1:30 PM	63.1	65.9	2.8	860	1.944

Contd…

1:30-2:00 PM	65.9	68.1	2.2	850	2.5
2:00-2:30 PM	68.1	69.5	1.4	826	2.5
2:30-3:00 PM	69.5	70.2	0.7	806	2.777

Table D.6: Calculations for various parameters for 60 l/hr mass flow rate using water-based copper oxide (CuO) nanofluid as working fluid

Time	Absorbed heat flux (W/m^2)	Useful heat gain(W)	Instantaneous efficiency	Thermal efficiency	Overall efficiency
9:30-10:00 AM	540.89	334.33	39.39	14.15	8.9
10:00-10:30 AM	552.09	292.54	33.77	12.13	
10:30-11:00 AM	565.38	306.47	34.54	12.41	
11:00-11:30 AM	582.88	271.65	29.7	10.67	
11:30-12:00 AM	595.47	278.61	29.82	10.71	
12:00-12:30 PM	610.17	264.68	27.64	9.93	
12:30-1:00 PM	619.26	243.78	25.09	9.01	
1:00-1:30 PM	601.77	195.03	20.65	7.42	
1:30-2:00 PM	594.77	153.24	16.42	5.9	
2:00-2:30 PM	577.98	97.51	10.75	3.86	
2:30-3:00 PM	563.98	48.76	5.51	1.98	

APPENDIX: E

(For water-based copper oxide nanofluid with 0.05% concentration)

Table E.1: Experimental readings for 20 l/hr mass flow rate using water-based copper oxide (CuO) nanofluid as working fluid

Experiment date: 02/06/2014					
Time	Inlet temperature (°C)	Outlet temperature (°C)	Temperature difference (°C)	Solar intensity (W/m^2)	wind speed m/sec
9:30-10:00 AM	32	37.1	5.1	774	1.111
10:00-10:30 AM	37.1	41.7	4.6	797	1.111
10:30-11:00 AM	41.7	45.8	4.1	827	0.8333
11:00-11:30 AM	45.8	50	4.2	848	0.8333
11:30-12:00 AM	50	54	4	875	1.666
12:00-12:30 PM	54	58.2	4.2	905	1.666
12:30-1:00 PM	58.2	61.3	3.1	929	2.5
1:00-1:30 PM	61.3	64.7	3.4	948	2.5
1:30-2:00 PM	64.7	67	2.3	923	3.333
2:00-2:30 PM	67	68.4	1.4	893	3.333
2:30-3:00 PM	68.4	68.9	0.5	860	3.888

Table E.2: Calculations for various parameters for 20 l/hr mass flow rate using water-based copper oxide (CuO) nanofluid as working fluid

Time	Absorbed heat flux (W/m^2)	Useful heat gain(W)	Instantaneous efficiency	Thermal efficiency	Overall efficiency
9:30-10:00 AM	541.59	117.52	13.83	14.9	
10:00-10:30 AM	557.69	106	12.11	13.05	
10:30-11:00 AM	578.68	94.48	10.4	11.21	
11:00-11:30 AM	593.37	96.78	10.39	11.2	
11:30-12:00 AM	612.27	92.17	9.59	10.34	
12:00-12:30 PM	633.26	96.78	9.74	10.5	

Contd…

12:30-1:00 PM	650.05	71.43	7	7.55	8.71
1:00-1:30 PM	663.35	78.35	7.53	8.11	
1:30-2:00 PM	645.85	53	5.23	5.64	
2:00-2:30 PM	624.86	32.26	3.29	3.55	
2:30-3:00 PM	601.77	11.52	1.22	1.32	

Table E.3: Experimental readings for 40 l/hr mass flow rate using water-based copper oxide (CuO) nanofluid as working fluid

Experiment date: 03/06/2014					
Time	Inlet temperature (°C)	Outlet temperature (°C)	Temperature difference (°C)	Solar intensity (W/m^2)	wind speed m/sec
9:30-10:00 AM	36.2	41.2	5	790	3.888
10:00-10:30 AM	41.2	45.9	4.7	818	3.888
10:30-11:00 AM	45.9	50	4.1	842	4.722
11:00-11:30 AM	50	54	4	860	4.722
11:30-12:00 AM	54	57.8	3.8	890	5
12:00-12:30 PM	57.8	61.5	3.7	918	5
12:30-1:00 PM	61.5	64.7	3.2	944	5
1:00-1:30 PM	64.7	67.3	2.6	905	5
1:30-2:00 PM	67.3	69.1	1.8	882	5.277
2:00-2:30 PM	69.1	70.4	1.3	851	5.277
2:30-3:00 PM	70.4	70.6	0.2	818	5.277

Table E.4: Calculations for various parameters for 40 l/hr mass flow rate using water-based copper oxide (CuO) nanofluid as working fluid

Time	Absorbed heat flux (W/m^2)	Useful heat gain(W)	Instantaneous efficiency	Thermal efficiency	Overall efficiency
9:30-10:00 AM	552.79	230.43	26.56	14.32	8.17
10:00-10:30 AM	572.38	216.61	24.12	13	
10:30-11:00 AM	589.17	188.96	20.44	11.01	
11:00-11:30 AM	601.77	184.35	19.52	10.52	
11:30-12:00 AM	622.76	175.13	17.92	9.66	
12:00-12:30 PM	642.35	170.52	16.92	9.12	
12:30-1:00 PM	660.55	147.48	14.23	7.67	
1:00-1:30 PM	633.26	119.83	12.06	6.5	
1:30-2:00 PM	617.16	82.96	8.57	4.62	
2:00-2:30 PM	595.47	59.91	6.41	3.46	
2:30-3:00 PM	572.38	9.22	1.03	0.55	

Table E.5: Experimental readings for 60 l/hr mass flow rate using water-based copper oxide (CuO) nanofluid as working fluid

Experiment date: 04/06/2014					
Time	Inlet temperature (°C)	Outlet temperature (°C)	Temperature difference (°C)	Solar intensity (W/m^2)	Wind speed (m/sec)
9:30-10:00 AM	36.5	41.8	5.3	786	1.666
10:00-10:30 AM	41.8	46.3	4.5	811	1.666
10:30-11:00 AM	46.3	51.2	4.9	842	1.944
11:00-11:30 AM	51.2	56.3	5.1	871	1.944
11:30-12:00 AM	56.3	60.7	4.4	912	2.5
12:00-12:30 PM	60.7	64.9	4.2	930	2.5
12:30-1:00 PM	64.9	68.4	3.5	946	3.333
1:00-1:30 PM	68.4	71.9	3.5	918	3.333

Contd…

1:30-2:00 PM	71.9	74.9	3	889	3.888
2:00-2:30 PM	74.9	76.6	1.7	851	3.888
2:30-3:00 PM	76.6	77	0.4	814	3.888

Table E.6: Calculations for various parameters for 60 l/hr mass flow rate using water-based copper oxide (CuO) nanofluid as working fluid

Time	Absorbed heat flux (W/m^2)	Useful heat gain(W)	Instantaneous efficiency	Thermal efficiency	Overall efficiency
9:30-10:00 AM	549.99	366.39	42.45	15.25	9.57
10:00-10:30 AM	567.48	311.09	34.94	12.55	
10:30-11:00 AM	589.17	338.74	36.64	13.16	
11:00-11:30 AM	609.47	352.56	36.86	13.24	
11:30-12:00 AM	638.16	304.17	30.38	10.91	
12:00-12:30 PM	650.75	290.35	28.43	10.21	
12:30-1:00 PM	661.95	241.96	23.29	8.37	
1:00-1:30 PM	642.35	241.96	24	8.62	
1:30-2:00 PM	622.06	207.39	21.25	7.63	
2:00-2:30 PM	595.47	117.52	12.58	4.52	
2:30-3:00 PM	569.58	27.65	3.09	1.11	

APPENDIX: F

Table F.1: Value of dimensionless numbers & h_f, F', F_R for water

Parameter	Water 20 l/hr	Water 40 l/hr	Water 60 l/hr
Re	631.08	1262.17	1886.75
Pr	2.605	2.605	2.605
Nu	5.863	10.208	14.08
h_f (W/m^2K)	144.84	252.175	347.84
F'	0.9132	0.9482	0.9619
F_R	0.8885	0.9348	0.9592

Table F.2: Value of dimensionless numbers & h_f, F', F_R for water-based Alumina (Al_2O_3) with 0.01% particle concentration

Parameter	Alumina 20 l/hr	Alumina 40 l/hr	Alumina 60 l/hr
Re	628	1256	1880
Pr	1.643	1.643	1.643
Nu	4.857	8.456	11.676
h_f (W/m^2K)	185.11	322.268	444.985
F'	0.931	0.959	0.97
F_R	0.9045	0.9448	0.9603

Table F.3: Value of dimensionless numbers & h_f, F', F_R for water-based Alumina (Al_2O_3) with 0.05% particle concentration

Parameter	Alumina 20 l/hr	Alumina 40 l/hr	Alumina 60 l/hr
Re	566.246	1132.49	1693.6
Pr	1.6311	1.6311	1.6311
Nu	4.457	7.76	10.71
h_f (W/m^2K)	189.67	330.23	455.77
F'	0.9323	0.9599	0.9706
F_R	0.9024	0.94395	0.9628

Table F.4: Value of dimensionless numbers & h_f, F', F_R for water-based copper oxide (CuO) with 0.01% particle concentration

Parameter	CuO 20 l/hr	CuO 40 l/hr	CuO 60 l/hr
Re	627.273	1254.55	1875
Pr	2.4089	2.4089	2.4089
Nu	5.655	9.8457	13.5786
h_f (W/m^2K)	143.89	250.522	345.505
F'	0.91265	0.94789	0.9617
F_R	0.8864	0.93373	0.95192

Table F.5: Value of dimensionless numbers & h_f, F', F_R for water-based copper oxide (CuO) with 0.05% particle concentration

Parameter	CuO 20 l/hr	CuO 40 l/hr	CuO 60 l/hr
Re	566.7	1132.665	1694.176
Pr	1.9015	1.9015	1.9015
Nu	4.743	8.254	11.39
h_f (W/m^2K)	139.48	242.73	334.95
F'	0.9101	0.9463	0.9605
F_R	0.8788	0.9292	0.9487

APPENDIX: G

Table G.1: Values of design parameters of Parabolic trough solar Collector (PTSC)

Specular reflectivity of the concentrated surface, β	0.93
Absorptivity of the receiver tube, α	0.90
Glass cover transmissivity for solar radiation, τ	0.88
Intercept factor, ϒ	0.95
Bond resistance, R_b	1

Table G.2: General properties of water used in the experiment (Dr. Kumar D.S., 2009)

Density of water, ρ	1000 kg/m^3
Specific heat of water, c_p	4.187 KJ/Kgk
Thermal conductivity of water, k	0.667 W/m-K
Viscosity of water, ν	0.415×10^{-6} m^2/s
Dynamic viscosity of nanofluids, μ	4.06×10^{-4} m^2/s

Table G.3: General properties of water-based alumina (Al_2O_3) nanofluid with 0.01% concentration used in the experiment

Density of nanofluid, ρ_{nf}	1029.7 kg/m^3
Specific heat of nanofluid, c_{pnf}	4.05507 KJ/Kgk
Thermal conductivity of nanofluid, k_{nf}	1.029 W/m-K
Viscosity of nanofluid, ν	0.405×10^{-6} m^2/s
Dynamic viscosity of nanofluids, μ_{nf}	4.169×10^{-4} m^2/s

Table G.4: General properties of water-based alumina (Al_2O_3) with 0.05% concentration nanofluid used in the experiment

Density of nanofluid, ρ_{nf}	1148.5 kg/m^3
Specific heat of nanofluid, c_{pnf}	3.59556 KJ/Kgk
Thermal conductivity of nanofluid, k_{nf}	1.149 W/m-K
Viscosity of nanofluid, ν	0.363×10^{-6} m^2/s
Dynamic viscosity of nanofluids, μ_{nf}	4.6211×10^{-4} m^2/s

Table G.5: General properties of water-based copper oxide with 0.01% concentration nanofluid used in the experiment

Density of nanofluid, ρ_{nf}	1054 kg/m^3
Specific heat of nanofluid, c_{pnf}	3.965 KJ/Kgk
Thermal conductivity of nanofluid, k_{nf}	0.6870 W/m-K
Viscosity of nanofluid, v	0.396×10^{-6} m^2/s
Dynamic viscosity of nanofluids, μ_{nf}	4.169×10^{-4} m^2/s

Table G.6: General properties of water-based copper oxide with 0.05% concentration nanofluid used in the experiment

Density of nanofluid, ρ_{nf}	1270 kg/m^3
Specific heat of nanofluid, c_{pnf}	3.266 KJ/Kgk
Thermal conductivity of nanofluid, k_{nf}	0.794 W/m-K
Viscosity of nanofluid, v	0.364×10^{-6} m^2/s
Dynamic viscosity of nanofluids, μ_{nf}	4.6211×10^{-4} m^2/s

APPENDIX: H

(Informative)

H.1: XRD Image Information of Alumina (Al_2O_3)

Measurement Conditions:

Dataset Name	Al_2O_3
File name	C:\Documents and Settings\Administrator\Desktop\SAI Labs\TU\Kundan Lal\Kapil sharma\Al_2O_3.xrdml
Comment	Configuration=Spinner Reflection-Transmission, Owner=User-1, Creation date=6/25/2009 11:03:49 AM
	Goniometer=PW3050/60 (Theta/Theta); Minimum step size 2Theta:0.001; Minimum step size Omega: 0.001
	Sample stage=Reflection-Transmission Spinner PW3064/60; Minimum step size Phi: 0.1
	Diffractometer system=XPERT-PRO
	Measurement program=Thapar_Spinner Stage, Owner=User-1, Creation date=2/5/2010 5:38:09 PM
Measurement Date / Time	6/12/2014 10:36:40 AM
Operator	Administrator
Raw Data Origin	XRD measurement (*.XRDML)
Scan Axis	Gonio
Start Position [°2Th.]	20.0116
End Position [°2Th.]	109.9846
Step Size [°2Th.]	0.0130
Scan Step Time [s]	29.0700
Scan Type	Continuous
PSD Mode	Scanning
PSD Length [°2Th.]	3.35
Offset [°2Th.]	0.0000
Divergence Slit Type	Automatic
Irradiated Length [mm]	10.00
Specimen Length [mm]	10.00
Measurement Temperature [°C]	25.00

Anode Material	Cu
K-Alpha1 [Å]	1.54060
Generator Settings	40 mA, 45 kV
Diffractometer Type	0000000011059259
Diffractometer Number	0
Goniometer Radius [mm]	240.00
Dist. Focus-Diverg. Slit [mm]	100.00
Incident Beam Monochromator	No
Spinning	Yes

Peak List:

Pos. [°2Th.]	Height [cts]	d-spacing [Å]	Rel. Int. [%]	Area [cps*°2Th.]	Area [cts*°2Th.]	FWHM [°2Th.]
25.5904	20.26	3.47817	0.31	13.59	395.14	4.0000
35.1585	6125.18	2.55045	94.56	31.50	915.76	0.1171
37.7864	2358.84	2.37890	36.42	10.82	314.65	0.1039
38.7920	6.31	2.31951	0.10	0.38	11.19	0.0013
39.2337	6.14	2.29441	0.09	0.39	11.46	4.0000
41.6511	57.56	2.16666	0.89	0.62	18.10	0.2629
43.3607	6477.27	2.08511	100.00	32.79	953.30	0.1155
46.1960	80.47	1.96352	1.24	0.42	12.26	0.1212
52.5566	2550.38	1.73988	39.37	13.68	397.65	0.1213
57.5058	5188.74	1.60134	80.11	27.03	785.76	0.1184
59.7461	85.42	1.54654	1.32	0.49	14.33	0.1314
61.1393	182.75	1.51459	2.82	0.55	16.02	0.0912
61.2920	381.39	1.51118	5.89	2.38	69.29	0.1438
66.5224	1704.86	1.40448	26.32	9.43	273.99	0.1256
68.2118	2600.91	1.37376	40.15	14.27	414.78	0.1245
68.3866	146.48	1.37067	2.26	0.22	6.31	4.0000

70.4244	85.70	1.33592	1.32	0.35	10.31	0.0951
74.3017	76.67	1.27551	1.18	0.33	9.65	0.0985
76.8848	656.33	1.23897	10.13	3.34	97.01	0.1165
77.2383	366.96	1.23418	5.67	1.98	57.63	0.1258
80.7002	269.87	1.18973	4.17	1.56	45.25	0.1308
83.1946	45.67	1.16028	0.71	0.28	8.27	0.1422
84.3517	208.12	1.14729	3.21	1.13	32.86	0.1233
86.3821	122.56	1.12546	1.89	0.94	27.24	0.1742
88.9963	335.21	1.09904	5.18	2.08	60.43	0.1407
90.7109	82.48	1.08267	1.27	0.56	16.37	0.1633
91.1873	375.57	1.07825	5.80	2.59	75.36	0.1582
95.2436	712.20	1.04276	11.00	4.93	143.23	0.1581
98.3714	103.16	1.01779	1.59	0.92	26.77	0.2038
101.0696	474.32	0.99778	7.32	2.40	69.89	0.1149
103.3250	84.57	0.98206	1.31	0.48	14.02	0.1296

Pattern List:

Visible	Ref. Code	Score	Compound Name	Displacement [°2Th.]	Scale Factor	Chemical Formula	SemiQuant [%]
*	01-073-6870	98	Corundum, syn	-0.002	0.949	Al2 O3	100

H.2: XRD Image Information of Copper Oxide (CuO)

Measurement Conditions:

Dataset Name	CuO
File name	C:\Documents and Settings\Administrator\Desktop\SAI Labs\TU\Kundan Lal\Kapil sharma\CuO.xrdml
Comment	Configuration=Spinner Reflection-Transmission, Owner=User-1, Creation date=6/25/2009 11:03:49 AM
	Goniometer=PW3050/60 (Theta/Theta); Minimum step size 2Theta:0.001; Minimum step size Omega:0.001
	Sample stage=Reflection-Transmission Spinner PW3064/60; Minimum step size Phi: 0.1
	Diffractometer system=XPERT-PRO
	Measurement program=Thapar_Spinner Stage, Owner=User-1, Creation date=2/5/2010 5:38:09 PM
Measurement Date / Time	6/12/2014 10:20:29 AM
Operator	Administrator
Raw Data Origin	XRD measurement (*.XRDML)
Scan Axis	Gonio
Start Position [°2Th.]	20.0116
End Position [°2Th.]	109.9846
Step Size [°2Th.]	0.0130
Scan Step Time [s]	29.0700
Scan Type	Continuous
PSD Mode	Scanning
PSD Length [°2Th.]	3.35
Offset [°2Th.]	0.0000
Divergence Slit Type	Automatic
Irradiated Length [mm]	10.00
Specimen Length [mm]	10.00
Measurement Temperature [°C]	25.00
Anode Material	Cu
K-Alpha1 [Å]	1.54060

Generator Settings	40 mA, 45 kV
Diffractometer Type	0000000011059259
Diffractometer Number	0
Goniometer Radius [mm]	240.00
Dist. Focus-Diverg. Slit [mm]	100.00
Incident Beam Monochromator	No
Spinning	Yes

Peak List:

Pos. [°2Th.]	Height [cts]	d-spacing [Å]	Rel. Int. [%]	Area [cps*°2Th.]	Area [cts*°2Th.]	FWHM [°2Th.]
23.2173	0.38	3.82803	0.01	5.71	166.07	4.0000
32.5625	384.24	2.74761	11.77	5.53	160.89	0.3410
35.5462	1583.53	2.52352	48.51	59.76	1737.17	0.8702
38.8098	3264.31	2.31849	100.00	84.67	2461.31	0.5961
45.3935	5.18	1.99635	0.16	0.73	21.32	0.0010
48.8624	256.98	1.86242	7.87	16.91	491.66	1.5133
51.3164	12.84	1.77898	0.39	0.00	0.00	0.4048
53.5594	103.20	1.70964	3.16	5.38	156.51	1.2359
58.2462	297.75	1.58274	9.12	8.30	241.14	0.6495
61.6300	371.27	1.50370	11.37	14.97	435.10	0.9345
66.1754	333.21	1.41100	10.21	19.71	572.88	1.3849
68.0606	622.39	1.37644	19.07	14.29	415.38	0.5449
72.3674	93.19	1.30476	2.85	5.12	148.70	1.3267
74.9903	102.42	1.26549	3.14	6.36	184.96	1.4696
75.2067	1279.05	1.26239	39.18	1.90	55.33	0.0335
80.5177	3.63	1.19197	0.11	0.00	0.00	0.0010
82.6209	95.14	1.16687	2.91	3.02	87.91	0.9362
83.3976	118.81	1.15797	3.64	3.94	114.60	0.8912

86.7146	4.65	1.12199	0.14	0.45	13.04	3.5115
89.9424	88.90	1.08992	2.72	1.97	57.39	0.5199
91.7358	23.54	1.07323	0.72	1.08	31.49	1.1171
99.2081	34.81	1.01144	1.07	2.45	71.10	1.6645
103.5198	77.05	0.98074	2.36	4.69	136.31	1.4082
107.0812	81.67	0.95775	2.50	0.41	11.84	0.1150

Pattern List:

Visible	Ref. Code	Score	Compound Name	Displacement [°2Th.]	Scale Factor	Chemical Formula	SemiQuant [%]
*	01-089-5897	86	Copper Oxide	0.026	1.111	Cu O	53
*	01-073-6023	81	Tenorite	0.009	1.007	Cu O	47

CONFERENCES

Sharma K., Lal K., (2013), A review on the performance of the nanofluid-based solar collectors-Solar Energy, Proceeding of 1st National Conference on Recent Advances in Renewable Energy & Environment Sciences 2013 (NCRAREES), page 15.